ARL 63-159

THEORETICAL AND EXPERIMENTAL INVESTIGATION OF MICROWAVE SCATTERING FROM A CYLINDRICAL PLASMA

S. W. BOWEN
D. W. CHEATHAM, JR.
J. A. NICHOLLS
B. P. SELBERG

UNIVERSITY OF MICHIGAN
ANN ARBOR, MICHIGAN

SEPTEMBER 1963

Contract AF 33(616)-8126
Project 7116
Task 7116-02

AEROSPACE RESEARCH LABORATORIES
OFFICE OF AEROSPACE RESEARCH
UNITED STATES AIR FORCE
WRIGHT-PATTERSON AIR FORCE BASE, OHIO

FOREWORD

This final report was prepared by The University of Michigan, Ann Arbor, Michigan, on Contract AF 33(616)-8126 for the Aerospace Research Laboratories, Office of Aerospace Research, United States Air Force. The work reported herein was accomplished on Task 7116-02 "Research in Energy Conversion Techniques" of Project 7116, "Energy Conversion Research" with E. D. Stephens of the Thermomechanics Research Laboratory as the Task Monitor.

Special appreciation goes to Dr. E. Åström of the Royal Institute of Technology, Stockholm, Sweden, who suggested the theoretical analysis and the use of the microwave interferometer.

The assistance of Prof. A. Olte, Department of Electrical Engineering, The University of Michigan, in many enlightening discussions and for suggesting the use of the microwave spectrum analyzer; K. Young, Department of Electrical Engineering, The University of Michigan for his aid in the elimination of the RF interference problem; Dr. R. F. Goodrich, Department of Electrical Engineering, The University of Michigan, for helpful discussions of plasma physics; J. Fu and G. Machnikowski of the Propulsion Laboratory for mathematical computation and data reduction, is gratefully acknowledged.

ABSTRACT

This investigation was concerned with the theoretical and experimental study of a modest temperature plasma obtained by seeding with low ionization potential elements. A detailed thermochemical analysis of nitrogen or air as the carrier gases and sodium, potassium, or cesium as the seeding elements was made. The results are presented for a range of seeding ratios and temperatures up to 4000°K.

The experimental facility consisted of an RF plasma generator which produced a low velocity cylindrical plasma at 1 atmosphere pressure and a temperature of 2750°K. Seeding was accomplished by using an atomizer and aqueous solutions of the nitrates of the seeding elements.

The phase and amplitude of 3 cm microwaves scattered from the finite length, cylindrical, thermal plasma were measured by a microwave interferometer. These measurements were compared to the theoretical predicted values as obtained from an IBM 7090 computer program which considered the scattering of a plane incident electromagnetic wave from a homogeneous, cylindrical, infinite length plasma with properties based on the Saha equation ionization and available collision cross section data.

A comprehensive discussion of the possible sources of error is included but consistent unexplained differences between experiment and theory remain.

TABLE OF CONTENTS

TABLE OF CONTENTS (continued)

LIST OF FIGURES

LIST OF FIGURES (continued)

LIST OF TABLES

SYMBOLS

a_i = stoichiometric coefficient reactants

A_i = species i, molecular weight of species i reactants

b_j = stoichiometric coefficient products

$\overline{B}$ = magnetic field, webers m^{-2}

B_j = species j, molecular weight of species j, products

C_m = coefficients of Hankel function series

c = velocity of light, 3×10^8 m sec^{-1}

D = distance from plasma to receiver, m

D_m = coefficient of Bessel function series

$\overline{E}$ = electric field strength, volts m^{-1}

E_i = electronic energy of i^{th} energy level, joules

E_o = peak value of incident microwave, volts m^{-1}

$\overline{E}_p$ = plane wave electric vector, volts m^{-1}

E_{scat} = peak value of scattered electric field, volts m^{-1}

e = electron charge, $- 1.602 \times 10^{-19}$ coulombs

F = free energy (Gibbs), kcal/mole

$H_m^{(2)}$ = Hankel function of 2nd kind, order m

H = enthalpy, kcal/mole

$i = \sqrt{-1}$

I = ionization potential of species i, ev

$\overline{j}$ = current density, amp m^{-2}

J_m = Bessel function, order m

k = Boltzmann constant, 1.380×10^{-23} joule $^{o}K^{-1}$

k = complex propagation constant

K_3 = equilibrium constant of reaction 3

K_p = equilibrium constant

K_I = ionization equilibrium constant

m = separation constant, integer

M_i = molecular weight of species i, kg

m_e = electron mass, 9.106×10^{-31} kg

n_e = electron density, m^{-3}

n_T = total particle density m^{-3}

N = seeding ratio, mole fraction of seeding element

N_0 = Avogadro's number = 6.02472×10^{23} molecules/gm mole

P_T = total pressure, atm., Newtons m^{-2}

P_i = partial pressure of species i, Newtons m^{-2}, atm.

$Q(\ )$ = partition function

q_i = charge of component i in multiples of electron charge

Q_i = cross section of species i for electron impact, m^2

R = plasma radius, m

R = universal gas constant kcal $mole^{-1}\ ^{o}K^{-1}$

$R(r)$ = function of r in separation of variables

r = radial coordinate, m

S = molar entropy kcal/mole ^{o}K

S = Poynting vector, watts m^{-2}

T = temperature, ^{o}K

t = time, seconds

U_i = internal energy per mole of the i^{th} species

$\bar{v}$ = velocity vector, m sec^{-1}

$\langle \bar{v} \rangle$ = mean electron velocity, m sec^{-1}

x = coordinate normal to incident plane wave, m

X = seeding element—Na, K, Cs

x_i = mole fraction of species i

Y_m = Neumann function, order m

Z = compressibility factor, moles at equilibrium per original mole of undissociated, unionized mixture

β = phase of E_{tot} with respect to E_p, radians

$\epsilon_o = 8.854 \times 10^{-12}$ farad m^{-1}

$\mu_o = 4\pi \times 10^{-7}$ henry m^{-1}

λ = phase of scattered wave with respect to plane wave, radians

ν = collision frequency of electrons, sec^{-1}

ν_c = collision frequency of electrons, sec^{-1}

$\pi = 3.14159\ldots$

ρ = mass density kg m^{-3}

ρ = charge density coulomb m^{-3}

σ = electrical conductivity mho m^{-1}

ϕ = cylindrical angular coordinate measured from x axis, radians

$\psi(\phi)$ = function of ϕ in separation of variables

ω_p = plasma frequency, radian sec^{-1}

ω = frequency of electromagnetic wave, radian sec^{-1}

I. INTRODUCTION

The cylindrical plasma model has become one of much interest recently in that it has several physical counterparts in natural plasma phenomena. The high energy wakes and jets of various flight vehicles and propulsive devices are typical examples.[1] Considerable work has been accomplished both experimentally and theoretically with infinite and semi-infinite plasma media, and much theory and data have been accumulated for the so-called "plasma slab" model;[2-10] but theory and data are quite limited for the finite plasma models which appear to exist in actual practice. The cylindrical plasma, whether it be a by-product of current aerospace and hypervelocity endeavors or the direct result of a laboratory arrangement, more nearly represents a finite ionized medium (and its accompanying difficulties) than the above mentioned ideal plasma models. Accurate experimental data for finite plasmas is yet to be available in sufficient quantity;[11] therefore it is felt that the study of cylindrical plasmas and the development of applicable diagnostic techniques for these types of ionized media will contribute to the further understanding of finite plasma problems. Specifically, it is of interest to study and measure both the electrical and thermodynamic properties of such a medium. Murphy, Edelberg, Pippert, deRidder, and Peterson have studied the cylindrical plasma.[1, 12, 13]

The initial theoretical model to be considered in this study was chosen to be as simple as possible: a homogeneous, infinitely long, steady state, equilibrium, partially ionized, cylindrical plasma column consisting of an effectively-inert diatomic carrier gas, and a singly ionized low ionization potential seeding element. The experimental plasma model chosen for study produced the above somewhat idealized conditions with certain exceptions which are to be discussed in later sections of this report. The theoretical model was chosen to be at one atmosphere of pressure within a temperature range of 2000-4000^{o}K. These conditions obviously indicated the existence of a high collision frequency of particles within the plasma. The experimental plasma facility was capable of temperatures ranging from 2000^{o}K to 3000^{o}K as measured by sodium line reversal techniques, and a plasma could be generated for a wide range of ionization levels at atmospheric pressure.

[1] Manuscript released July 19, 1963 by the authors for publication as an ARL Technical Documentary Report.

A primary interest of this study was the consideration of the techniques and the effectiveness of seeding a finite plasma as a means of increasing the electrical conductivity of the medium. The plasma facility was capable of using a wide selection of carrier gases and a variety of seeding elements. The gases chosen for the experiment were N_2 and air. The seeding elements chosen were the alkali metals, Na, K, and Cs. These elements were mixed with the carrier gas prior to ionization by various methods. Two of these techniques proved more practical than others. In one seeding method the element in nitrate form was injected as an atomized aqueous solution, and in the second method the metal vapor was mixed with the carrier gas in a heating chamber, but was not used here.

An equilibrium constant analysis (Saha Equation) for the assumed theoretical plasma conditions was completed. Various combinations of carrier gases and seeding elements over the specific range of temperatures were considered in order to predict chemical composition, free electron mole fraction, and electron number densities as a function of the mole fraction seeding ratio of the elements involved.[14, 15, 16] A survey of recent collision cross section and collision frequency data[15, 17, 30, 31] was made in order to choose the appropriate collision frequency or range of collision frequencies for the assumed plasma conditions. Predicted values of the DC electrical conductivity were computed for a range of plasma conditions. The AC electrical conductivity could have been calculated as well. For the chosen theoretical plasma conditions the complex electrical conductivity was determined approximately by the predicted values of electron number density and collision frequency, the parameters which appear in the Lorentz formula for the electrical conductivity.[6, 19, 26, 27]

It was through consideration of the two parameters, electron density and collision frequency, that the experimental diagnostic methods were selected. Due to the nature of the r-f generated plasma the usual probe techniques were considered to be impractical. Thus microwave measurements, spectroscopic measurements, or a combination of both were considered applicable to this study. Due to the cylindrical geometry of the plasma and the predicted values of plasma properties,

X band microwave scattering measurements were chosen as being most applicable. Sodium line reversal measurements were selected as a means of determining the plasma temperature.

A plane polarized electromagnetic wave was transmitted via a wave guide horn to be normally incident upon the plasma column, with the electric field vector parallel to the cylinder axis.[12] Forward scattered field measurements were made giving the amplitude and the phase values of the scattered electric field surrounding the plasma column. These measurements were compared to the predicted values of amplitude and phase. The experimental measurements were not used to determine plasma frequency and collision frequency although in principle this could be done.

The remaining sections of this report include a detailed discussion of both the theoretical and experimental aspects of this study. In the following section, the thermo-chemistry of the seeded partially ionized gas is developed. Data including free electron mole fractions and densities, electrical conductivities, and plasma frequencies for a variety of plasma conditions is presented in graphical form. In other sections the microwave diagnostic method with its accompanying theory is discussed and the results of an electronic computer program for the computation of microwave scattering values are included. The plasma test conditions are discussed in light of the theoretical assumptions. The experimental arrangement and technique is described and experimental data is presented. A discussion of the experimental data, including an error analysis, is also included.

II. THERMO-CHEMICAL ANALYSIS OF AN EQUILIBRIUM SEEDED PLASMA—PLASMA PROPERTIES

In order to derive the properties of a plasma for given temperature and pressure values, the important chemical reactions which take place in the plasma must be analyzed. In the case of the seeded plasma these chemical reactions depend upon the seeding elements as well as the carrier gas. The low ionization potential elements chosen for analysis were the alkali metals, Na, K, and Cs; the carrier

gases to be considered were air, oxygen, and nitrogen. Thus for the various combinations of these flow components the important chemical reactions must be recognized. The equilibrium constants for the important chemical reactions must be determined, and the theoretical ionization process must be developed. The simultaneous solution of the resulting equilibrium reaction equations will yield the free electron mole fraction, x_e, for the seeded fluid. The electron density, n_e, then may be determined from the electron mole fraction for the given temperature and pressure, and the appropriate collision frequency, ν, may be selected for these same conditions. Finally the electrical conductivity, σ, of the plasma may be found using the electron density and collision frequency values. The electron density may also be written in the form of the plasma frequency, ω_p.

The properties thus derived, however, are restricted to the certain limiting assumptions or conditions which must be specified in order to make such an analysis in closed form.

For the analysis which follows:

1. The plasma is assumed to be in thermodynamic equilibrium.
2. The seeding element is assumed to be singly thermally ionized in an electrically neutral plasma.
3. The carrier gas and seeding element are assumed to be a mixture of perfect gases.
4. The pressure is assumed to be atmospheric throughout a temperature range of 2000° to 4000°K.

II-A. Equilibrium Plasma Analysis

For an equilibrium plasma consisting of a mixture of perfect gases the following equations will apply generally to the analysis of the free electron mole fraction versus seeding ratio of additive elements. The law of mass action may be represented by the equilibrium equation

$$K_P(T) = \frac{\prod_j P_{B_j}^{b_j}}{\prod_i P_{A_i}^{a_i}} \tag{2-1}$$

where P_{B_j} and P_{A_i} represent the partial pressure of the products and the reactants of the reaction respectively and b_j and a_i the associated stoichiometric coefficients of the reaction. The conservation of mass may be written

$$\sum_i a_i A_i = \sum_j b_j B_j \tag{2-2}$$

where A_i and B_j represent the molecular weights of the reactants and products respectively. The conservation of electric charge may be written

$$n_e = \sum_i q_i n_i \tag{2-3}$$

where n_e is the number of free electrons per unit volume, q_i is the charge (in units of electron charge) of the i^{th} component per unit volume.

For the temperature and pressure conditions of either seeded air or seeded nitrogen it becomes reasonable to consider only single thermal ionization of the gas atoms and the alkali seeding metals; then Equation (2-3) may be written as

$$n_e = n_{ions} \tag{2-4}$$

The equilibrium constants, $K_p(T)$, of Equation (2-1) represent the ionization or chemical reactions involved in the plasma and $K_p(T)$ may be evaluated through the use of the relation

$$\ln K_p(T) = \frac{-\Delta F^o}{RT} \tag{2-5}$$

where ΔF^o is the change in Gibbs free energy for the reaction at standard pressure. For certain chemical reactions, however, Equation (2-5) has been

evaluated and $K_p(T)$ is directly available as a function of temperature. For others it may be evaluated using data for the thermodynamic properties of the constituents of the appropriate chemical reactions at elevated temperatures. For some reactions it may be convenient to evaluate ΔF^o in terms of the partition functions, Q, of the reaction species.[24]

$$Q^{(tot)} = \sum_i g_i \exp\left(\frac{-E_i}{kT}\right) \tag{2-6}$$

where E_i is the energy associated with the i^{th} energy level, and g_i represents the number of quantum states of the i^{th} energy level of the species. The molar free energy in terms of the thermodynamic properties is given by

$$F = H - TS \tag{2-7}$$

The properties H(T) and S(T) may be written in terms of the partition function, Q; thus ΔF^o and $K_p(T)$ may be evaluated in terms of Q.

It has been assumed that all species within the plasma follow a Boltzmann distribution and that the plasma is a mixture of perfect gases. For the reaction

$$\sum_i a_i A_i = \sum_j b_j B_j \tag{2-8}$$

the equilibrium constant may be written

$$K_p(T) = \frac{\prod_j \left[(2\pi m_j)^{3/2} h^{-3} (kT)^{5/2} Q_j^{(i)}\right]^{b_j}}{\prod_i \left[(2\pi m_i)^{3/2} h^{-3} (kT)^{5/2} Q_i^{(i)}\right]^{a_i}} \exp\left(-\frac{\sum_j b_j U_j(0) - \sum_i a_i U_i(0)}{RT}\right) \tag{2-9}$$

where $Q_j^{(i)}$ is the internal partition function of the j^{th} species, $U_j(0)$ is the internal energy of the j^{th} species at 0^oK, m_j is the mass of the j^{th} species and h is the Planck constant. The general partition function here has been written $Q^{(tot)} = Q^{(tr)} \prod_i Q^{(i)}$ where $Q^{(tr)}$ is the translational motion partition function.[15]

If the important chemical reactions are known for a given equilibrium plasma, Equations (2-1) - (2-9) may be used in the appropriate combination to solve for the desired species mole fractions.

Consider for example the reaction for the single thermal ionization of the additive element, X,

$$X = X^+ + e^- \tag{2-10}$$

Equation (2-1) may be written, using Equations (2-2) and (2-4),

$$K_{P_I}(T) = \frac{P_{X^+} P_e}{P_X} = \frac{x_{X^+} x_e}{x_X} P_T = \frac{x_{X^+}^2 P_T}{x_X} = \frac{x_{X^+}^2 P_T}{NZ^{-1} - x_{X^+}}$$

$$x_{X^+}^2 P_T + K_{P_I}(T)\, x_{X^+} - NZ^{-1} K_{P_I}(T) = 0 \tag{2-11}$$

where x_i is the mole fraction of species i, moles i^{th} species per total moles of mixture and where $x_X = NZ^{-1} - x_{X^+}$ and N is the mole fraction seeding ratio of the additive element, moles X per initial moles of mixture and $Z = \frac{1}{1 - x_e}$, moles of mixture per initial moles of mixture. Thus the mole fraction of free electrons for such a simple reaction may be determined for the mole fraction seeding ratio, N, of a given seeding element X and a given temperature, provided K_{P_I} may be evaluated by means of Equation (2-9), for example. Equation (2-9) may be written

$$K_{P_I}(T) = \frac{Q_{x^+}^{(i)} Q_e^{(i)}}{Q_X^{(i)}} (2\pi m_e)^{3/2} h^{-3} (kT)^{5/2} \exp\left(-\frac{U_{x^+}(0) + U_e(0) - U_x(0)}{RT}\right) \tag{2-12}$$

where the approximation $m_{X^+} = m_X$ has been used. The numerator of the exponential represents the ionization energy per mole. This corresponds to U for the molecule where U = 23,053 I and I is the ionization potential of the element in electron volts. A further reduction of Equation (2-12) now, in terms of U, yields for

the reaction

$$\log K_{P_I}(T) = \log \frac{2Q_{x^+}^{(i)}}{Q_x^{(i)}} - \frac{5041\, I}{T} + 5/2 \log T - 6.491 \qquad (2\text{-}13)$$

For the case of negligible excited states above ground level the $Q^{(i)}$ may be replaced by g_o (ground level terms) and Equation (2-13) reduces to that attributed to M. N. Saha.[25] It is apparent then that, for a given seeded plasma with known chemical and ionization reactions, the free electron mole fraction may be determined in closed form. In order to complete an analysis of this sort the important chemical reactions as well as the ionization process must be determined for the specific plasmas to be studied. In the case where several governing chemical and ionization reactions are involved in the plasma a simultaneous solution of the equilibrium equations must be made.

Two basic plasmas are considered in this work, a nitrogen plasma with additives and an air plasma with additives. Specifically the additives or seeding elements are the low ionization potential alkali metals, Na, K, and Cs. In an earlier study of these plasmas Buchanan[15] has made a detailed analysis of the chemical reactions for a wide variety of seeding elements for similar plasma conditions.

II-B. Nitrogen Plasma with Alkali Metal Additives

In the case of the nitrogen plasma there are no important chemical reactions other than the single thermal ionization of the seeding element X for the temperatures and pressure considered.[15] It should be noted here that for the chosen conditions the plasma consists of molecular nitrogen and a singly ionized alkali metal in a gaseous state. Under these conditions then the nitrogen is effectively inert and serves as a carrier gas for the singly ionized seeding element. The appropriate equation for the solution of the free electron mole fraction as function of seeding element, temperature, pressure, and the mole fraction seeding ratio of the additive element is Equation (2-11) which is repeated here in terms of x_e.

$$x_e^2 P_T + K_{P_I}(T)\, x_e - NZ^{-1} K_{P_I}(T) = 0 \qquad (2\text{-}11)$$

The ionization equilibrium constants, $K_{P_I}(T)$, for the seeding elements are determined using Equation (2-13) where only the ground level terms for the partition function are used, i. e., the Saha Equation. Figure 1 presents $K_{P_I}(T)$ versus temperature for Na, K, and Cs. Figures 2 through 4 present the solution of the ionization equation, Equation (2-11), for free electron mole fraction versus temperature for a select set of mole fraction seeding ratios of the alkali additives. Due to the relatively small electron mole fraction (10^{-4}), the value of Z was taken to be unity.[28]

Having determined the electron mole fractions for the seeded nitrogen plasma the free electron number density may be found using the relation

$$n_e = x_e\, n_T \qquad (2\text{-}14)$$

where n_T is the total number of particles per unit volume in the plasma and is given by the relation

$$n_T = \frac{P_T}{kT} = N_o \rho_o \left(\frac{\rho}{\rho_o}\right) \frac{1}{\sum_i x_i M_i} \qquad (2\text{-}15)$$

where x_i and M_i are the mole fraction and molecular weight of the i^{th} species respectively. Figures 5 through 7 represent the seeding ratio of the additives versus the free electron number density for several temperatures for the seeded nitrogen plasma. Using the determined values of electron density and a selected value of the effective collision frequency of the plasma, $\nu = 7.5 \times 10^{10}$ coll./sec. (see Section IV), the DC electrical conductivities, σ_{DC}, were computed using the relation

$$\sigma_{DC} = \frac{n_e}{\nu} (e^2/m_e) \qquad (2\text{-}16)$$

and these results are shown in Figures 8 through 12 for each seeding element and for several temperatures. The conductivity is plotted versus the mole fraction seeding ratio of the seeding element in order to indicate directly the effect of seeding on the electrical conductivity of the plasma. The plasma frequency ω_p of the plasma is related to the electron density by the equation

$$\omega_p = \left[\frac{n_e e^2}{\epsilon_o m_e}\right]^{1/2} \tag{2-17}$$

where e, m_e, and ϵ_o are the charge of the electron, the mass of the electron, and the free space dielectric constant respectively. Figure 13 presents the plasma frequency, versus seeding ratio, N, for 2700°K.

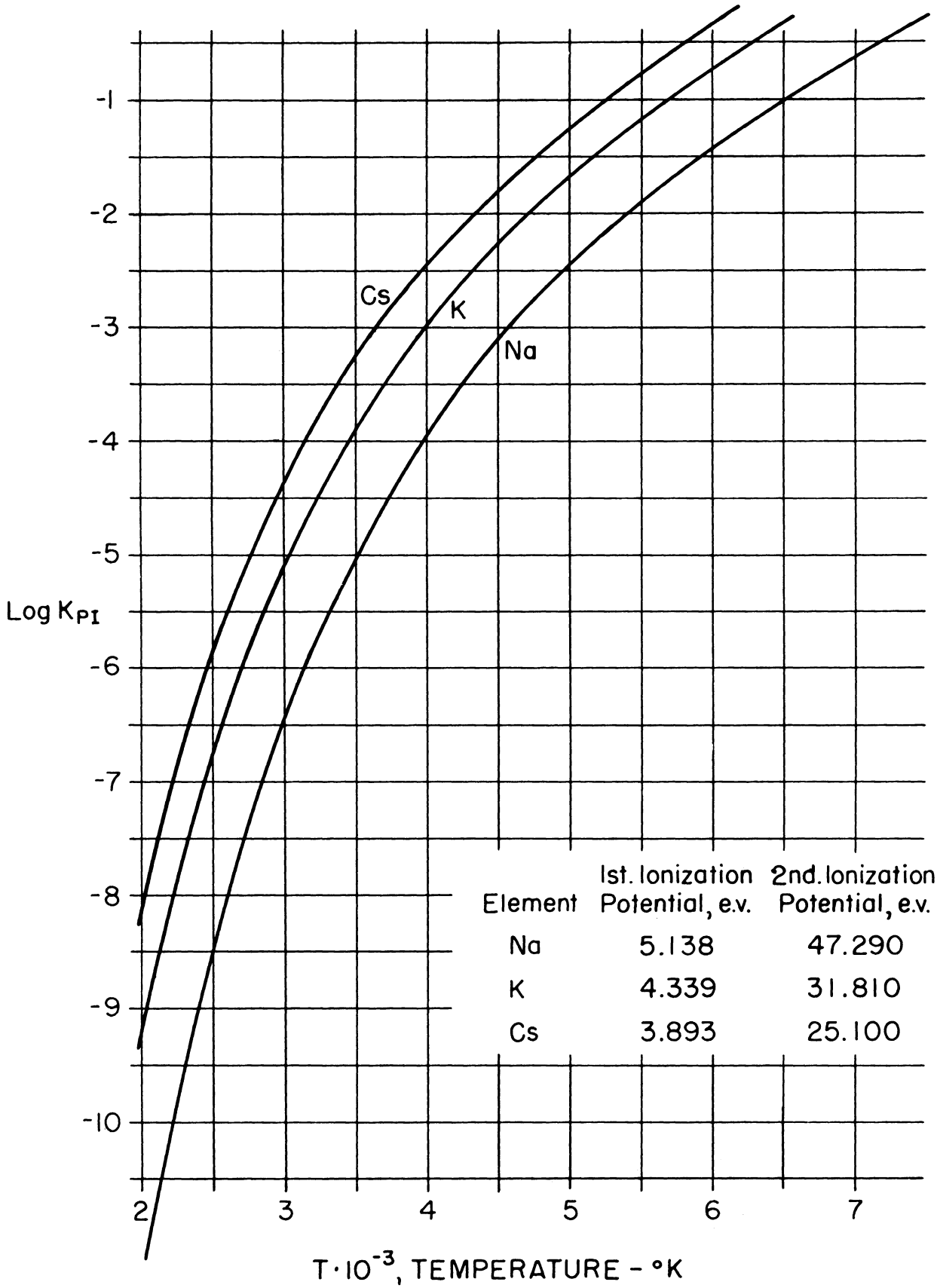

FIGURE 1. IONIZATION EQUILIBRIUM CONSTANT vs. TEMPERATURE

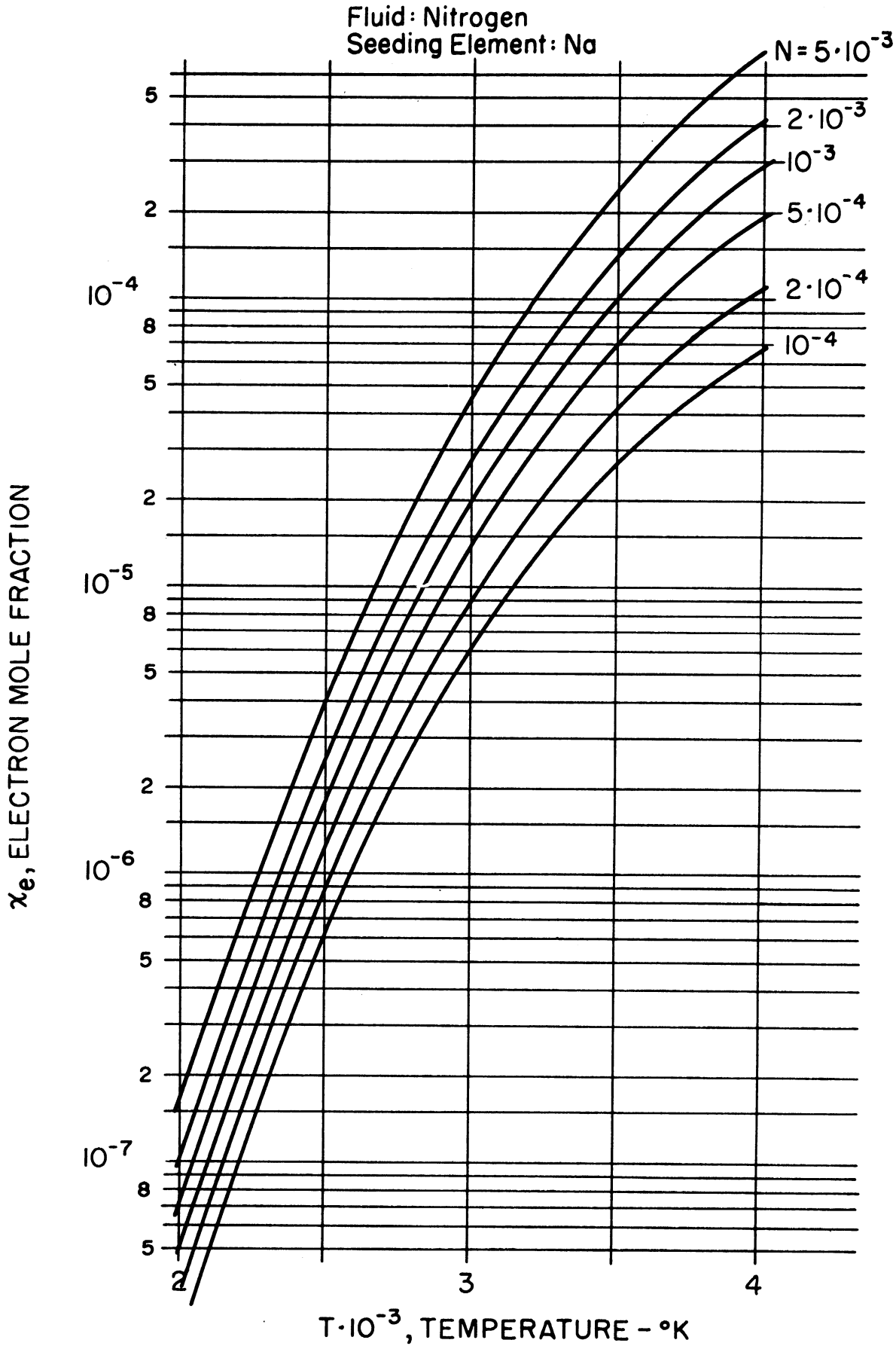

FIGURE 2. ELECTRON MOLE FRACTION vs. TEMPERATURE (N_2 and Na)

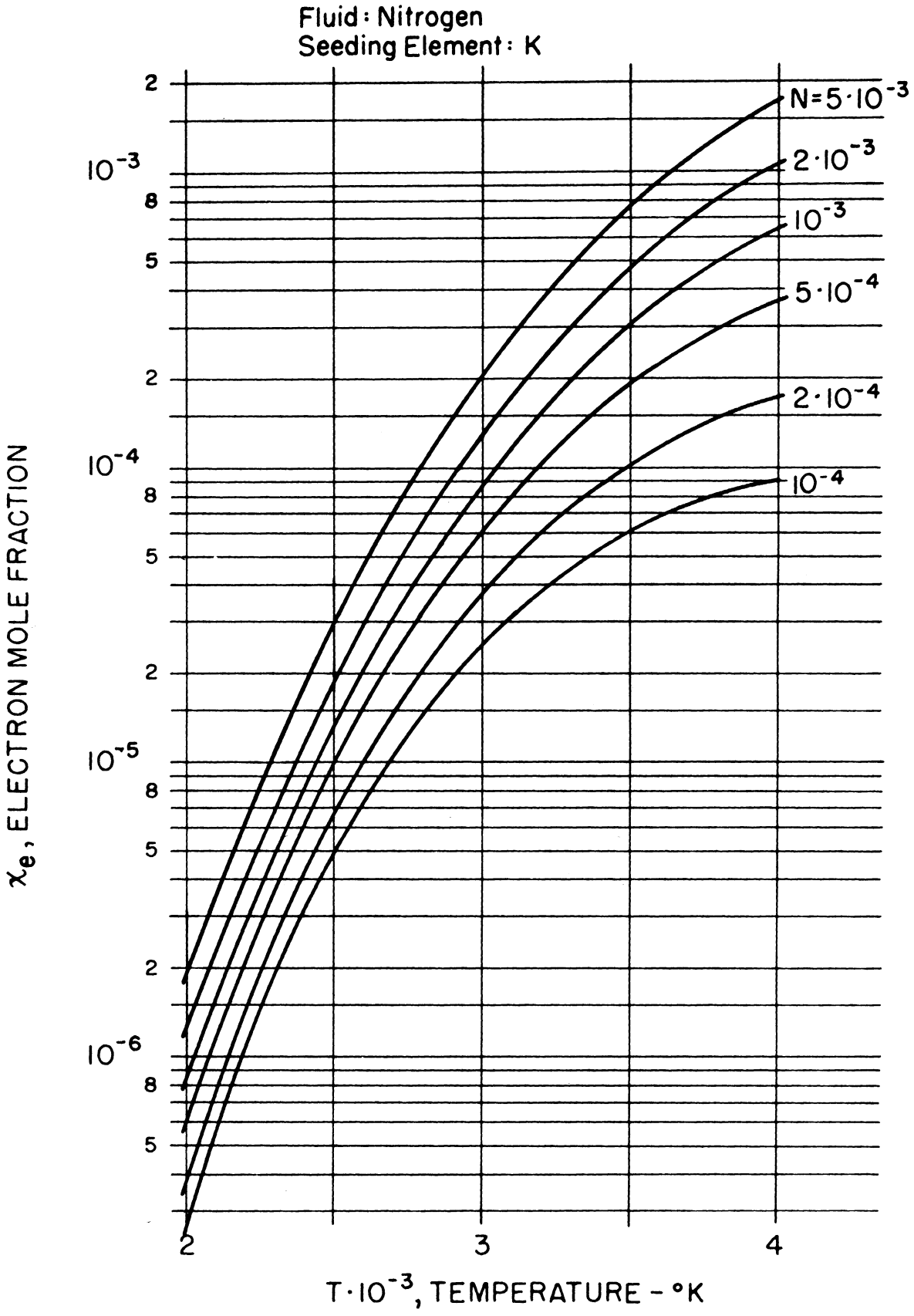

FIGURE 3. ELECTRON MOLE FRACTION vs. TEMPERATURE (N_2 and K)

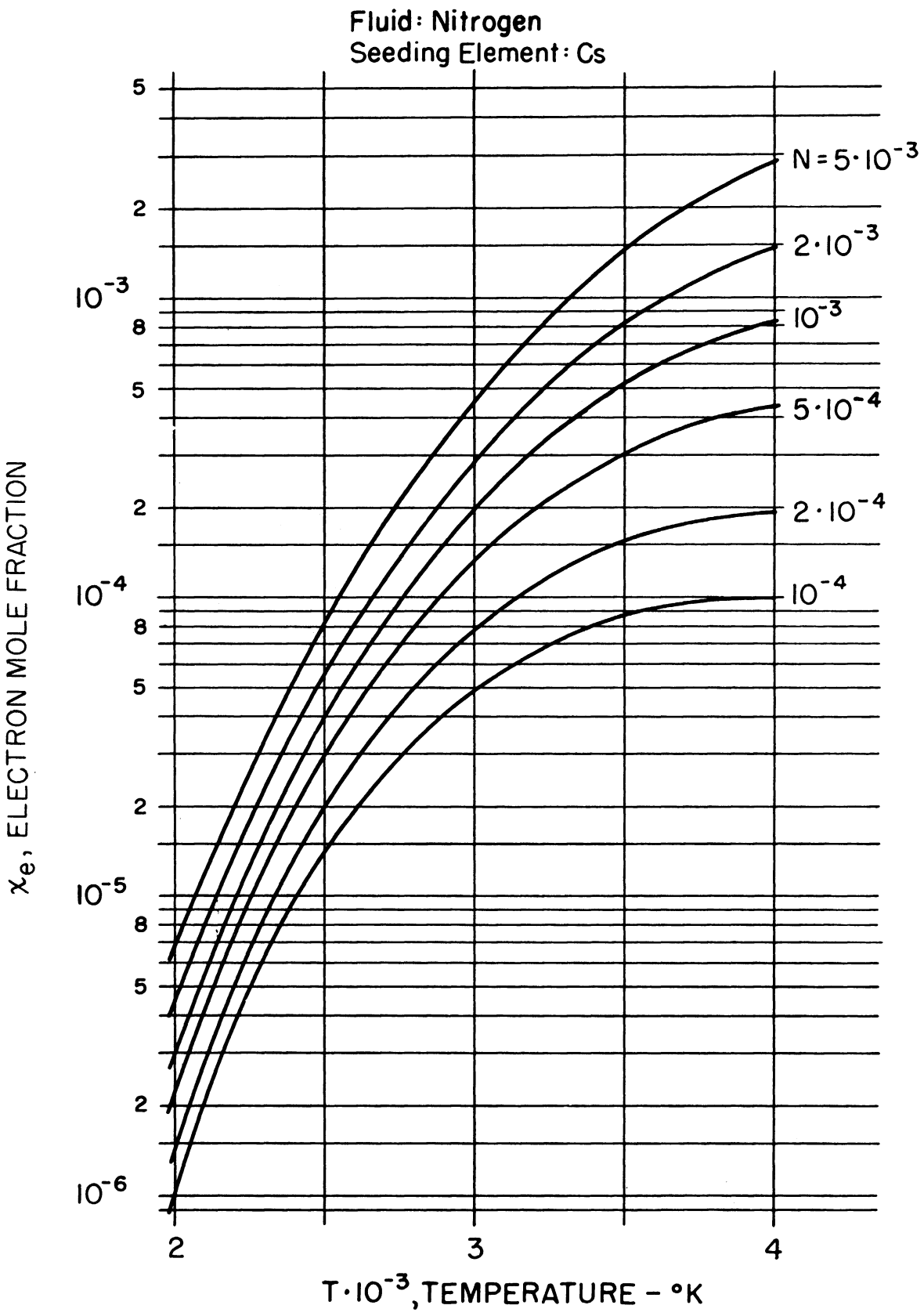

FIGURE 4. ELECTRON MOLE FRACTION vs. TEMPERATURE (N_2 and Cs)

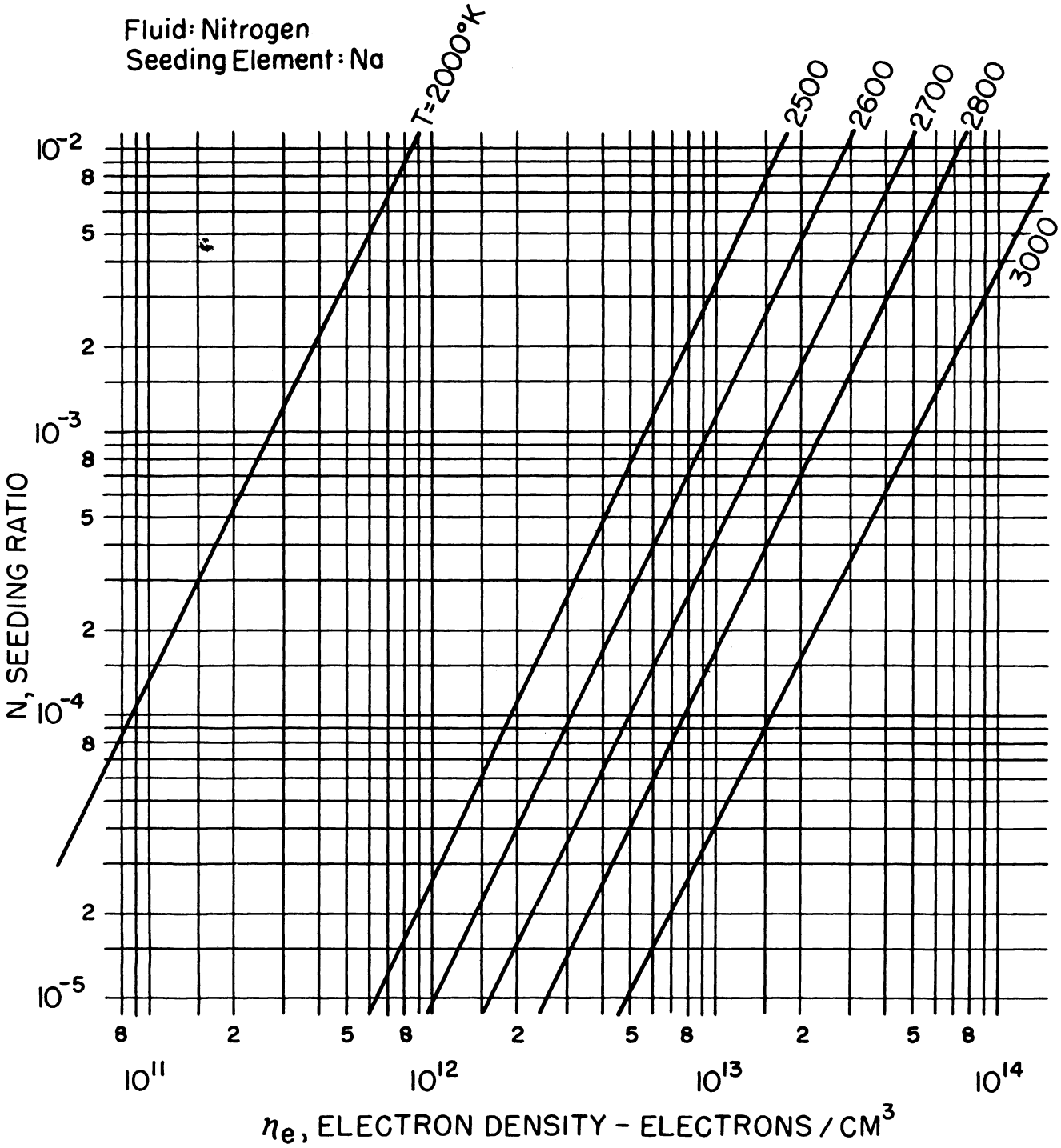

FIGURE 5. SEEDING RATIO vs. ELECTRON DENSITY (N_2 and Na)

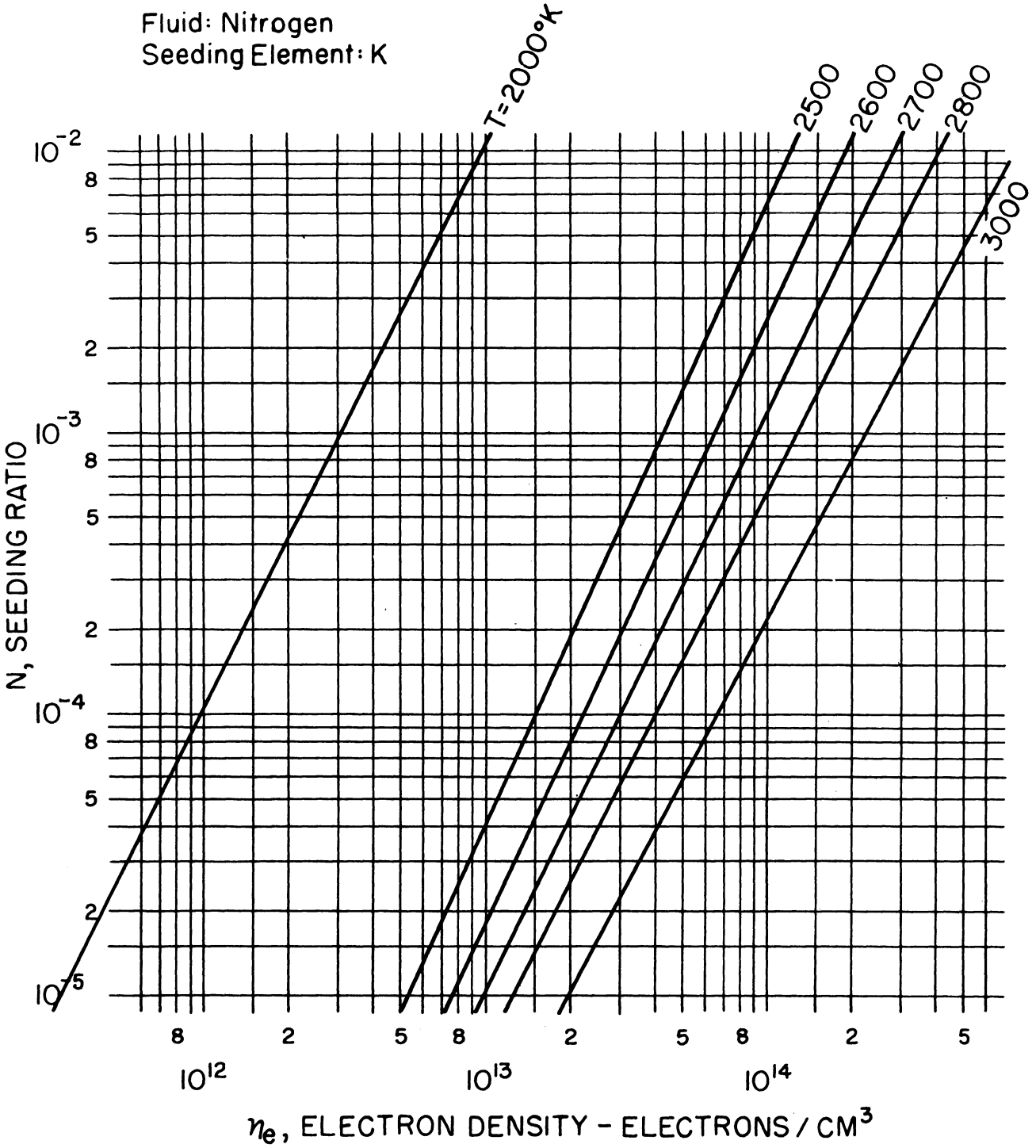

FIGURE 6. SEEDING RATIO vs. ELECTRON DENSITY (N_2 and K)

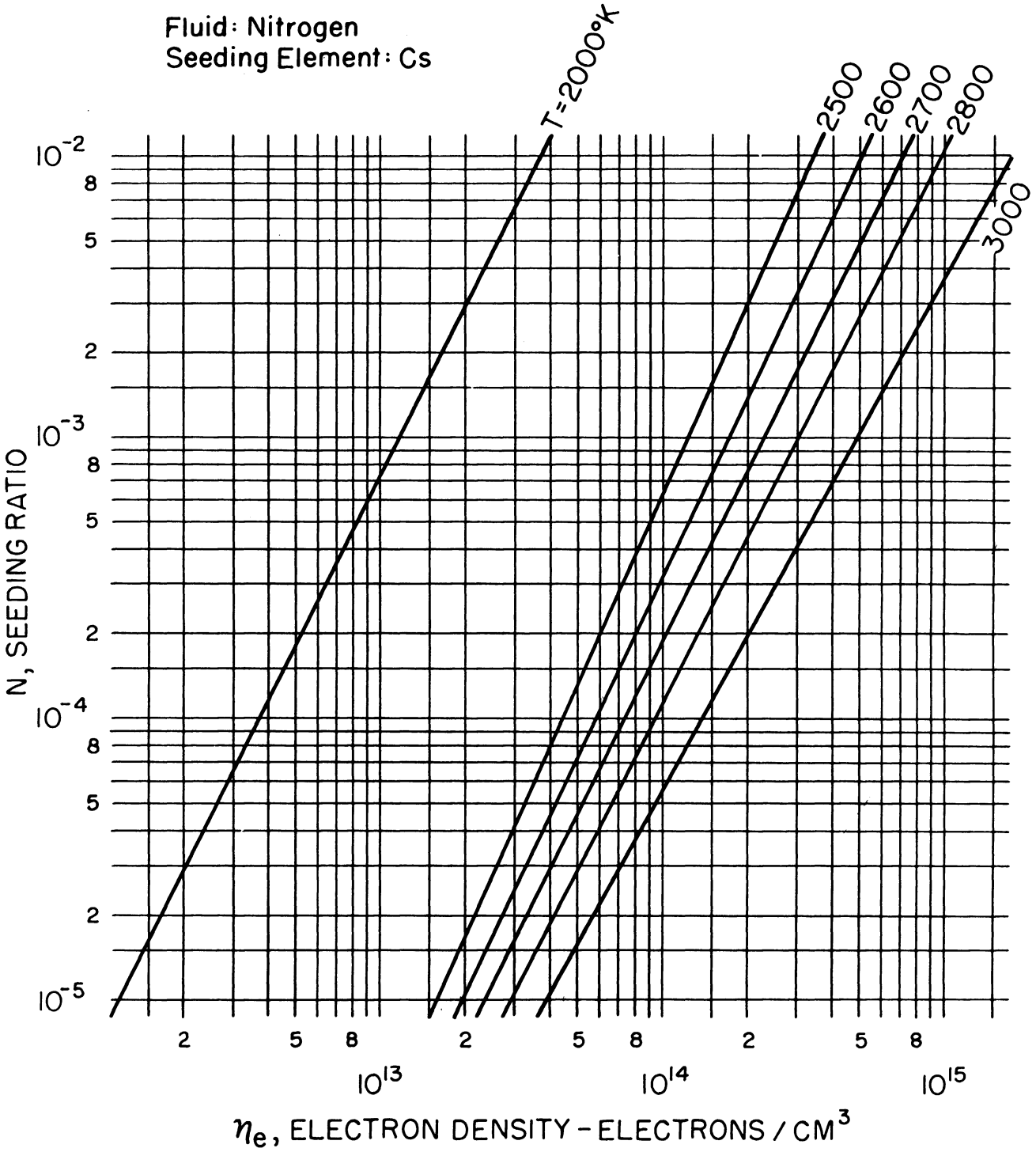

FIGURE 7. SEEDING RATIO vs. ELECTRON DENSITY (N_2 and Cs)

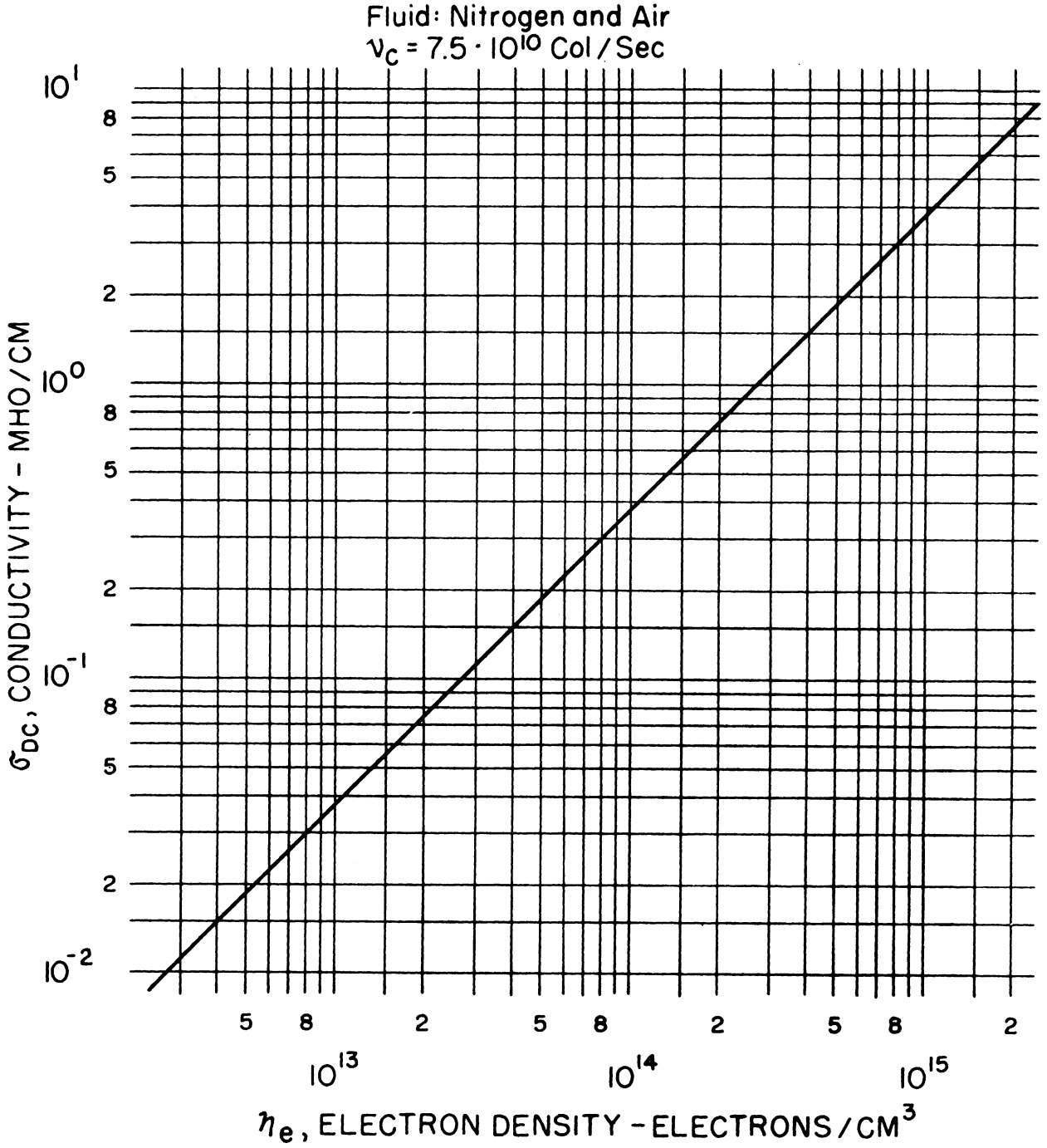

FIGURE 8. DC ELECTRICAL CONDUCTIVITY vs. ELECTRON DENSITY

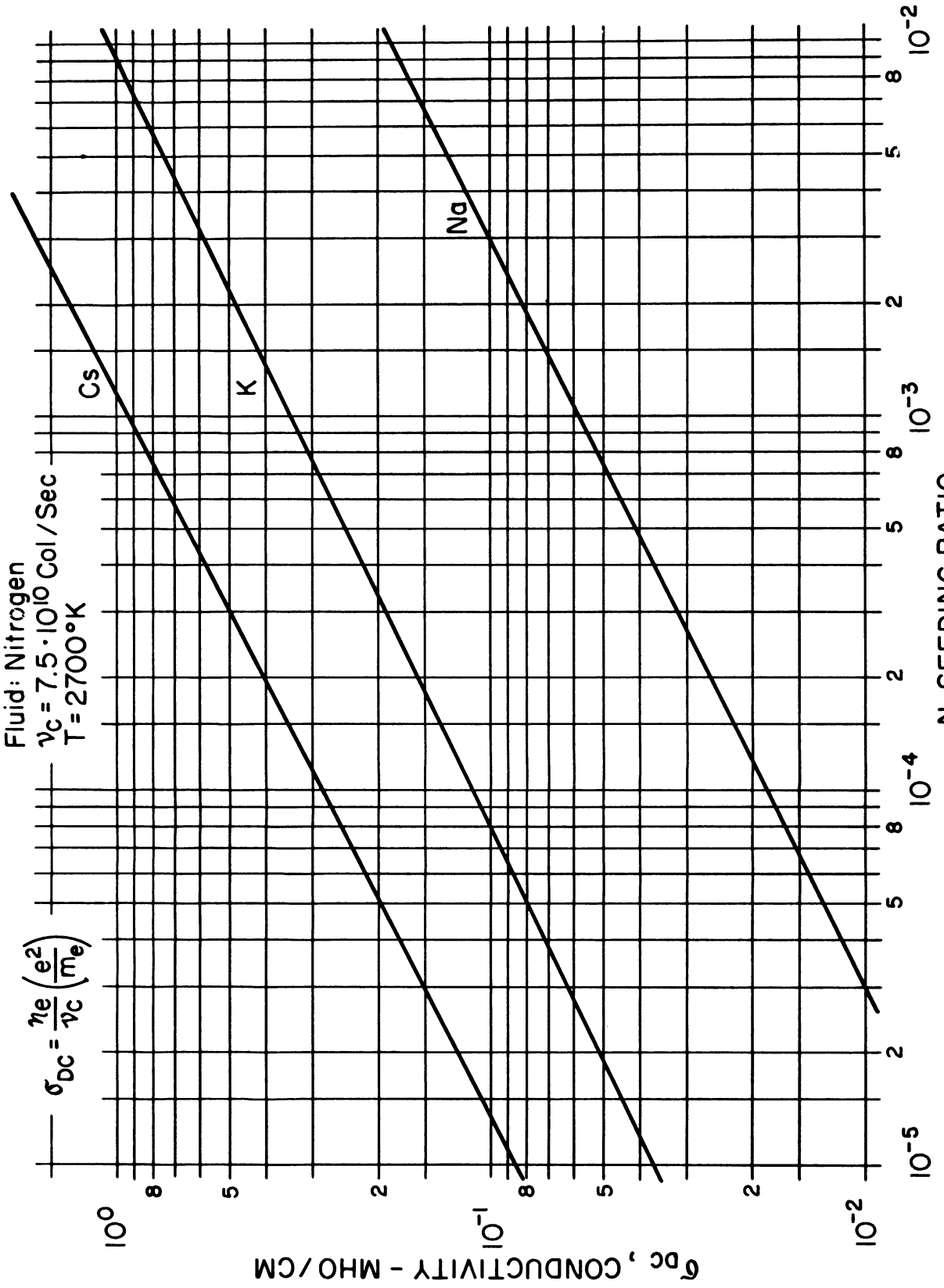

FIGURE 9. DC ELECTRICAL CONDUCTIVITY vs. SEEDING RATIO (N_2 and Na, K, or Cs, at 2700°K)

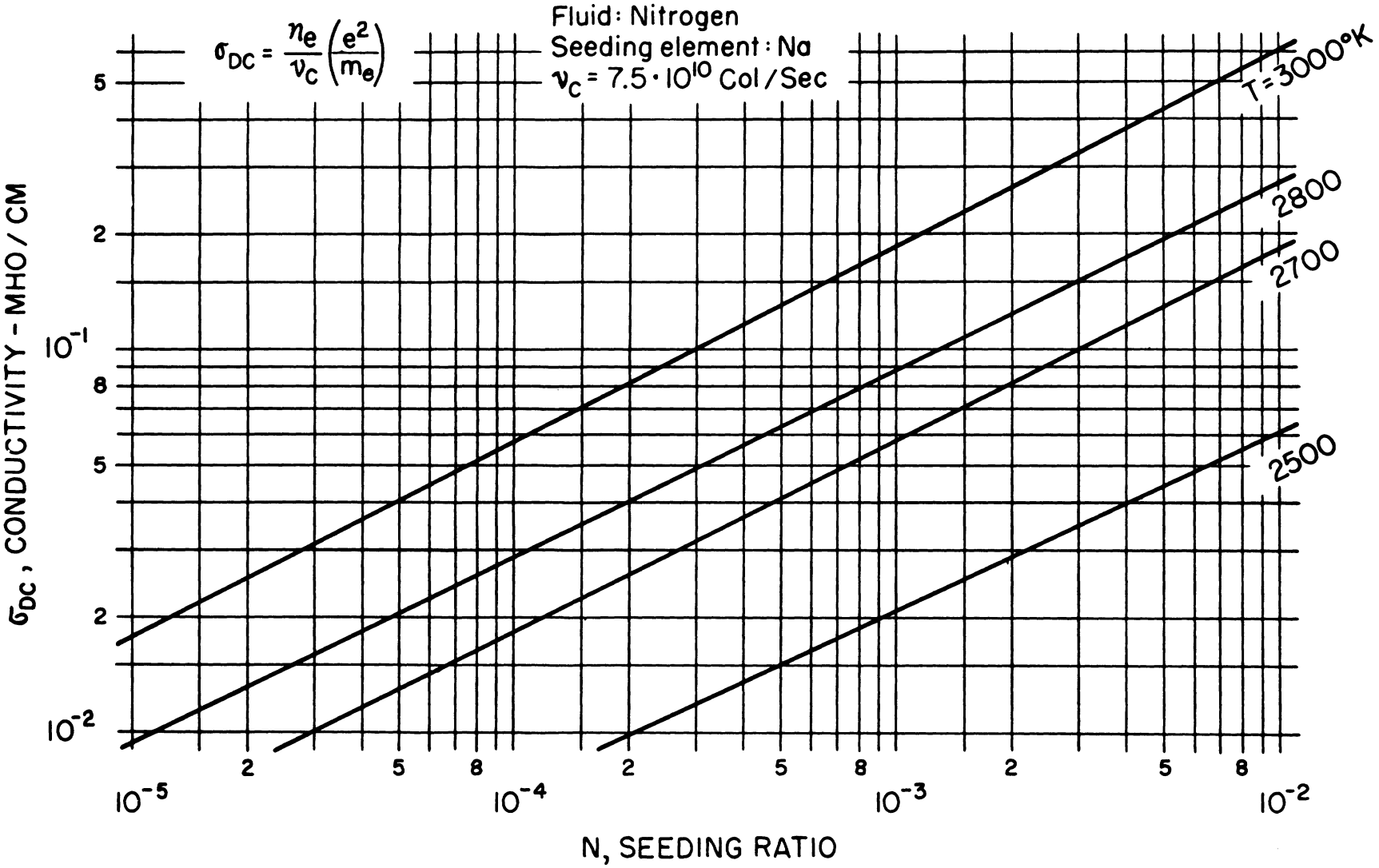

FIGURE 10. DC ELECTRICAL CONDUCTIVITY vs. SEEDING RATIO
(N_2 and Na)

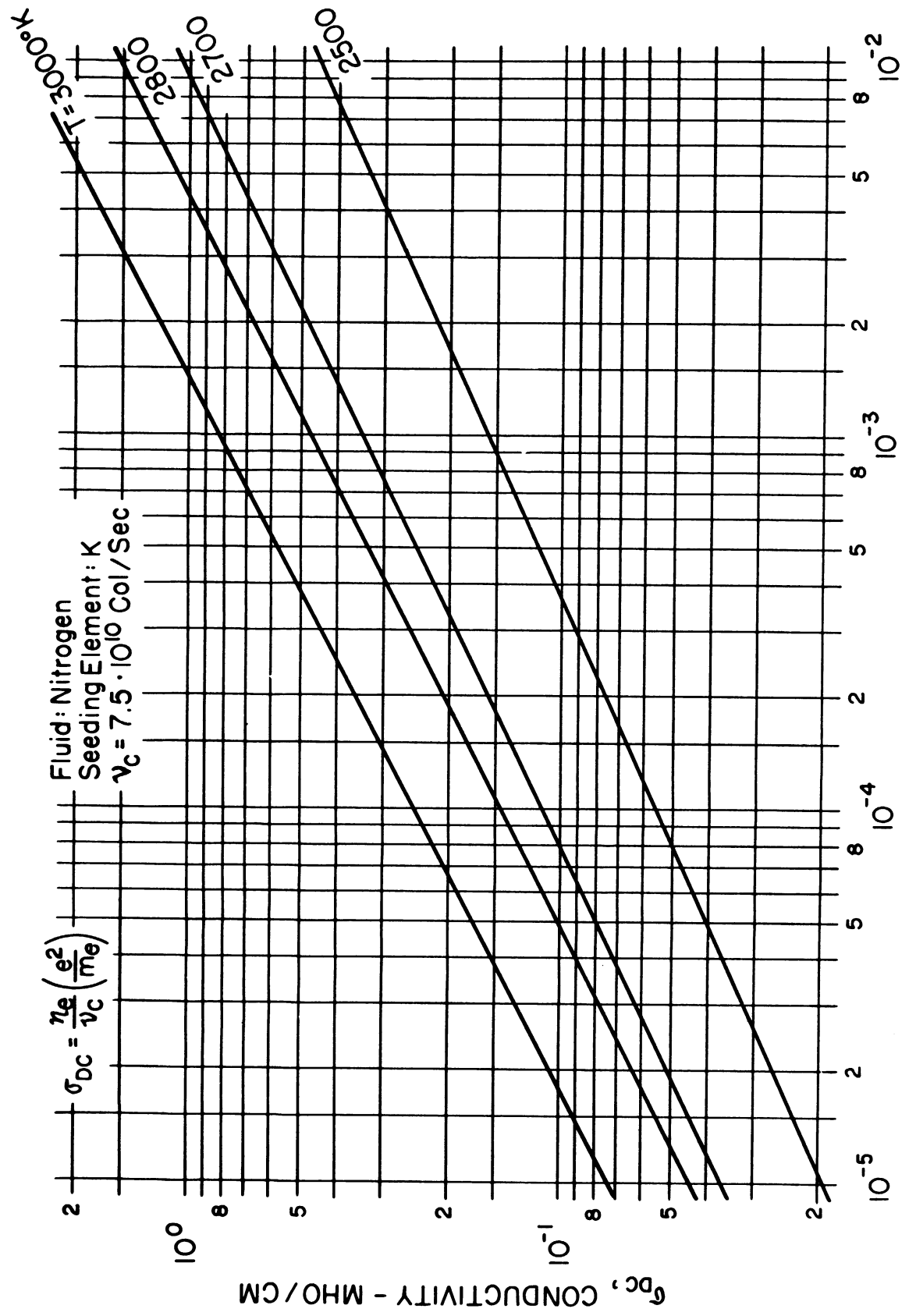

FIGURE 11. DC ELECTRICAL CONDUCTIVITY vs. SEEDING RATIO (N_2 and K)

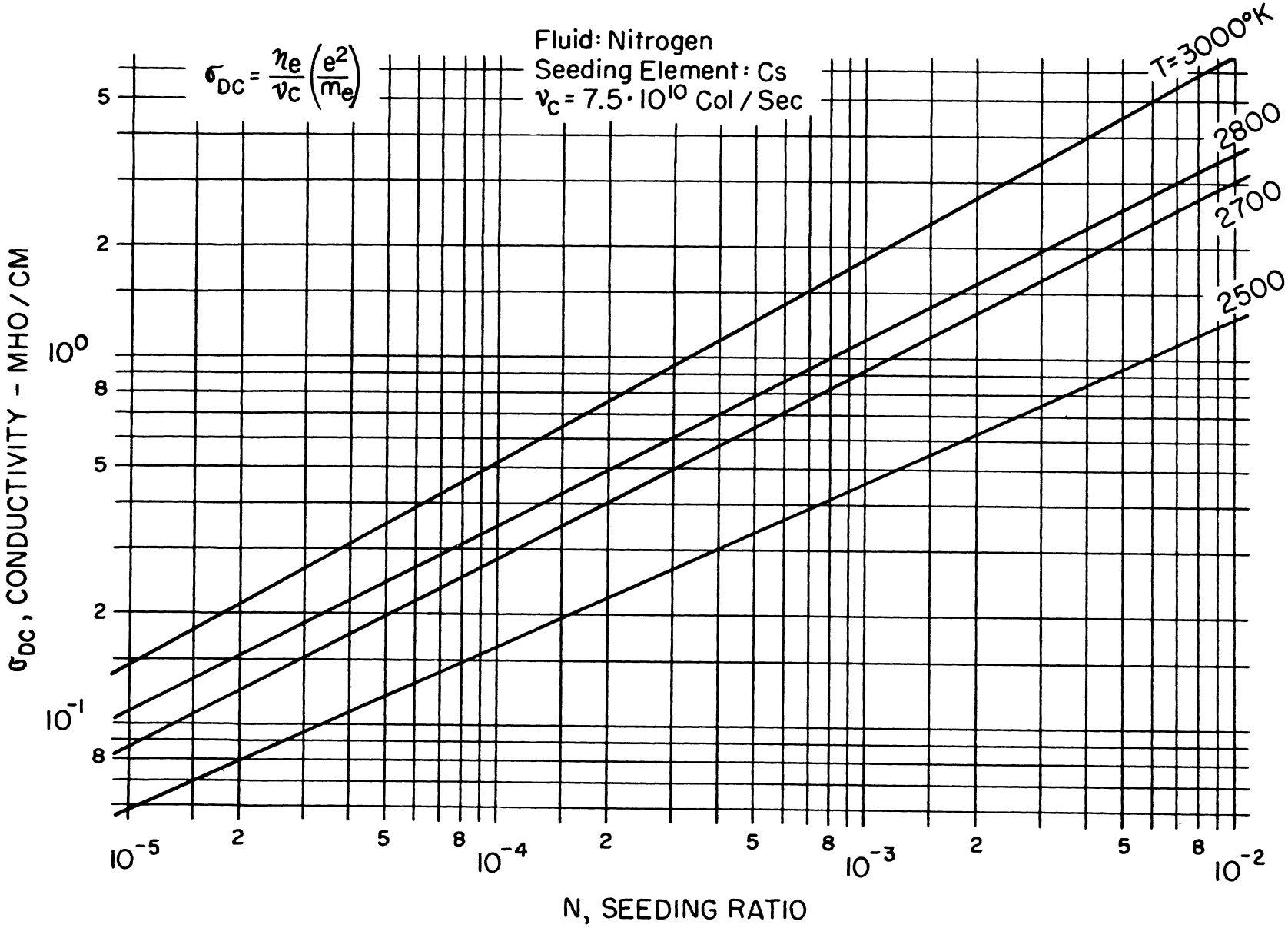

FIGURE 12. DC ELECTRICAL CONDUCTIVITY vs. SEEDING RATIO (N_2 and Cs)

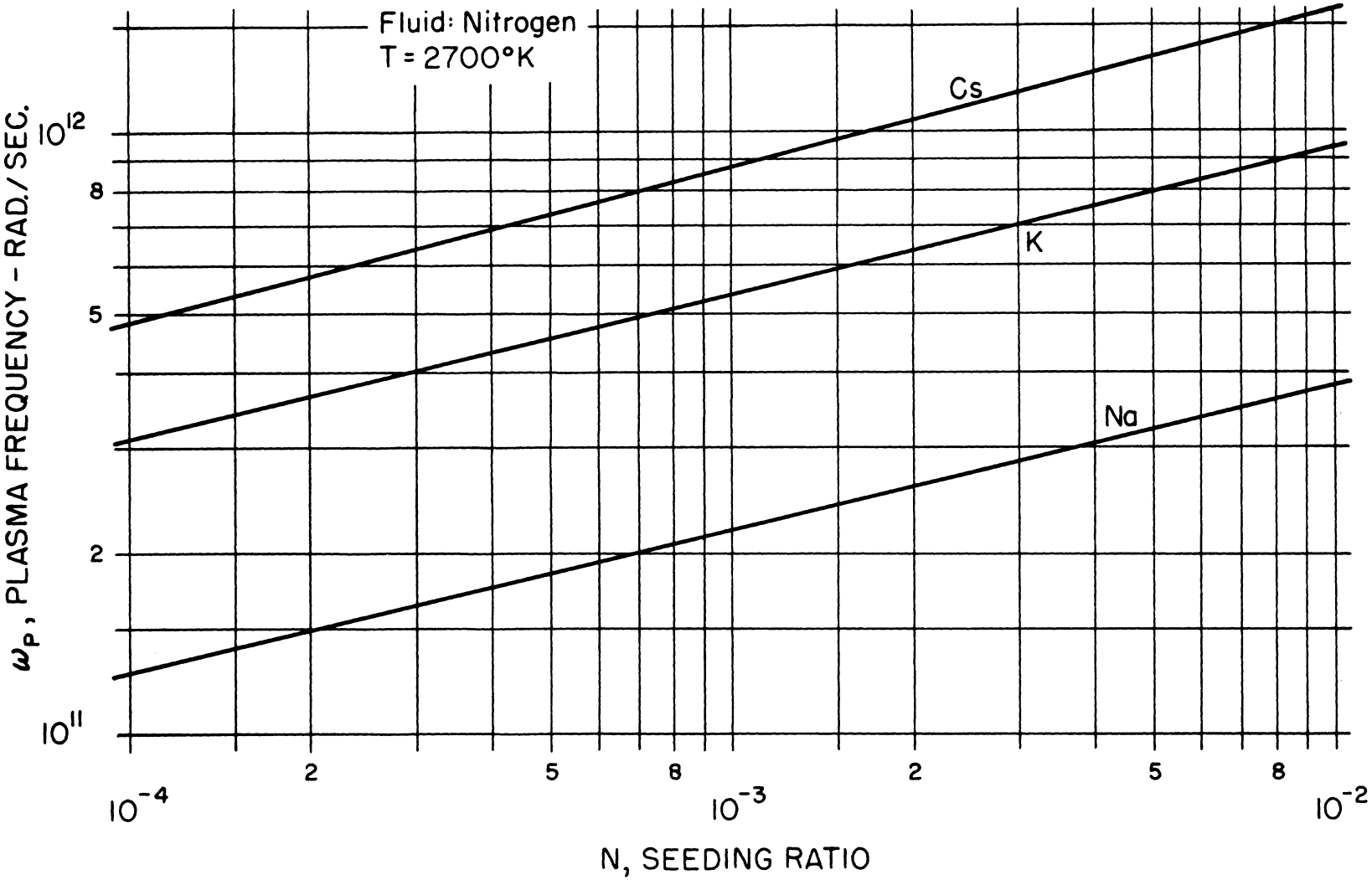

FIGURE 13. PLASMA FREQUENCY vs. SEEDING RATIO
(N_2 and Na, K, Cs at 2700°K)

II-C. Air Plasma with Alkali Metal Additives

Now for the case of the seeded air plasma all of the predominant reactions must be considered simultaneously through the use of Equations (2-1) through (2-13). Both unseeded and seeded air properties have been determined similarly by other authors.[14, 15, 16, 20, 21] For the case of oxygen as the carrier gas the predominant reactions are

$$XO(g) = X(g) + O \tag{2-21}$$

$$1/2\, O_2 = O \tag{2-22}$$

$$X = X^+ + e^- \tag{2-23}$$

$$O_2 = O_2^+ + e^- \tag{2-24}$$

$$O = O^+ + e^- \tag{2-25}$$

where the latter two ionization reactions may be considered negligible for the temperature and pressure restrictions considered here. The equilibrium equations then become, from reaction (2-21),

$$K_3(T) = \frac{x_X\, x_O}{x_{XO}}\, P_T \tag{2-26}$$

from (2-22),

$$K_P(T) = \frac{x_O}{x_{O_2}^{1/2}}\, P_T^{1/2} \tag{2-27}$$

from (2-23),

$$K_{P_I}(T) = \frac{x_{X^+}\, x_e}{x_X}\, P_T \tag{2-28}$$

A simultaneous solution of Equations (2-26) - (2-28) along with the mass conservation relation

$$x_{XO} + x_X + x_{X^+} = NZ^{-1} \tag{2-29}$$

and the conservation of charge relation

$$x_e = x_{X^+} \tag{2-30}$$

yields the following quadratic equation which may be solved for the free electron mole fraction, x_e:

$$\left[x_O P_T^2 + K_3(T)\, P_T\right] x_e^2 + \left[K_3(T)\, K_{P_I}(T)\right] x_e - NZ^{-1} K_3(T)\, K_{P_I}(T) = 0 \tag{2-31}$$

where the values of $K_3(T)$ may be determined from available thermodynamic property data,[15, 22, 23, 24] x_O from readily available values of $K_p(T)$,[22] Z,[28] and $K_{P_I}(T)$ from the ground level form of Equation (2-13), the Saha Equation.

For seeded air under the imposed temperature-pressure conditions and for seeding ratios in the order of 10^{-2} to 10^{-4}, Equation (2-31) may be used to determine the free electron mole fraction with an error of not greater than 1% provided the values used for x_O and Z are those for equilibrium air at the specified plasma conditions.[15]

Figure 14 represents the solution of $K_3(T)$ versus temperature using thermodynamic property data, and Figure 1 again represents the values of $K_{P_I}(T)$ for the additive elements as a function of temperature.

Figures 15, 16, and 17 then present the solution of Equation (2-31) for the free electron mole fraction, x_e, versus temperature for selected seeding ratios, N, and the three seeding elements using both Z = 1 and Z for equilibrium air. At $3000^{\circ}K$ the error due to the use of unity for Z is less than 3%.

As in the case of the nitrogen plasma, Equations (2-14) and (2-15) may be used to determine the electron density, n_e, for the air plasma. Figures 18, 19, and 20 show the seeding ratio versus free electron density for several temperatures for the three additive elements, Na, K, and Cs.

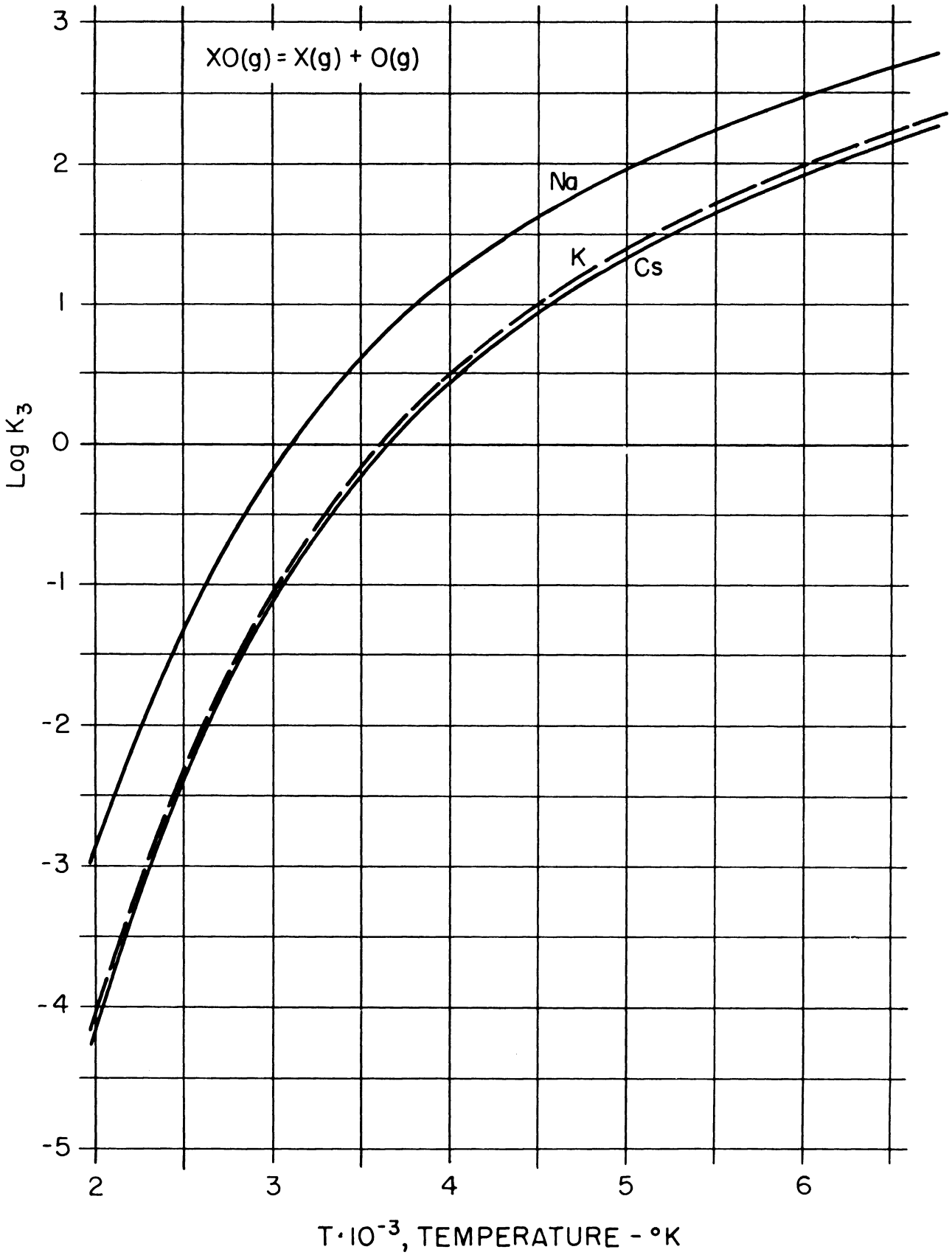

FIGURE 14. EQUILIBRIUM CONSTANT, K_3, vs. TEMPERATURE (XO = X + O)

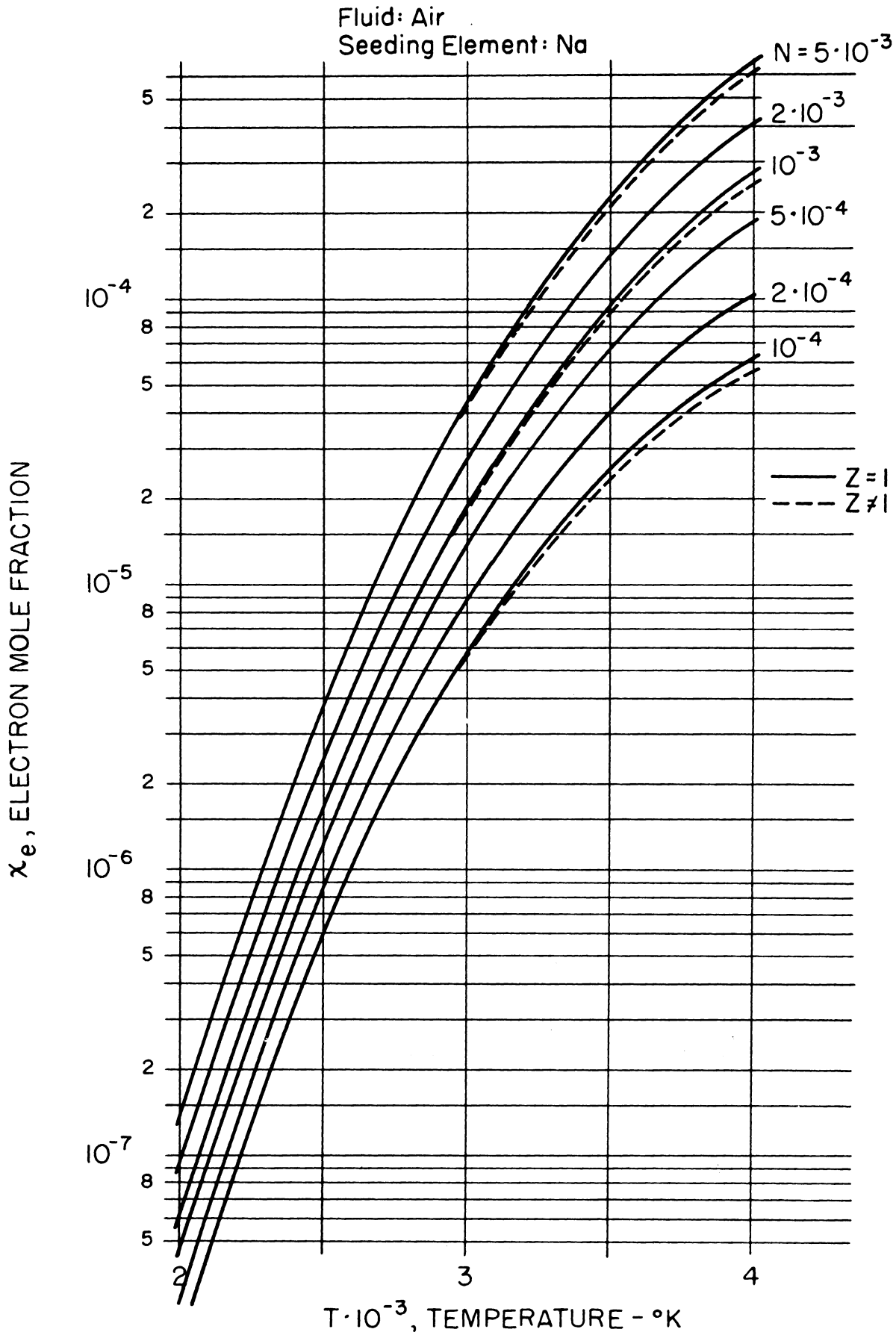

FIGURE 15. ELECTRON MOLE FRACTION vs. TEMPERATURE
(Air and Na)

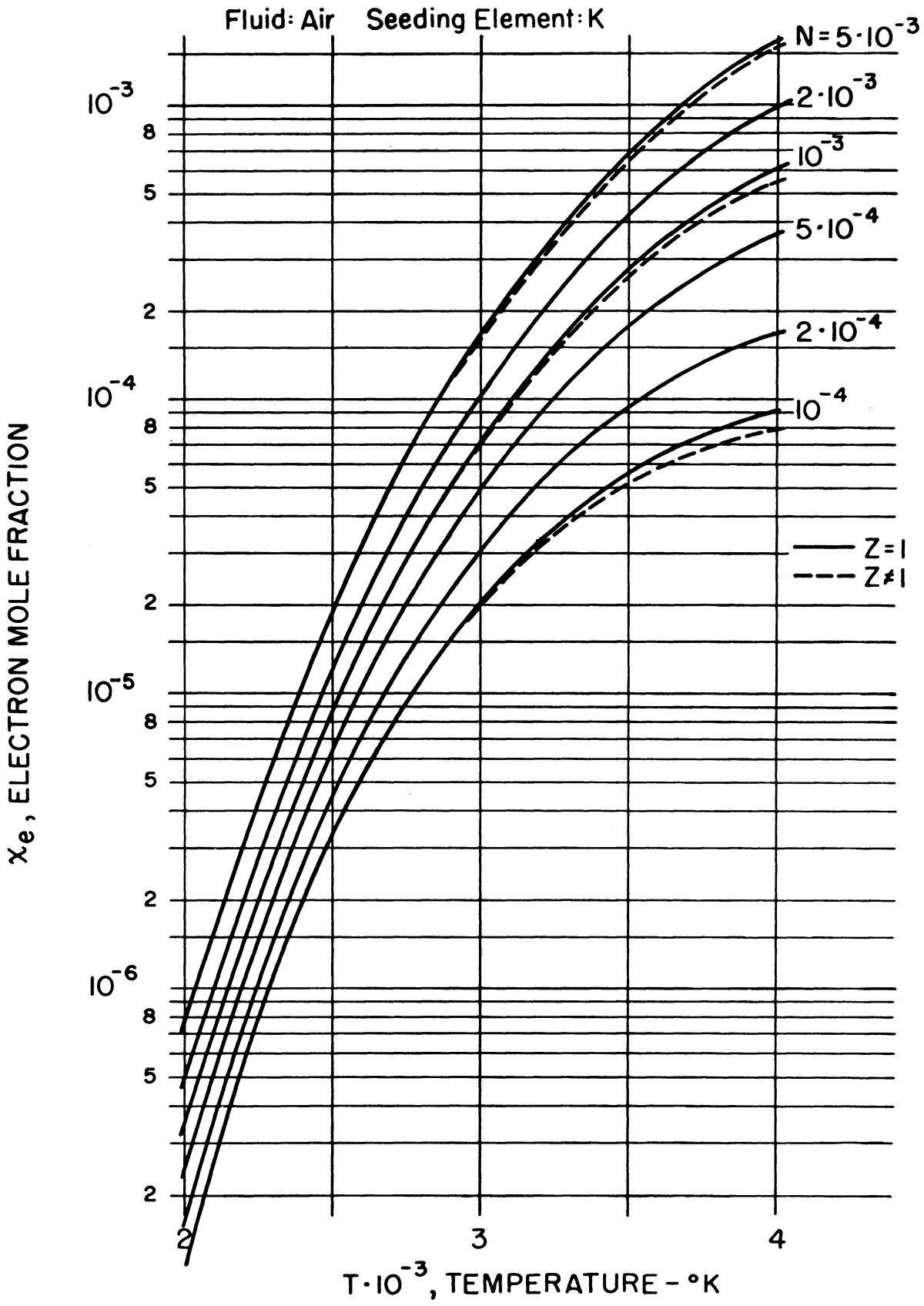

FIGURE 16. ELECTRON MOLE FRACTION vs. TEMPERATURE (Air and K)

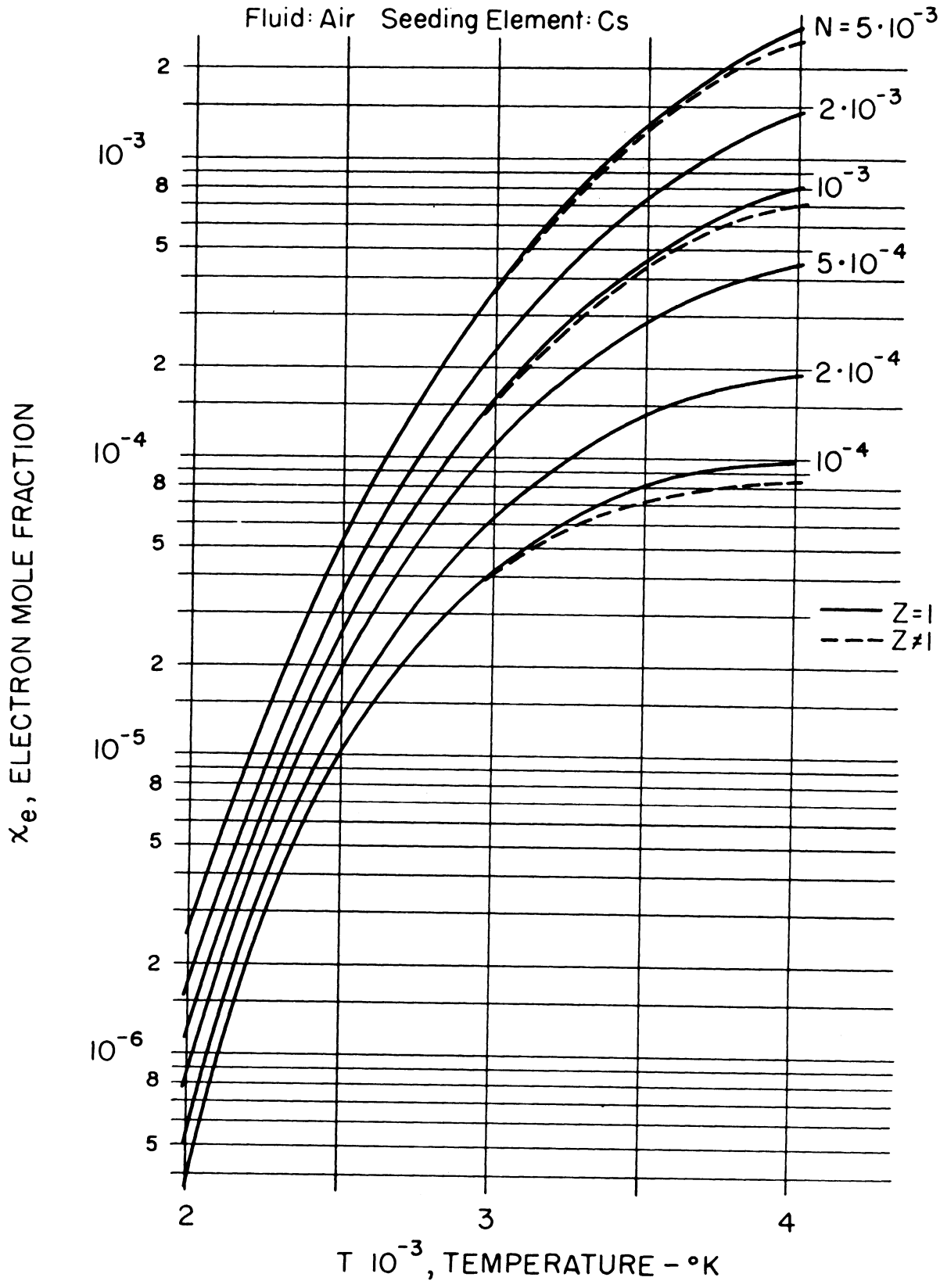

FIGURE 17. ELECTRON MOLE FRACTION vs. TEMPERATURE
(Air and Cs)

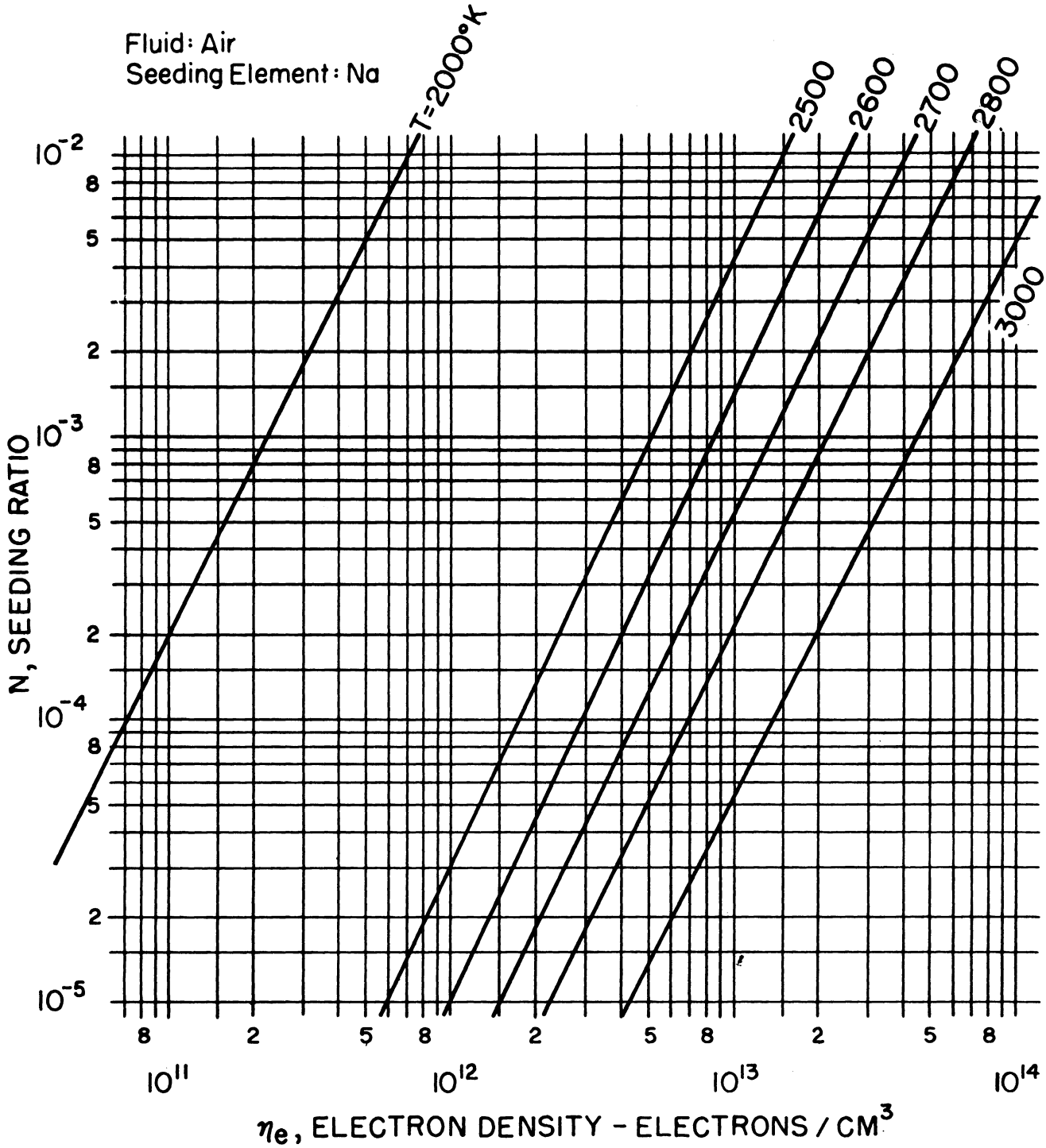

FIGURE 18. SEEDING RATIO vs. ELECTRON DENSITY
(Air and Na)

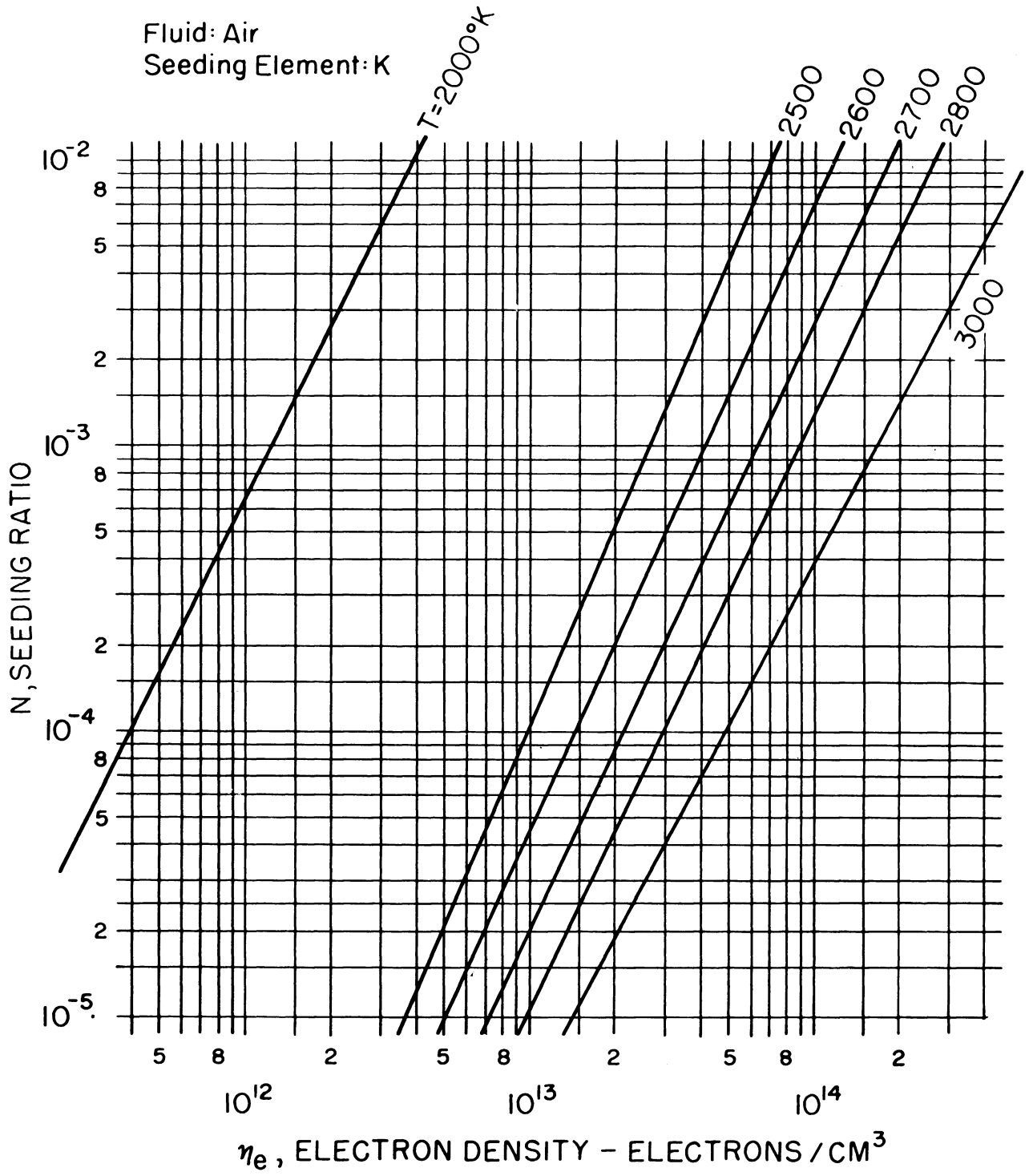

FIGURE 19. SEEDING RATIO vs. ELECTRON DENSITY
(Air and K)

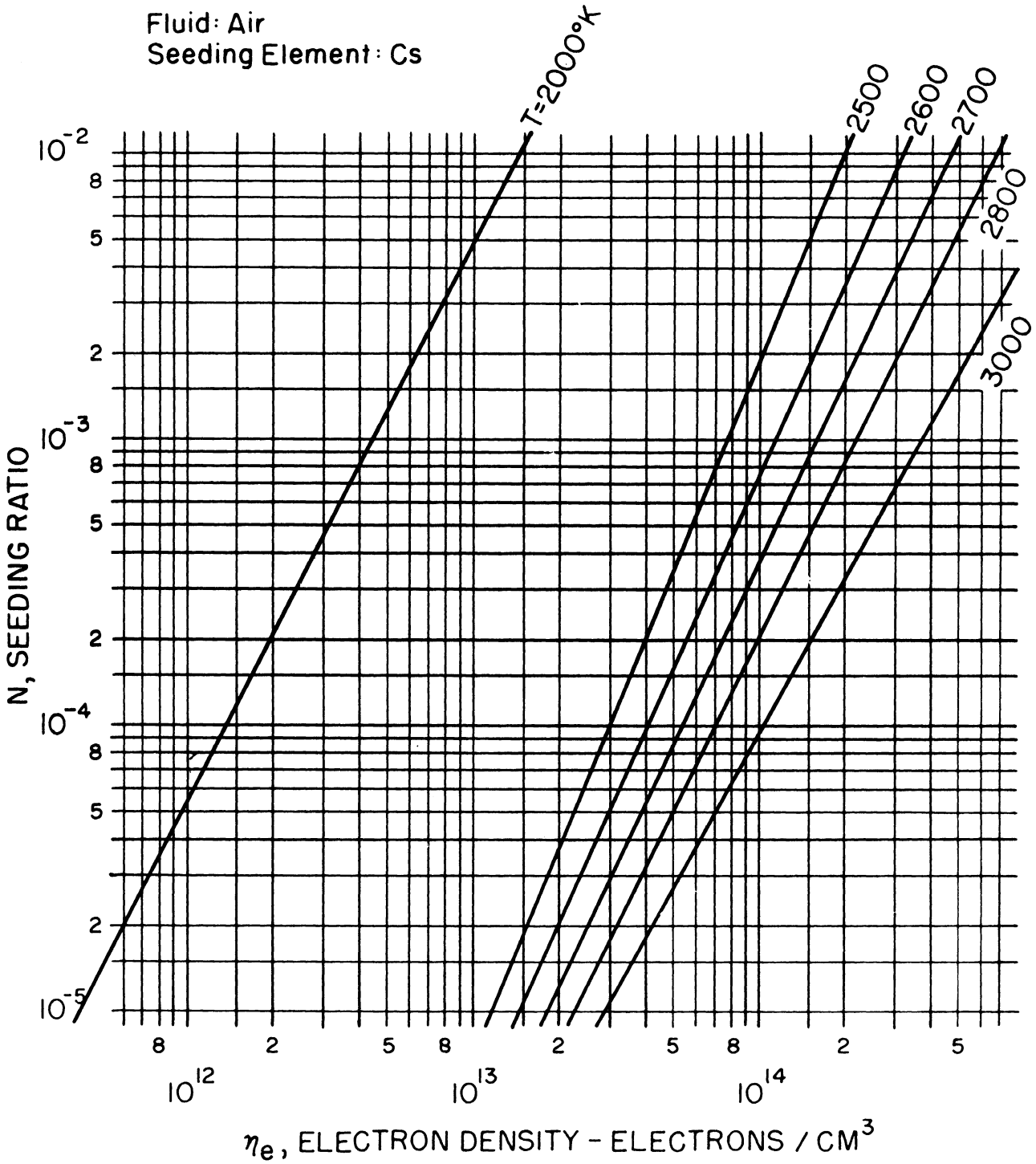

FIGURE 20. SEEDING RATIO vs. ELECTRON DENSITY
(Air and Cs)

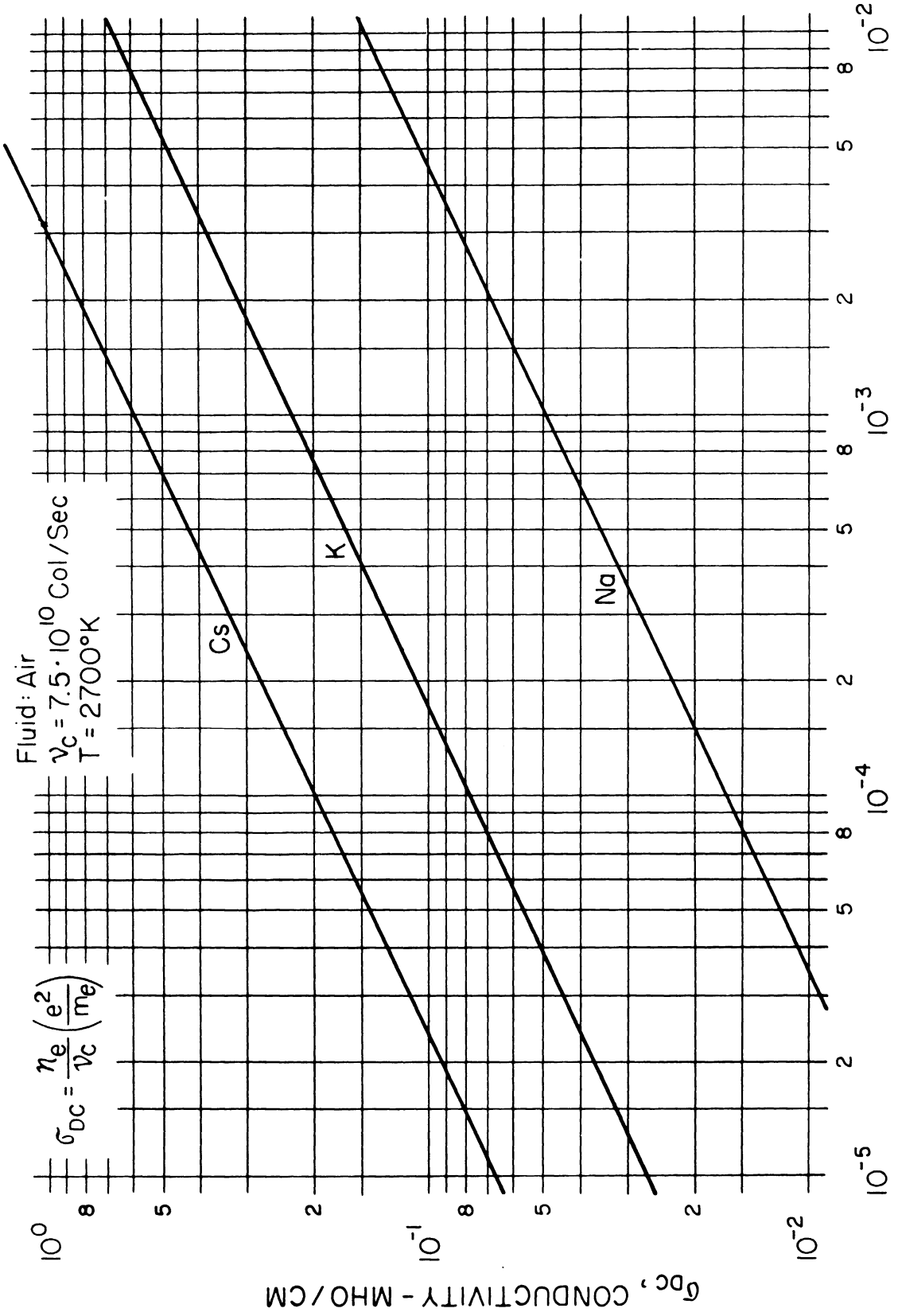

FIGURE 21. DC ELECTRICAL CONDUCTIVITY vs. SEEDING RATIO
(Air and Na, K, or Cs at 2700°K)

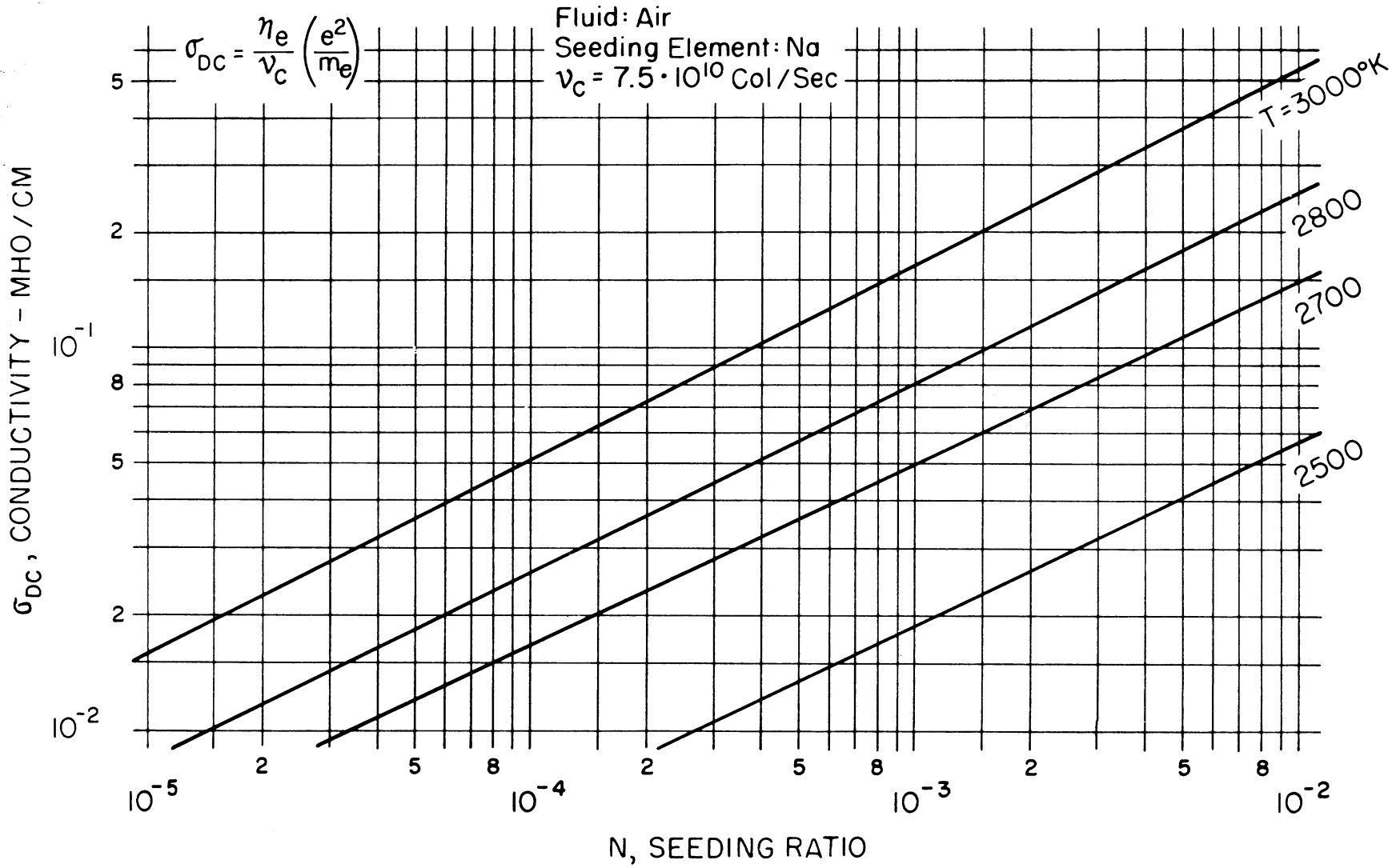

FIGURE 22. DC ELECTRICAL CONDUCTIVITY vs. SEEDING RATIO
(Air and Na)

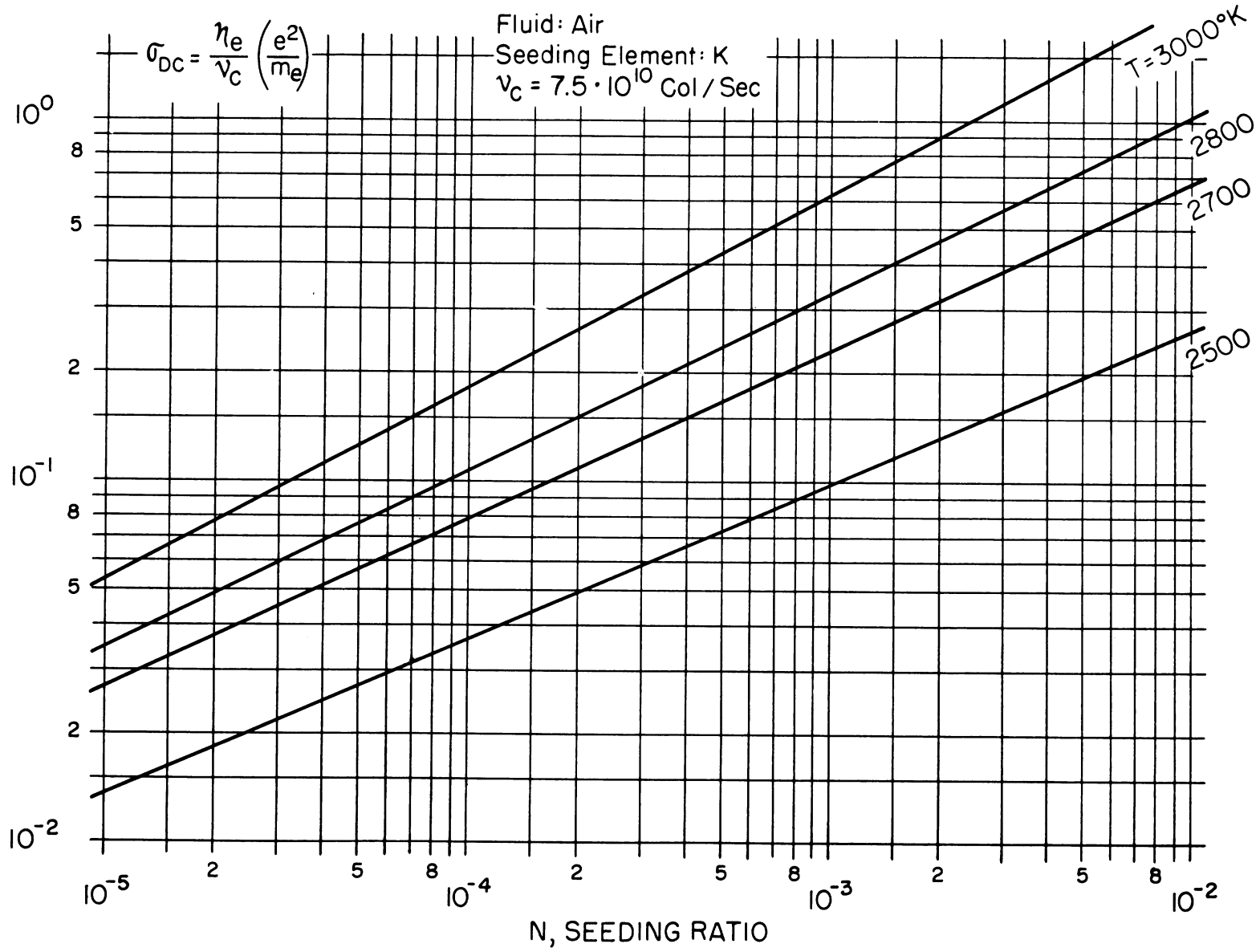

FIGURE 23. DC ELECTRICAL CONDUCTIVITY vs. SEEDING RATIO
(Air and K)

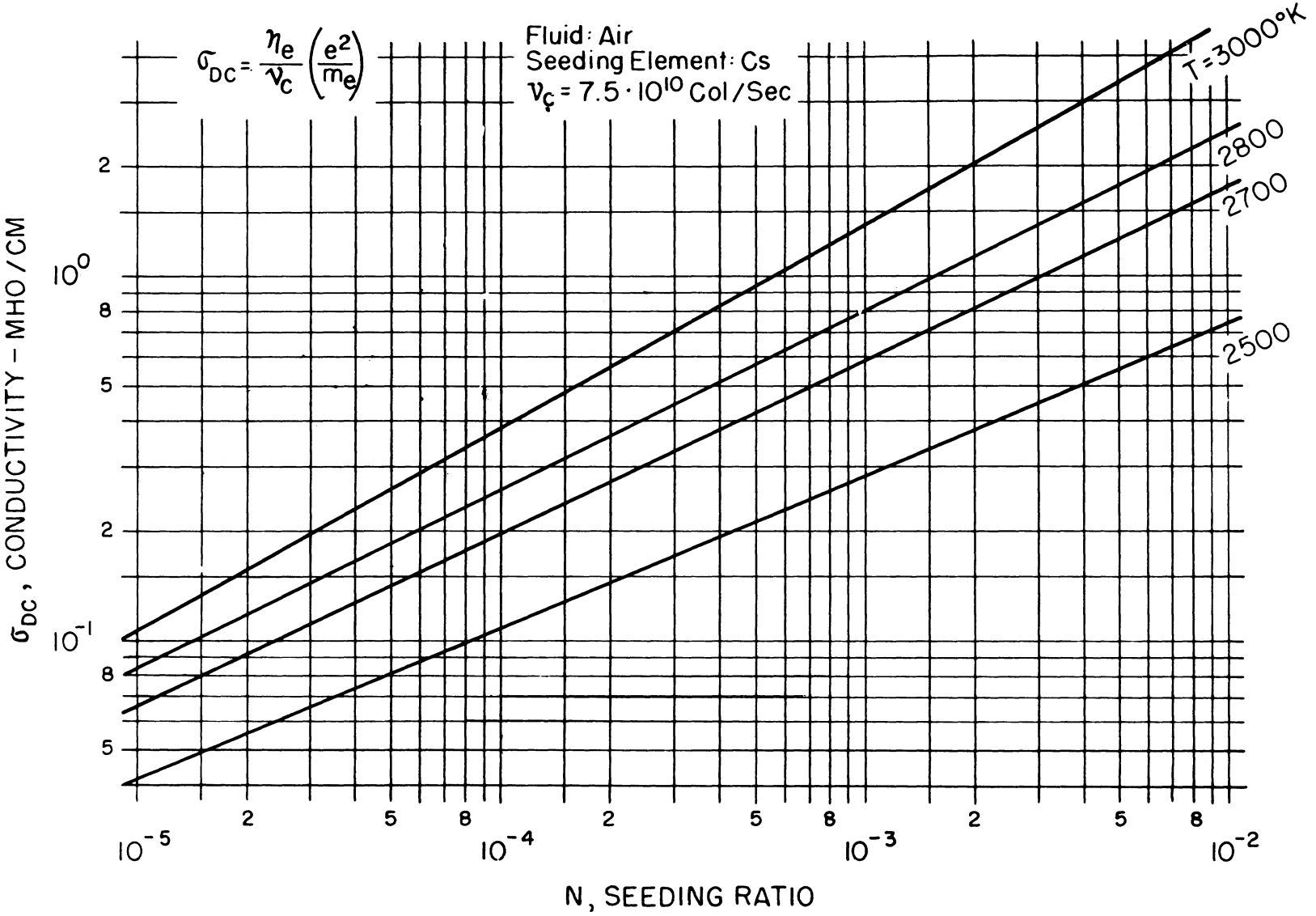

FIGURE 24. DC ELECTRICAL CONDUCTIVITY vs. SEEDING RATIO
(Air and Cs)

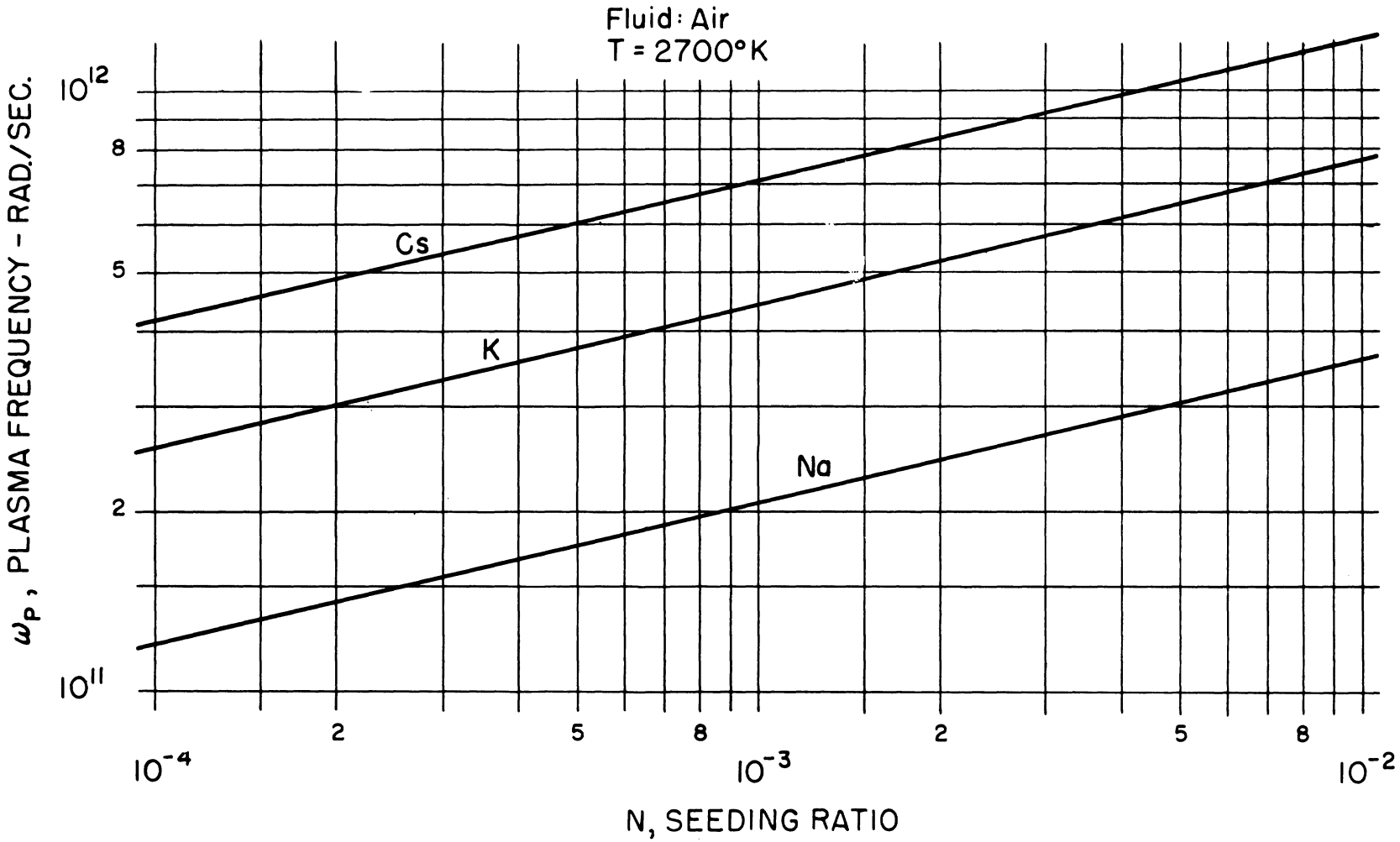

FIGURE 25. PLASMA FREQUENCY vs. SEEDING RATIO
(Air and Na, K, or Cs at 2700°K)

Also as in the case of the seeded nitrogen plasma Figures 21 through 25 present the electrical conductivity and plasma frequency values for seeded air.

The values of the plasma collision frequency, ν, used in this study were selected from the currently available values for the plasma conditions imposed in the analysis.[17] A detailed treatment of collision frequency and collision cross sections is contained in Section IV of this report. For Na seeded N_2, ν is of the order 7.5×10^{10} coll/sec, and for convenience this value was used in the conductivity calculation for both air and N_2 plasmas (as indicated in the figures).

With the determination of the collision frequency of the plasma the important plasma properties are now available, namely: plasma frequency or free electron density, collision frequency, and the electrical conductivity. Figures 1 through 25 then represent these plasma properties as derived for the equilibrium plasma under the imposed temperature-pressure conditions for both nitrogen and air with additives (for one value of the collision frequency). Thus, with the plasma properties and seeding effects which result from the previous analysis, it remains to study the experimental plasma in detail in order to determine the actual test conditions and to determine the plasma properties for comparison and interpretation with these theoretical properties.

III. MICROWAVE SCATTERING FROM A CYLINDRICAL PLASMA

III-A. Assumptions

The simplest theoretical microwave scattering model thought to adequately approximate the experimental conditions makes the following assumptions.

1. The cylindrical plasma is of infinite length, radius R.
2. The plasma properties are uniform within the cylinder, i.e., there are no radial or axial gradients of temperature, density, etc. There is a discontinuity of properties at the plasma surface. The region outside the plasma is assumed to be a vacuum for electromagnetic waves.
3. Inside the plasma, because of the uniform properties, electrical neutrality is maintained.

4. Because of the small mass of the electrons relative to the ions, the only electrically active species of particle is the electron. The ions are considered at rest relative to the electrons.
5. The particles inside the plasma are assumed to be in thermal equilibrium. This implies that the electric fields present are small.
6. A plane polarized electromagnetic wave is normally incident on the plasma with the electric vector parallel to the plasma axis.
7. The plasma is assumed to consist of charges interacting in a vacuum so that $\mu = \mu_o$ and $\epsilon = \epsilon_o$.
8. The time dependence is taken as exp ($i\omega t$) so that steady state solutions are obtained.
9. The polarizability of the plasma is neglected.

Assumptions 1, 2, and 5 will be discussed in the section on errors.

III-B. Scattering of a Plane Wave by a Cylindrical Plasma

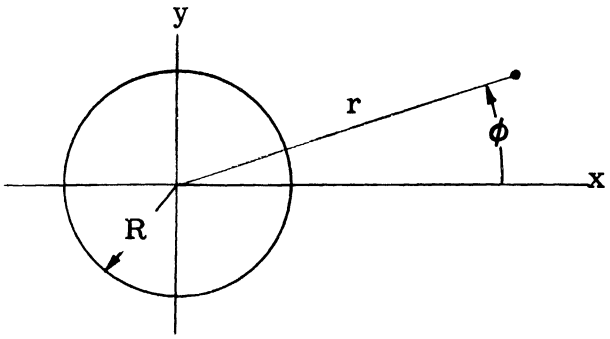

The incident plane polarized wave propagating in the x direction shown on Figure 26 is represented by

$$\bar{E}_p = E_o \exp\left(i\omega t - \frac{i\omega x}{c}\right) \bar{e}_z \qquad (3\text{-}1)$$

where E_o is the peak value of the electric field $\bar{E}_p$, ω is the frequency of the wave, t is the time, x is the coordinate normal to the plane wave, c is the velocity of light, $\bar{e}_z$ is a unit vector in the z direction and $i = \sqrt{-1}$.

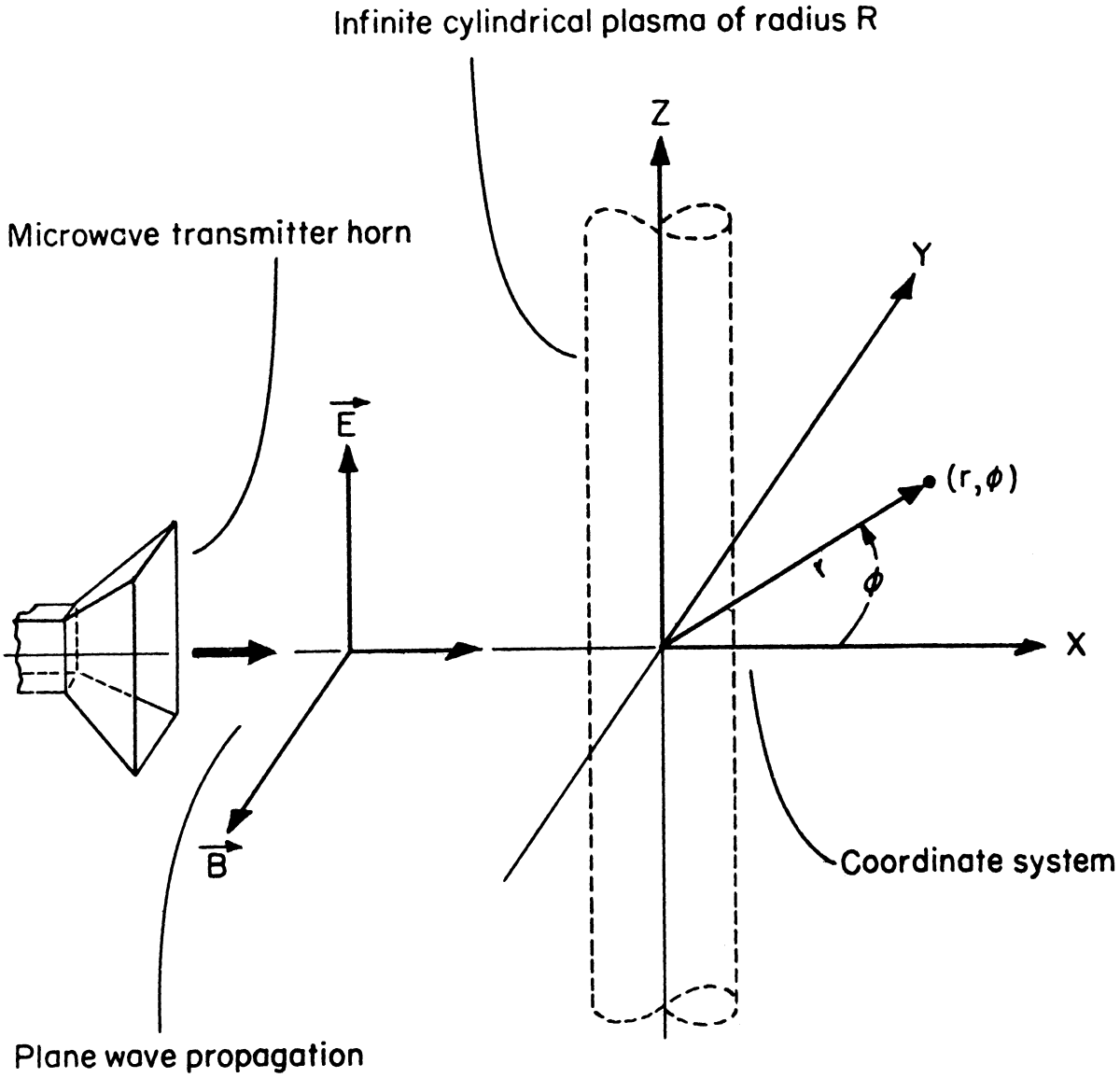

FIGURE 26. COORDINATE SYSTEM AND FIELD ORIENTATION

The Maxwell equations in MKS units are

$$\nabla \times E = - \frac{\partial \overline{B}}{\partial t} \tag{3-2}$$

$$\nabla \times \frac{\overline{B}}{\mu_o} = \overline{j} + \frac{\partial(\epsilon_o \overline{E})}{\partial t} \tag{3-3}$$

$$\nabla \cdot \overline{E} = \rho / \epsilon_o \tag{3-4}$$

$$\nabla \cdot \overline{B} = 0 \tag{3-5}$$

where $\overline{B}$ is the magnetic field, ρ is the net charge density and the current density is given by

$$\overline{j} = \sum_k n_k e_k \overline{v}_k \tag{3-6}$$

$\overline{v}_k$ is the drift velocity of the k^{th} species. The sum is over the various species present in the plasma. By assumption 4

$$\overline{j} = n_e e \overline{v} \tag{3-7}$$

The equation of motion for the electrons is

$$m_e \frac{d\overline{v}}{dt} = e\overline{E} - m_e \nu \overline{v} + e\overline{v} \times \overline{B} \tag{3-8}$$

$\nu = \sum_k \nu_k$ is the total collision frequency. The term $- m_e \nu \overline{v}$ represents the effect of collisions and is discussed in Ratcliff.[38] The sum is over all species with which the electrons interact.

Since $\overline{B}$ fields are not externally applied, the Lorentz force term $e\overline{v} \times \overline{B}$ due to the wave is of order v/c compared to the electric force $e\overline{E}$ and therefore neglected in (3-8).

Assuming that all time varying quantities are proportional to exp ($i\omega t$), the equation of motion (3-8), using linearization and therefore neglecting $(\overline{v} \cdot \nabla)\overline{v}$, gives

$$\overline{v} = \frac{-i\frac{e}{m_e}\overline{E}}{\omega - i\nu} \tag{3-9}$$

so that (3-7) becomes

$$\overline{j} = n_e e\overline{v} = -i\frac{\epsilon_o \omega_p^2}{\omega - i\nu}\overline{E} \tag{3-10}$$

where $\omega_p = \sqrt{\frac{n_e e^2}{m_e \epsilon_o}}$ = plasma frequency.

The Maxwell equations (3-2) and (3-3) become, inserting (3-10), noting $c^2 = \frac{1}{\mu_o \epsilon_o}$ and assumption 8,

$$\nabla \times \overline{E} = -i\omega\overline{B} \tag{3-11}$$

$$\nabla \times \overline{B} = -\frac{i}{c^2}\frac{\omega_p^2 \overline{E}}{\omega - i\nu} + \frac{i\omega\overline{E}}{c^2}$$

$$= \frac{ik^2}{\omega}\overline{E} \tag{3-12}$$

where

$$k = \frac{\omega}{c}\sqrt{1 - \frac{\omega_p^2}{\omega^2 + \nu^2} - i\frac{\nu}{\omega}\frac{\omega_p^2}{\omega^2 + \nu^2}}$$

$$= \frac{\omega}{c}\sqrt{\frac{1 - \frac{\omega_p^2}{\omega^2 + \nu^2} + \sqrt{\left(1 - \frac{\omega_p^2}{\omega^2 + \nu^2}\right)^2 + \left(\frac{\nu}{\omega}\frac{\omega_p^2}{\omega^2 + \nu^2}\right)^2}}{2}}$$

$$- i\frac{\omega}{c}\sqrt{\frac{-\left(1 - \frac{\omega_p^2}{\omega^2 + \nu^2}\right) + \sqrt{\left(1 - \frac{\omega_p^2}{\omega^2 + \nu^2}\right)^2 + \left(\frac{\nu}{\omega}\frac{\omega_p^2}{\omega^2 + \nu^2}\right)^2}}{2}} \qquad (3\text{-}13)$$

k is the complex propagation constant in the plasma and lies in the 4th quadrant. Alternatively, the complex dielectric constant of the plasma is the quantity inside the first square root.

Taking the curl of (3-11) and substituting (3-12) gives

$$\nabla \times (\nabla \times \overline{E}) = k^2 \overline{E} \qquad (3\text{-}14)$$

The plasma is seen to remain neutral by taking the divergence of (3-12). $\nabla \cdot (\nabla \times \overline{B}) \equiv 0 = \nabla \cdot \left(\frac{ik^2}{\omega}\overline{E}\right)$ so that wherever k is independent of position $\nabla \cdot \overline{E} = 0 = \rho/\epsilon_o$. Therefore

$$\rho = 0 \qquad (3\text{-}15)$$

Since $\overline{E}$ (0, 0, E_z) has a z component only and E_z is a cartesian component in cylindrical coordinates, $\nabla \times (\nabla \times E) = \nabla(\nabla \cdot \overline{E}) - \nabla^2 \overline{E}$. Therefore, noting (3-15), the vector Equation (3-14) becomes a scalar equation

$$\nabla^2 E_z + k^2 E_z = 0 \tag{3-16}$$

Solving (3-16) by separation of variables, let $E_z = R(r)\psi(\phi)$. There is no z dependence since E_z is assumed independent of z. Equation (3-16) becomes

$$\frac{1}{R} r \frac{d}{dr}\left(r \frac{dR}{dr}\right) + k^2 r^2 = -\frac{1}{\psi} \frac{d^2\psi}{d\phi^2} = m^2 \tag{3-17}$$

where, since each side is a function only of its own independent variable r or ϕ, it has been set equal to a constant m^2. Thus

$$\frac{d^2\psi}{d\phi^2} = -m^2\psi \tag{3-18a}$$

$$\frac{1}{r}\frac{d}{dr}\left(r \frac{dR}{dr}\right) + \left(k^2 - \frac{m^2}{r^2}\right) R = 0 \tag{3-18b}$$

The solution to (3-18a) is $\psi = A_{1m} \cos m\phi + A_{2m} \sin m\phi$ where A_{1m}, A_{2m}, etc., are arbitrary constants. Since $\psi(\phi)$ is an even function of ϕ, $\psi(-\phi) = \psi(\phi)$, therefore $A_{2m} = 0$, and $\psi = \cos(m\phi)$, $m = 0, 1, 2, 3 \ldots$ neglecting arbitrary constants. So that ψ will be single valued, m is integral.

Equation (3-18b) is Bessels equation, which has solutions that are linear combinations of $J_m(kr)$ and $Y_m(kr)$. Therefore $R = A_{3m} J_m(kr) + A_{4m} Y_m(kr)$. Since Y_m has a log singularity at the origin, the coefficient of Y_m is set equal to zero inside the plasma. Thus, neglecting the arbitrary constant, $R(r) = J_m(kr)$, $r < R$.

Outside the plasma the combination of J_m and Y_m that varies as $\frac{\exp(\pm ir)}{\sqrt{r}}$ for large r is chosen. These combinations are $H_m^{(1)}(kr) = J_m(kr) + i\,Y_m(kr)$ for $\frac{\exp(+ir)}{\sqrt{r}}$, known as the Hankel function of the 1st kind and similarly $H_m^{(2)}(kr) = J_m(kr) - i\,Y_m(kr)$ for $\frac{\exp(-ir)}{\sqrt{r}}$, the Hankel function of the 2nd kind. Thus $R(r) = A_{5m}H_m^{(1)}(kr) + A_{6m}H_m^{(2)}(kr)$, $r > R$. Since the time variation has been taken as $\exp(+i\omega t)$, $\frac{\exp(+ir)}{\sqrt{r}}$, i. e, $H_m^{(1)}$, represents an incoming wave, and $\frac{\exp(-ir)}{\sqrt{r}}$, i. e., $H_m^{(2)}$, represents an outgoing wave. Because there is only an outgoing scattering wave, the coefficient of $H_m^{(1)}$ is set equal to zero. The solution outside the plasma is, neglecting the arbitrary constant;

$$R(r) = H_m^{(2)}(kr), \qquad r > R$$

The most general solution of (3-16) is the superposition of all the m solutions. Reinserting the arbitrary constants, which are used to satisfy the boundary conditions,

$$E_{z\,in} = \sum_{m=0}^{\infty} D_m J_m(kr)\cos(m\phi)\exp(i\omega t), \qquad r < R \tag{3-19}$$

$$E_{z\,scat} = \sum_{m=0}^{\infty} C_m H_m^{(2)}\left(\frac{\omega r}{c}\right)\cos m\phi \exp(i\omega t), \qquad r > R \tag{3-20}$$

since, for $r > R$, $\omega_p = 0$ and $k = \frac{\omega}{c}$.

Now $x = r\cos\phi$, so the incident plane wave given by (3-1) is

$$E_{zp} = E_o \exp\left(-i\frac{\omega r}{c}\cos\phi\right)\exp(i\omega t) \tag{3-21}$$

Note that $e^{i\alpha\cos\phi} = \sum_{m=-\infty}^{\infty} i^m \exp(im\phi) J_m(\alpha) = J_o(\alpha) + \sum_{m=1}^{\infty} i^m \exp(im\phi) J_m(\alpha)$

$+ \sum_{m=-\infty}^{-1} i^m \exp(im\phi) J_m(\alpha)$ and using $J_{-m}(\alpha) = (-)^m J_m(\alpha)$ for integral m,

$(-)^m = i^{2m}$, $2\cos m\phi = \exp(im\phi) + \exp(-im\phi)$ so consequently one sees that

$\exp(i\alpha\cos\phi) = J_o(\alpha) + 2\sum_{m=1}^{\infty} i^m J_m(\alpha)\cos m\phi$. The plane wave (3-21) can be represented as

$$E_{zp} = E_o J_o\left(\frac{\omega r}{c}\right) + 2\sum_{m=1}^{\infty} (-i)^m J_m\left(\frac{\omega r}{c}\right)\cos m\phi \exp(i\omega t) \tag{3-22}$$

The total electric field outside is given by the sum of (3-20) and (3-22)

$$E_{z\,tot} = E_{z\,scat} + E_{zp} = \left[\sum_{m=0}^{\infty} C_m H_m^{(2)}\left(\frac{\omega r}{c}\right)\cos m\phi + E_o\left(J_o\left(\frac{\omega r}{c}\right) + 2\sum_{m=1}^{\infty}(-i)^m \cos m\phi\, J_m\left(\frac{\omega r}{c}\right)\right)\right]\exp(i\omega t) \tag{3-23}$$

To match the inside and outside solutions (3-19), (3-23), the tangential components of $\overline{E}$ and $\frac{\overline{B}}{\mu_o}$, E_z and B_ϕ, are made continuous at r = R.

For continuity of E_z, equate (3-23) and (3-19) at r = R.

$$\sum_{m=0}^{\infty} D_m J_m(kR)\cos m\phi = \sum_{m=0}^{\infty} C_m H_m^{(2)}\left(\frac{\omega R}{c}\right)\cos m\phi + E_o\left\{J_o\left(\frac{\omega R}{c}\right) + 2\sum_{m=1}^{\infty}(-i)^m \cos m\phi\, J_m\left(\frac{\omega R}{c}\right)\right\} \tag{3-24}$$

Now $B = \frac{i}{\omega} \nabla \times \overline{E}$ from (3-11) so

$$B_\phi = \frac{i}{\omega}\left(\cancel{\frac{\partial E_r}{\partial z}}^{0} - \frac{\partial E_z}{\partial r}\right) = -\frac{ik}{\omega}\frac{\partial E_z}{\partial (kr)} \tag{3-25}$$

Using (3-19) and (3-23), noting $k = \frac{\omega}{c}$ outside, continuity of B_ϕ at $r = R$ gives

$$\begin{aligned}\frac{kc}{\omega}\sum_{m=0}^{\infty} D_m J'_m(kR)\cos m\phi = \sum_{m=0}^{\infty} C_m H'^{(2)}_m\left(\frac{\omega R}{c}\right)\cos m\phi \\ + E_o\left(J'_o\left(\frac{\omega R}{c}\right) + 2\sum_{m=1}^{\infty}(-i)^m J'_m\left(\frac{\omega R}{c}\right)\cos m\phi\right)\end{aligned} \tag{3-26}$$

where the prime indicates differentiation with respect to the argument given. We equate terms for each value of m.

For $m = 0$

$$\begin{aligned}D_o J_o(kR) &= C_o H_o^{(2)}\left(\frac{\omega R}{c}\right) + E_o J_o\left(\frac{\omega R}{c}\right) \\ \frac{ck}{\omega} D_o J'_o(kR) &= C_o H'^{(2)}_o\left(\frac{\omega R}{c}\right) + E_o J'_o\left(\frac{\omega R}{c}\right)\end{aligned} \tag{3-27}$$

Divide the first equation by the second equation. Note $Z'_m = \frac{Z_{m-1} - Z_{m+1}}{2}$

and $Z_{m-1} + Z_{m+1} = \frac{2m}{z} Z_m(z)$ so $Z'_m = Z_{m-1} - \frac{m}{z} Z_m$, where $Z_m = J_m$, or H_m. Solving for C_o/E_o yields

$$\frac{C_o}{E_o} = \frac{\left[\frac{kc}{\omega}\frac{J_1(kR)}{J_o(kR)}\right] J_o\left(\frac{\omega R}{c}\right) - J_1\left(\frac{\omega R}{c}\right)}{H_1^{(2)}\left(\frac{\omega R}{c}\right) - H_o^{(2)}\left(\frac{\omega R}{c}\right)\left[\frac{kc}{\omega}\frac{J_1(kR)}{J_o(kR)}\right]} \tag{3-28}$$

Similarly for $m = 1, 2, \ldots$

$$\frac{C_m}{E_o} = -2(-i)^m \left[\frac{J_{m-1}\left(\frac{\omega R}{c}\right) - J_m\left(\frac{\omega R}{c}\right)\left[\frac{kc}{\omega}\frac{J_{m-1}(kR)}{J_m(kR)}\right]}{H_{m-1}^{(2)}\left(\frac{\omega R}{c}\right) - H_m^{(2)}\left(\frac{\omega R}{c}\right)\left[\frac{kc}{\omega}\frac{J_{m-1}(kR)}{J_m(kR)}\right]}\right] \tag{3-29}$$

Dividing Equation (3-23) through by E_o, the total wave due to the incident plane wave plus the scattered cylindrical wave, dropping the understood sub z and time dependence exp (iωt), is

$$\frac{E_{tot}}{E_o} = \frac{E_{scat}}{E_o} + \exp\left(-i\frac{\omega x}{c}\right) = \frac{E_{scat}}{E_o} + \cos\left(\frac{\omega x}{c}\right) - i\sin\left(\frac{\omega x}{c}\right) \tag{3-30}$$

where

$$\frac{E_{scat}}{E_o} = \sum_{m=0}^{\infty} \frac{C_m}{E_o} H_m^{(2)}\left(\frac{\omega r}{c}\right)\cos m\phi \tag{3-31}$$

with the C_m/E_o given by (3-28), and (3-29).

E_{scat}/E_o is a complex number with phase angle generally not equal to that of the plane wave, $-\frac{\omega x}{c}$.

III-C. Numerical Results of the Theoretical Model

Equations (3-30) and (3-31) were programmed on an IBM 7090. Arbitrary values of ω_p, ν, R, D and ϕ were assumed and the resulting phase and amplitude of the scattered wave given by Equation (3-31) determined. The scattered wave combines with the plane wave given by Equation (3-1) to give the total wave. The results are shown on Figures 27 through 32.

The notation is shown in the following sketch.

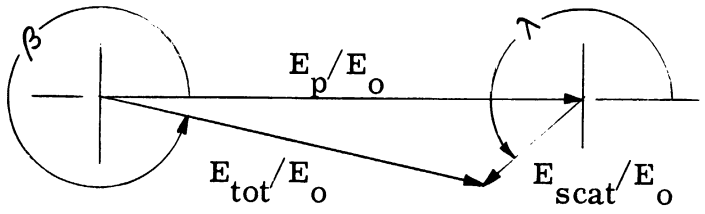

λ is the phase of E_{scat} with respect to the plane wave E_p, β is the phase of E_{tot} with respect to E_p. Note that the incident plane wave E_p/E_o has unit amplitude. λ and β are measured in radians. E_{scat}/E_o is the absolute value of Equation (3-31) and λ is the phase of Equation (3-31) relative to the phase of the plane wave of Equation (3-1). R is the radius of the plasma, D is the distance of the point of observation from the center of the plasma, and ϕ is the angle that the point of observation makes with the x axis, i. e., the angle measured from the forward direction. $\omega = 2\pi \times 10^{10}$ for all calculations.

The following observations are made for R = .2 to .8 cm, $\omega_p = 10^{10}$ to 10^{12}, $\nu = 10^{10}$ to 10^{12}, $\omega = 2\pi \times 10^{10}$ and $\phi = 0$.

1. The shape of the λ vs. ω_p curves appears to depend mainly on ν.
2. The right hand asymptote of λ vs. ω_p depends mainly on R.
3. The left hand asymptote of λ vs. ω_p depends mainly on ν.
4. Increasing ν reduces E_{scat}/E_o at low ω_p.
5. Increasing radius increases E_{scat}/E_o relatively independent of ω_p.
6. E_{scat}/E_o more strongly depends on ω_p than on ν.

Although curves are not presented here for ϕ other than zero, E_{tot}/E_o can be greater than 1 for $\phi > 0$.

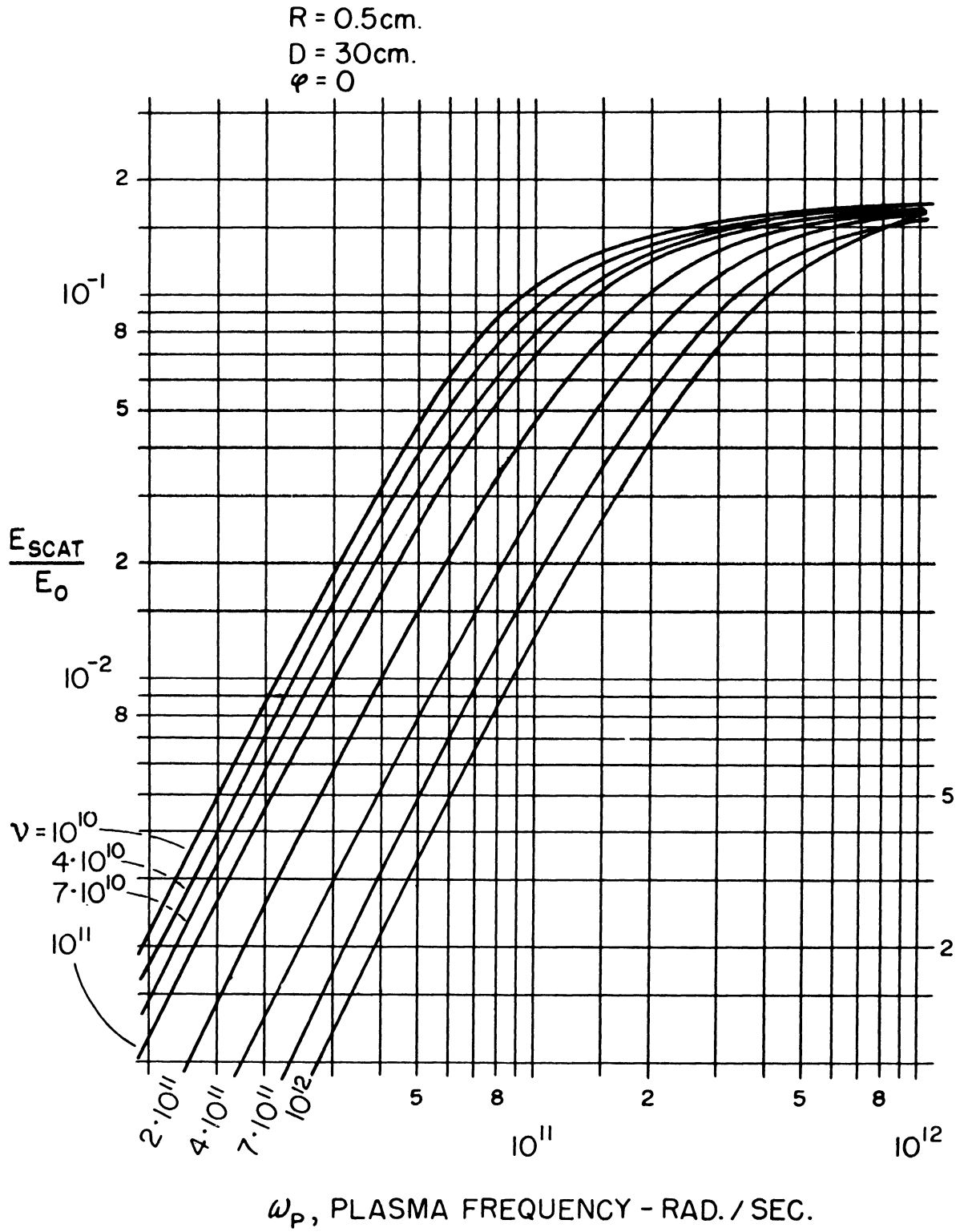

FIGURE 27. AMPLITUDE OF SCATTERED WAVE vs. PLASMA FREQUENCY

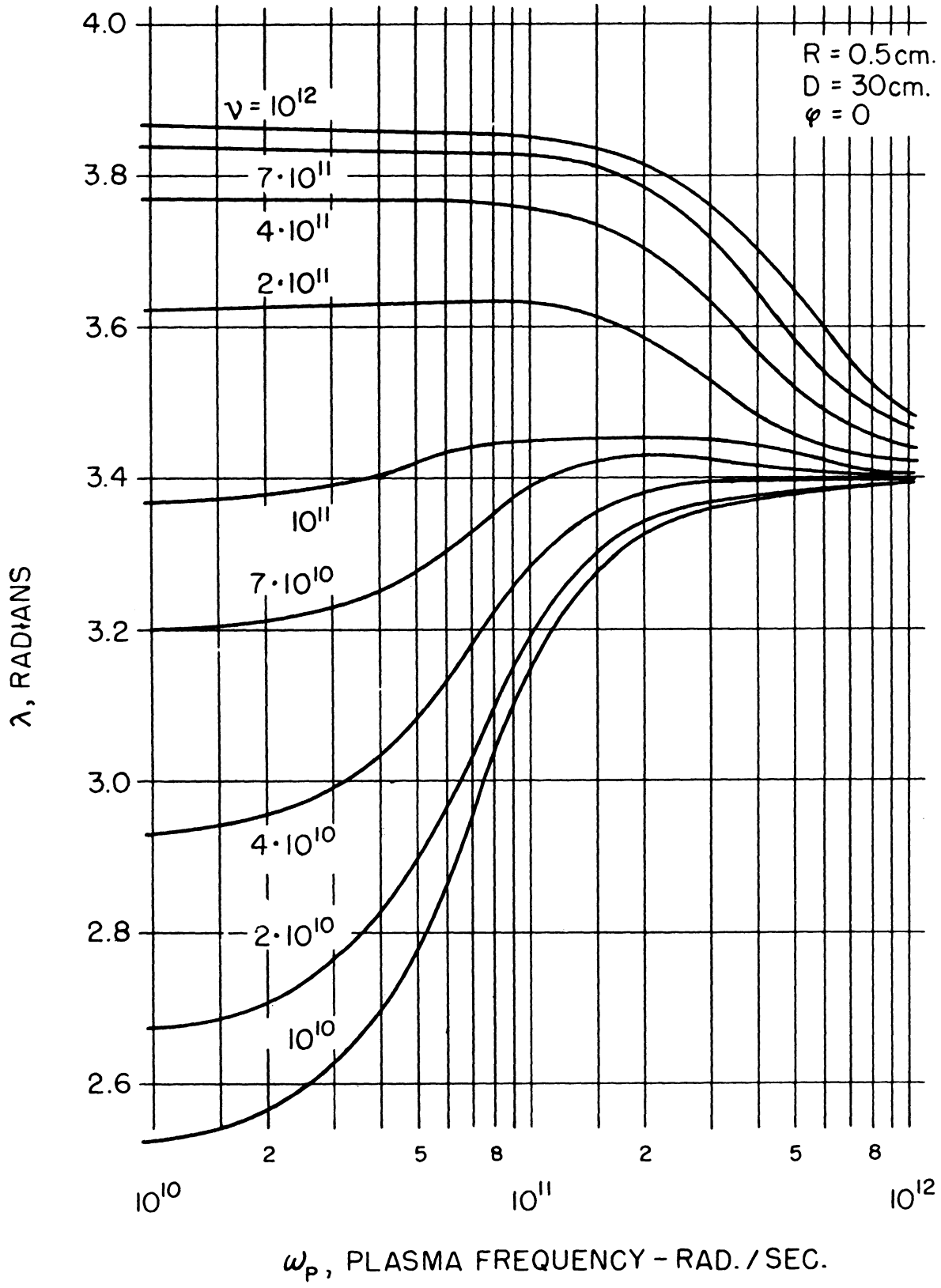

FIGURE 28. PHASE OF SCATTERED WAVE vs. PLASMA FREQUENCY

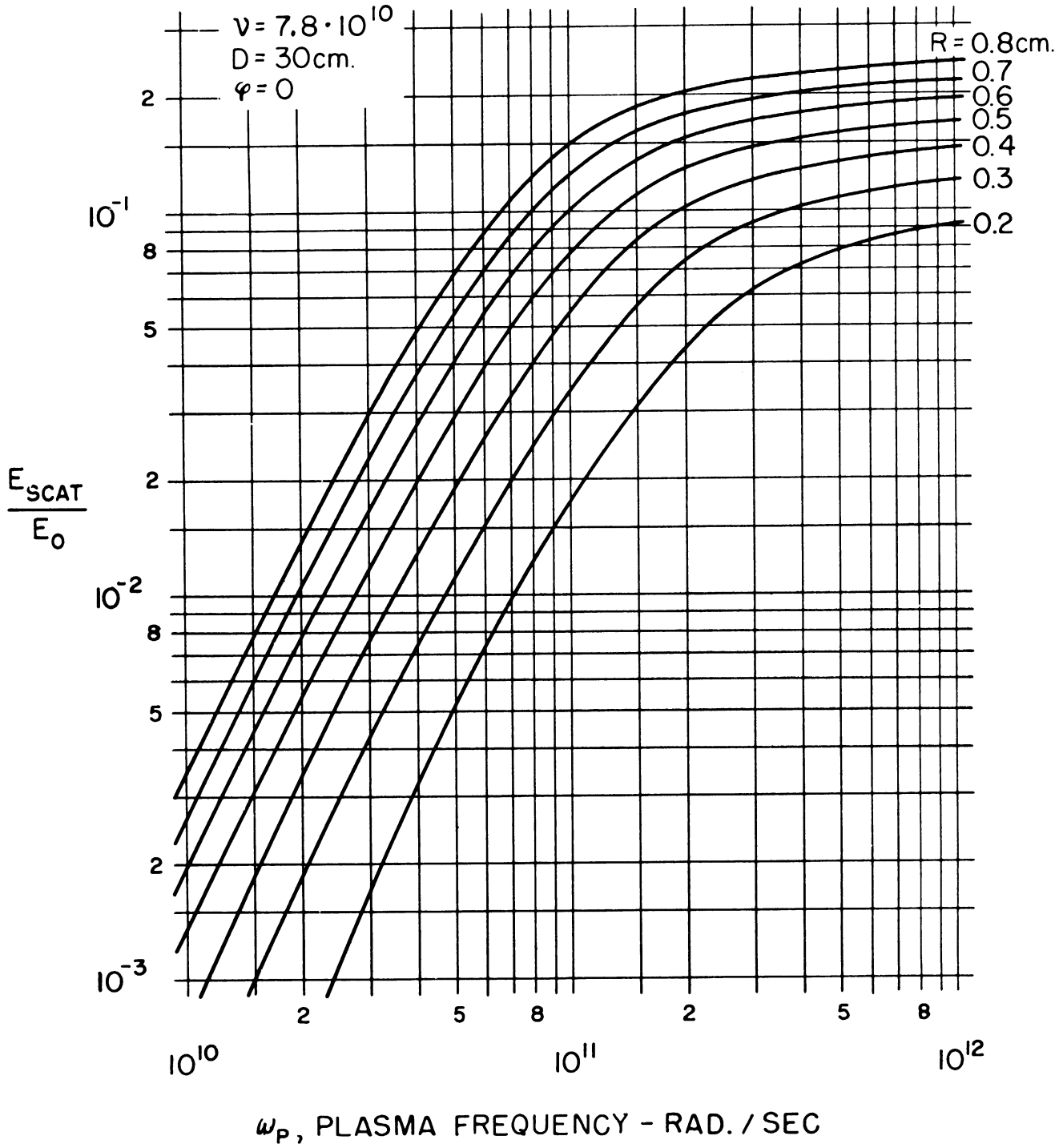

FIGURE 29. AMPLITUDE OF SCATTERED WAVE vs. PLASMA FREQUENCY

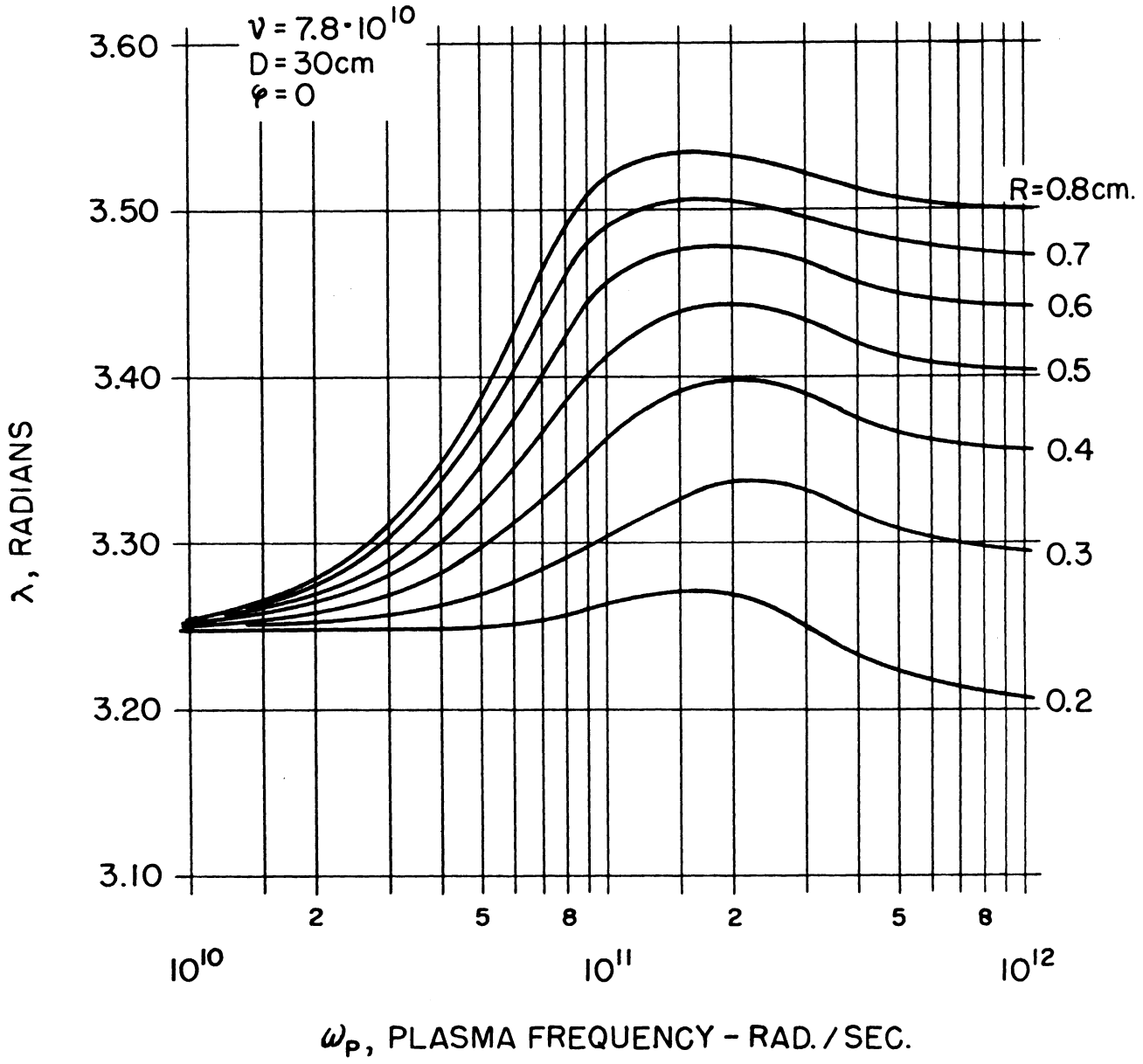

FIGURE 30. PHASE OF SCATTERED WAVE vs. PLASMA FREQUENCY

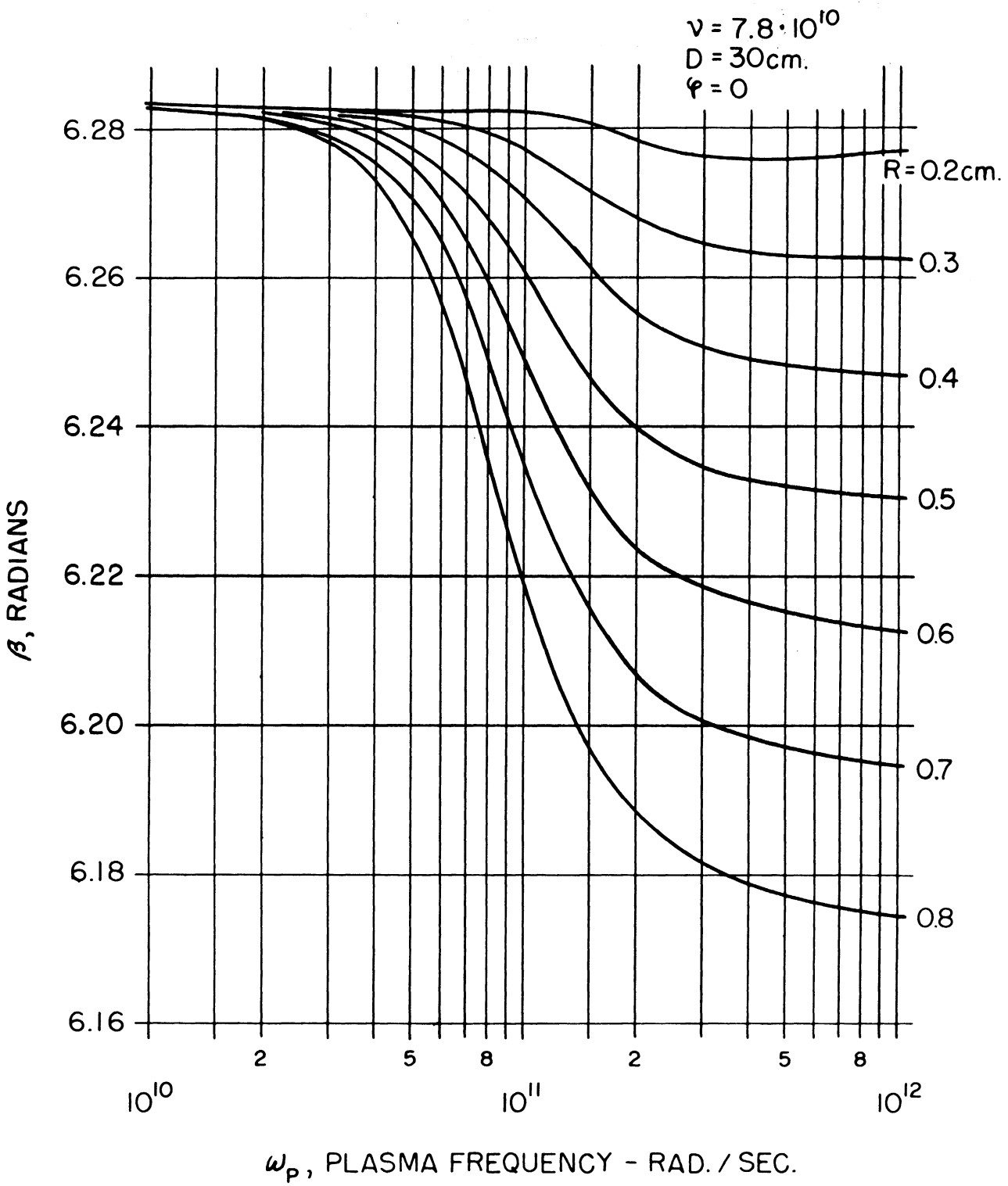

FIGURE 31. PHASE OF TOTAL WAVE vs. PLASMA FREQUENCY

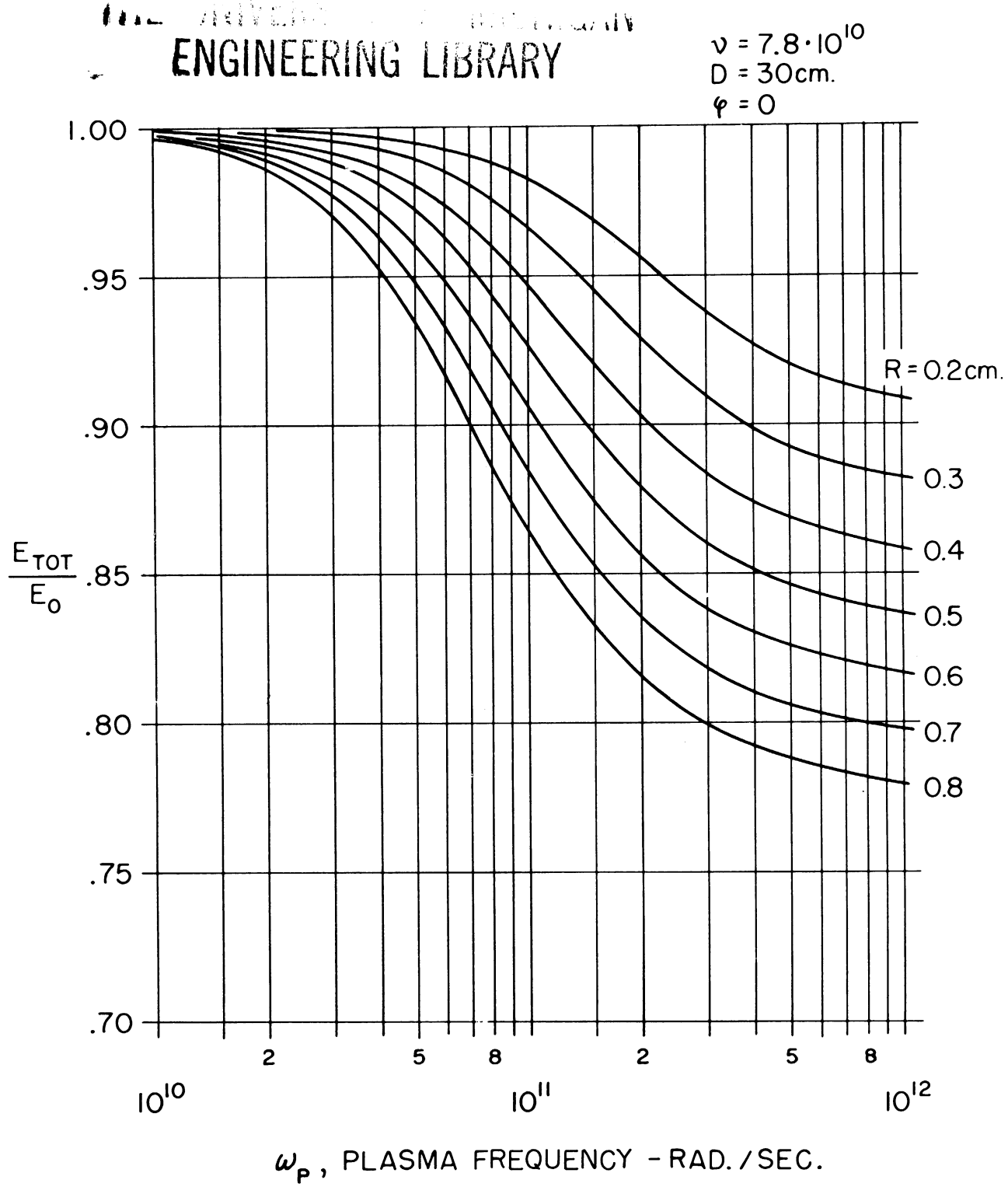

FIGURE 32. AMPLITUDE OF TOTAL WAVE vs. PLASMA FREQUENCY

IV. PLASMA PROPERTIES—PREDICTED

IV-A. Relation Between Plasma Properties and Complex Conductivity

It is useful to relate the plasma frequency ω_p and collision frequency ν in a plasma to the complex conductivity σ in such a medium.

Assume that ohms law

$$\overline{j} = \sigma \overline{E} \tag{4-1}$$

holds inside the medium, with $\mu = \mu_o$ and $\epsilon = \epsilon_o$ everywhere. For fields varying as exp ($i\omega t$), Maxwells Equation (3-3) becomes, using Equation (4-1) and noting $c^2 = \frac{1}{\mu_o \epsilon_o}$

$$\nabla \times \overline{B} = \frac{ik^2}{\omega} \overline{E} \tag{4-2}$$

where

$$k = \frac{\omega}{c} \sqrt{1 - \frac{i\sigma}{\omega \epsilon_o}} \tag{4-3}$$

Separating k into real and imaginary parts,

$$k = \frac{\omega}{c} \sqrt{\frac{1}{2} + \frac{1}{2} \sqrt{1 + \left(\frac{\sigma}{\epsilon_o \omega}\right)^2}} - i \frac{\omega}{c} \sqrt{-\frac{1}{2} + \frac{1}{2} \sqrt{1 + \left(\frac{\sigma}{\epsilon_o \omega}\right)^2}} \tag{4-4}$$

The propagation constant k lies in the 4th quadrant.

If we insert

$$\sigma = \sigma_r + i\sigma_i \tag{4-5}$$

into Equation (4-4) and equate the real and imaginary parts of (4-4) to the real and imaginary parts of k in a plasma given by Equation (3-13), we find that

$$\left.\begin{aligned} \sigma_r &= \frac{\omega_p^2 \nu \epsilon_o}{\omega^2 + \nu^2} \\ \sigma_i &= -\frac{\omega_p^2 \omega \epsilon_o}{\omega^2 + \nu^2} \end{aligned}\right\} \tag{4-6}$$

or

$$\left.\begin{aligned} \nu &= \frac{\omega \sigma_r}{\sigma_i} \\ \omega_p^2 &= -\frac{\omega \sigma_i}{\epsilon_o}\left[1 + \left(\frac{\sigma_r}{\sigma_i}\right)^2\right] \end{aligned}\right\} \tag{4-7}$$

Equations (4-6) and (4-7) relate the plasma frequency and collision frequency to real and imaginary parts of the conductivity.

The DC value of the conductivity is obtained by setting $\omega = 0$ in Equation (4-6)

$$\sigma_{DC} = \frac{\omega_p^2 \epsilon_o}{\nu} = \frac{n_e e^2}{m\nu}$$

IV-B. Predicted Plasma Frequency vs. Seeding Ratio for Seeded Nitrogen

Using Figures 5, 6, and 7 in Section II and $\omega_p = \sqrt{\frac{n_e e^2}{m\epsilon_o}}$

we obtain the plasma frequency ω_p vs. seeding ratio N for a nitrogen seeded stream at 2754°K. The results are shown in Figure 33.

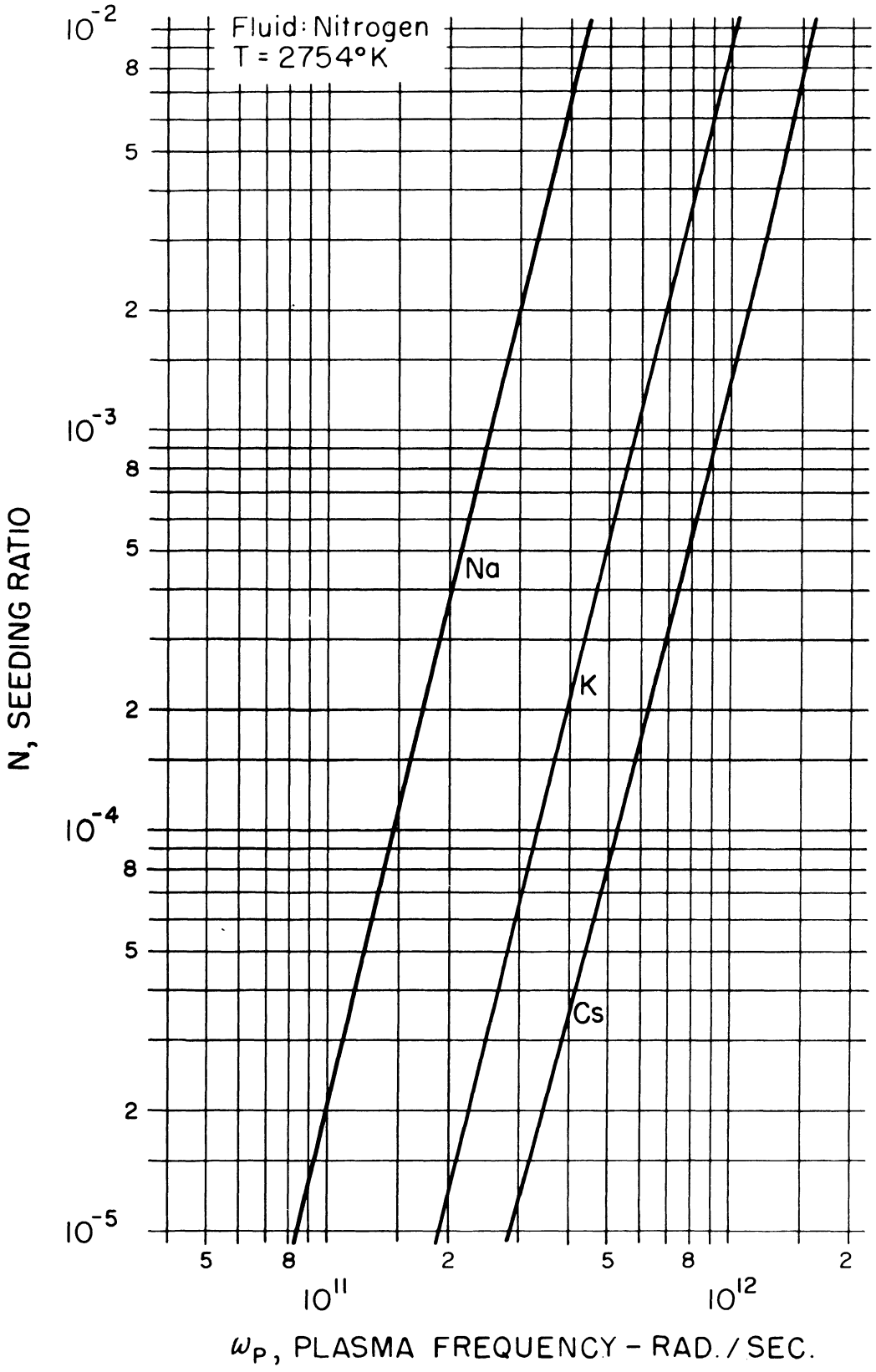

FIGURE 33. SEEDING RATIO vs. PLASMA FREQUENCY

IV-C. Predicted Collision Frequency vs. Seeding Ratio for Seeded Nitrogen

The collision frequency of the electrons with species k is given by

$$\nu_k = \langle \bar{v} \rangle n_k Q_k \tag{4-8}$$

where n_k is the number density of species k, Q_k is the velocity averaged, elastic cross section of species k for electron collision, and $\langle \bar{v} \rangle = \sqrt{\frac{8\,kT}{\pi\, m_e}}$ is the mean electron velocity.

The total collision frequency ν is given by

$$\nu = \sum_k \nu_k \tag{4-9}$$

The various species k are N_2, H_2O introduced in seeding (see Section I-B) the seeding element Na, K or Cs, Na^+, K^+ or Cs^+, O_2, H_2, OH, NO, H, O, etc.

Shkarofsky[17] lists cross sections for N_2, N, NO, O_2, and O. Molmud[30] gives cross sections for H_2O. Brown[31] gives data for H_2, neutral Na, K, and Cs. Values for H and OH were estimated by comparison with this data.

The cross section radius for ionized particles is roughly the distance of closest approach. A more accurate value for Q_+ is obtained from Spitzer,[32] by combining his Equation 5-32, 5-36 and using Equation (4-8) above, giving

$$Q_+ = \frac{\pi\, 2e^4}{(1.164)\,8\,(kT)^2} \ln \Lambda \tag{4-10}$$

where

$$\Lambda = \frac{3\,(kT)^{3/2}}{2e^3\sqrt{\pi\, n_e}} \tag{4-11}$$

is the ratio of Debye shielding distance to the 90^o impact parameter. Note the above formulas are in Gaussian units. Equation (4-10) includes the effect of electron-electron encounters.

Noting

$$n_K = n_T x_K \tag{4-12}$$

where x_K is the mole fraction of species K, Equation (4-9) becomes

$$\nu = n_T \langle \bar{v} \rangle \sum_k x_k Q_k \tag{4-13}$$

Equations (4-10) and (4-8) give reasonable accurate values of an effective collision frequency in the fully ionized cases. Equation (4-13) will give adequate collision frequencies for mixtures of neutral gases if proper cross-sections are used. However for the strongly ionized plasma, Equation (4-13) will not give accurate collision frequencies due to nonlinear effects. A strongly ionized plasma is one where the fraction of particles ionized is on the order of 10^{-3} or greater.

The only justification for the use of Equation (4-13) is that for the seeding ratios and temperatures considered here the contribution of the ions to the total collision frequency is small enough so the linear approximation represented by Equation (4-13) may not be seriously in error.

To calculate ν for the aqueous seeded N_2 stream described in Section V-B, the following steps were followed.

1. Because the amount of salt dissolved in the water was small, less than 10^{-3} mole fraction, the equilibrium at $2754^{o}K$, 1 atmosphere was calculated initially considering only N_2, H_2O present. The atomizer seeded the N_2 with .028 gms solution (here H_2O) per gm of N_2.

   Therefore the initial mole fractions were

$$x_{H_2O} = .0435$$

$$x_{N_2} = .9565$$

2. Considering the following reactions at 2754°K, 1 atmosphere total pressure

$$H_2 + \frac{1}{2} O_2 \rightarrow H_2O$$

$$\frac{1}{2} O_2 \rightarrow O$$

$$\frac{1}{2} H_2 \rightarrow H$$

$$\frac{1}{2} O_2 + \frac{1}{2} H_2 \rightarrow OH$$

$$\frac{1}{2} N_2 + \frac{1}{2} O_2 \rightarrow NO$$

with K_p taken from Penner,[24] the mole fractions at equilibrium are

$$x_{N_2} = .94233$$

$$x_{H_2O} = .02688$$

$$x_{H_2} = .01026$$

$$x_{O_2} = .002442$$

$$x_H = .006989$$

$$x_O = .002344$$

$$x_{OH} = .004558$$

$$x_{NO} = .004198$$

3. Since the mole fraction seeding ratio N ~ 10^{-3} it was assumed that introduction of the seeding element in the form of a nitrate would not materially affect the above equilibrium for collision frequency calculations. The error in the collision frequency calculation is less than .1%.

4. Using the data from Figures 2, 3, and 4, x_{M^+}, tabulated in Table 1, and the mole fraction of the seeding element that did not ionize, given in Table 2, were determined as a function of seeding ratio. N is the initial condition molar seeding ratio. Note that $x_{M^+} = x_e$.

TABLE 1

MOLE FRACTION OF IONIZED SEEDING ELEMENT

N	x_{Na^+}	x_{K^+}	x_{Cs^+}
10^{-4}	2.18×10^{-6}	1.23×10^{-5}	2.9×10^{-5}
2×10^{-4}	3.15×10^{-6}	1.73×10^{-5}	4.35×10^{-5}
5×10^{-4}	4.7×10^{-6}	2.65×10^{-5}	6.9×10^{-5}
10^{-3}	6.6×10^{-6}	3.65×10^{-5}	9.8×10^{-5}
2×10^{-3}	9.2×10^{-6}	5.3×10^{-5}	1.35×10^{-4}
5×10^{-3}	1.5×10^{-5}	8.3×10^{-5}	2.07×10^{-4}

TABLE 2

MOLE FRACTION OF NEUTRAL SEEDING ELEMENT

N	x_{Na}	x_K	x_{Cs}
10^{-4}	$.9782 \times 10^{-4}$	$.877 \times 10^{-4}$	$.71 \times 10^{-4}$
2×10^{-4}	1.9685×10^{-4}	1.827×10^{-4}	1.565×10^{-4}
5×10^{-4}	4.953×10^{-4}	4.735×10^{-4}	4.31×10^{-4}
10^{-3}	$.9934 \times 10^{-3}$	$.9635 \times 10^{-3}$	$.902 \times 10^{-3}$
2×10^{-3}	1.9908×10^{-3}	1.947×10^{-3}	1.865×10^{-3}
5×10^{-3}	4.985×10^{-3}	4.917×10^{-3}	4.793×10^{-3}

5. The values of collision cross sections and their source are shown in Table 3.

TABLE 3

CROSS SECTIONS FOR SPECIES AT 2754°K

	Source
$Q_{H_2O} = 4.73 \times 10^{-15}\ cm^2$	(30)
$Q_{O_2} = 5.35 \times 10^{-16}\ cm^2$	(17)
$Q_O = 9.35 \times 10^{-16}\ cm^2$	(17)
$Q_{N_2} = 9.22 \times 10^{-16}\ cm^2$	(17)
$Q_{NO} = 8.9 \times 10^{-16}\ cm^2$	(17)
$Q_N = 1.34 \times 10^{-16}\ cm^2$	(17)
$Q_{Na} = 3.25 \times 10^{-14}\ cm^2$	(31)
$Q_K = 3.89 \times 10^{-14}\ cm^2$	(31)
$Q_{H_2} = 14.2 \times 10^{-16}\ cm^2$	(31)
$Q_H = 2 \times 10^{-16}\ cm^2$	estimated
$Q_{OH} = 10 \times 10^{-16}\ cm^2$	estimated

6. Utilizing these values of collision cross section along with Equation (4-10) for Q_+ and noting $n_e = x_e\, n_T$, where $n_T = \frac{P_T}{kT}$ is the total number of particles per unit volume, we obtain the collision frequency of a nitrogen seeded plasma given in Figure 34.

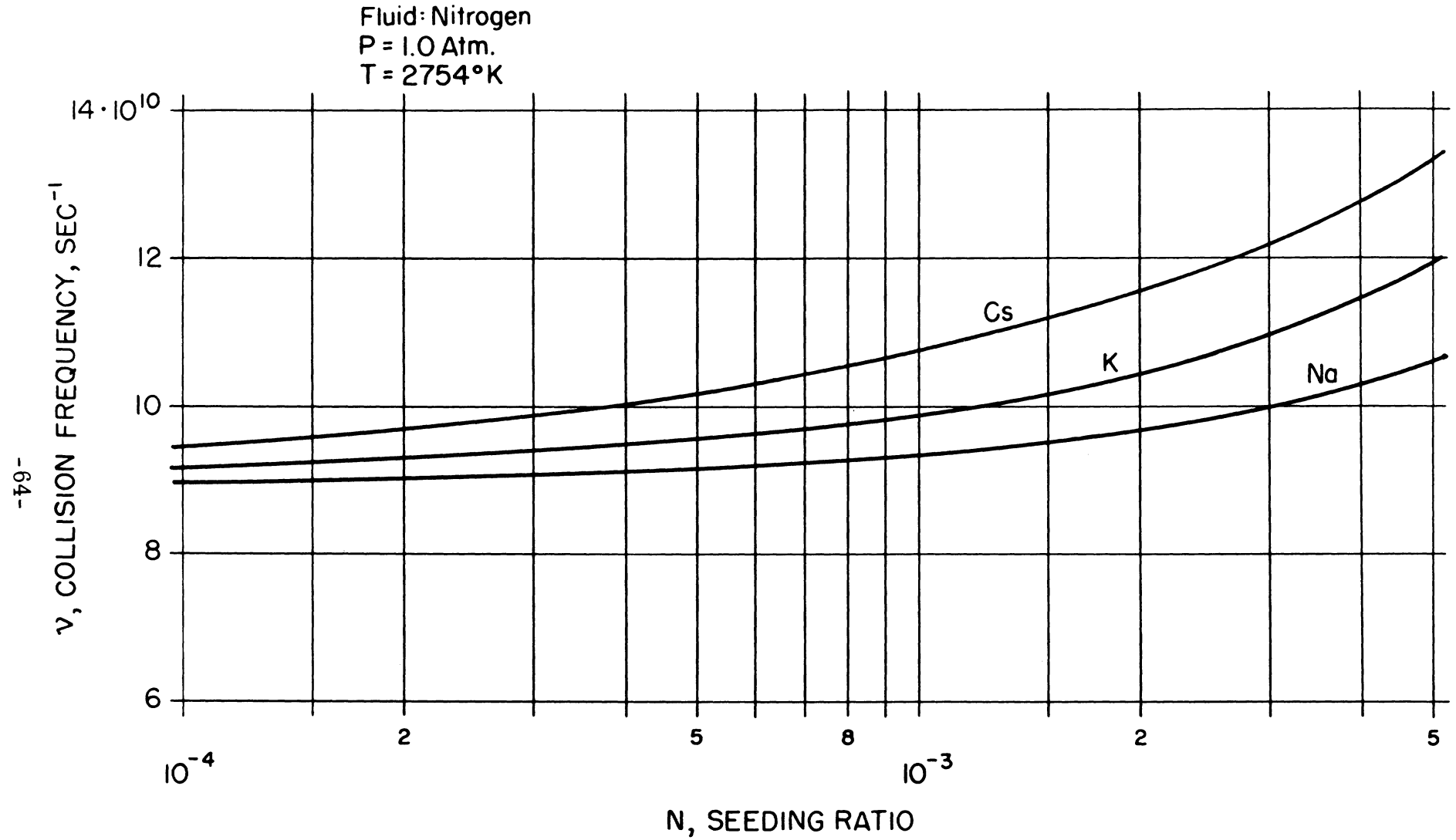

FIGURE 34. COLLISION FREQUENCY vs. SEEDING RATIO FOR SEEDED N_2 PLASMA

V. EXPERIMENTAL FACILITIES AND ARRANGEMENT

V-A. Plasma Generator

A schematic of the Plasma Generator is shown in Figure 35 and a photograph in Figure 40. The generator delivers approximately 1 KW to the plasma. It is a modification of the design given by Roddy and Green.[33] The generator uses a 304 TH triode operating at 30 MC/sec, and a 3/8" copper rod with a hemispherical end for the high voltage electrode, or probe.

The plasma is started by touching the electrode with an insulated metal object to give a spark to furnish an initial electron supply for the seeded gas flowing past the probe. These electrons are accelerated by the high electric field and collide with the seed element to produce ions and more electrons.

The seeded gas stream produces a luminous plasma, 15-20 cm long and 1 cm in diameter, with a mean temperature of 2754^{o}K as measured by Na D line reversal.

No copper contamination was visible in a spectrogram taken of an unseeded air "plasma".

V-B. Seeding Technique

Nitrogen or air is forced through a DeVilbiss No. 40 nebulizer containing salt solution, shown in Figure 36. The atomizer is immersed in a constant temperature water bath. The seeded gas stream leaves the atomizer in a saturated condition, passes upward through the high field produced at the electrode tip, where the seed element is ionized by electron impact producing a plasma about 20 cm long and 1 cm in diameter, depending on seeding ratio. The flow velocity in the tube is on the order of 20 cm/sec.

The pressure driving the atomizer is kept fixed using the manometer. The seeding ratio, i. e., the mole fraction of Na, K, Cs, etc., in the stream increases with driving pressure. The final pressure used was 9. 8 cm Hg, being the highest that did not splash solution out of the atomizer up into the glass tube.

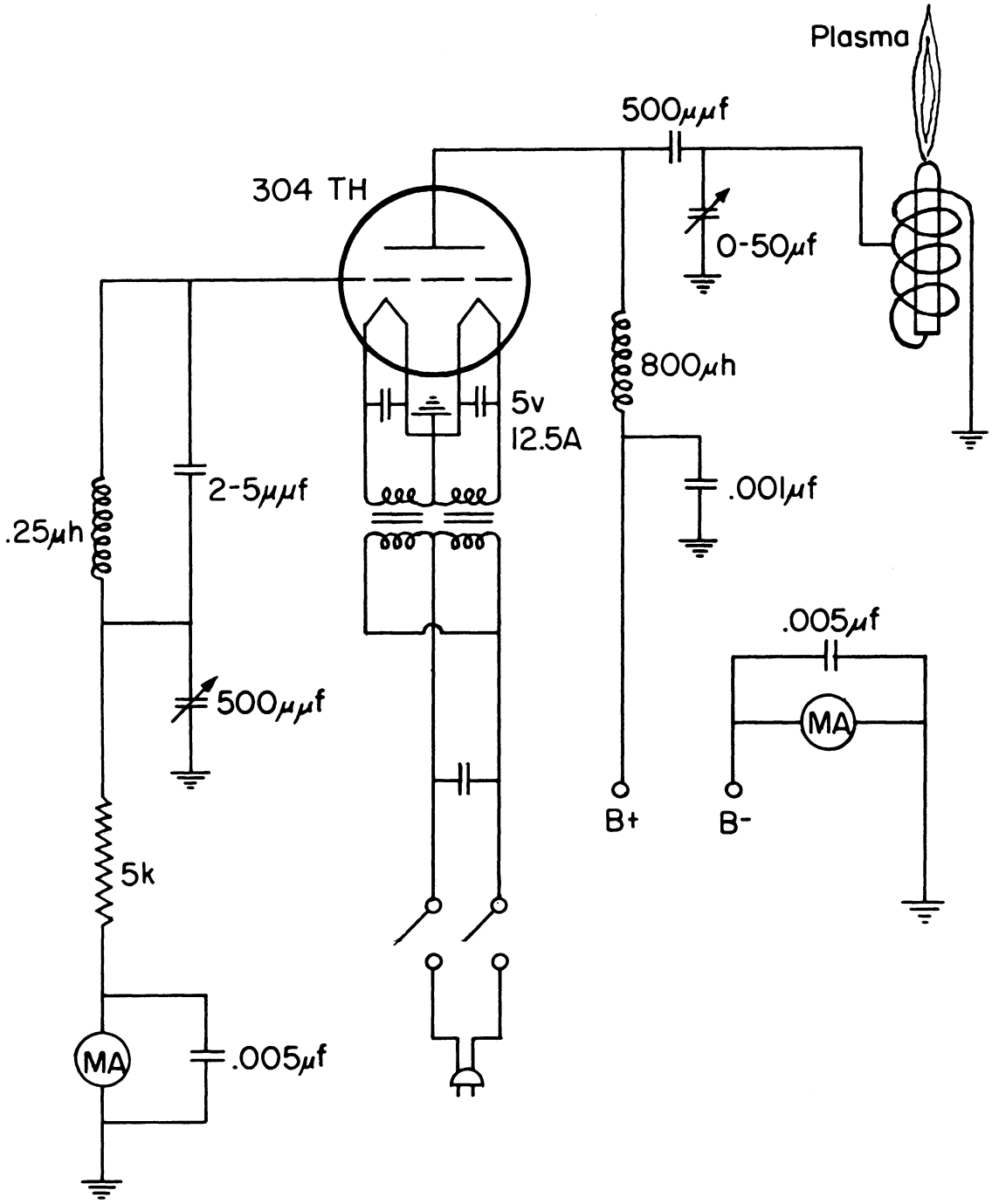

FIGURE 35. SCHEMATIC OF PLASMA GENERATOR

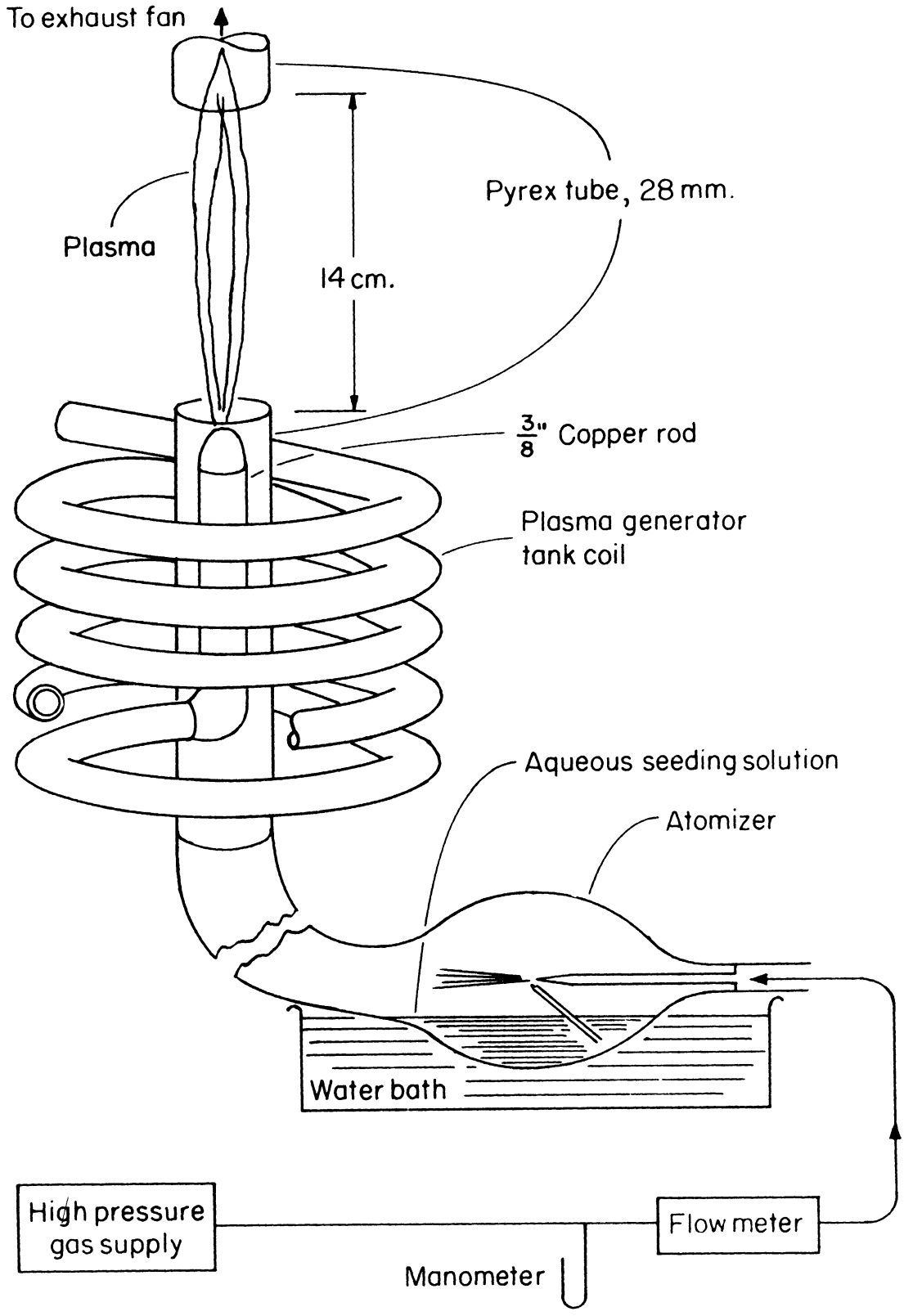

FIGURE 36. SEEDING OF PLASMA

The seeding ratio also increases with water bath temperature. The final temperature used, $87^{o}F$, was the highest that did not give over saturation of the gas stream, resulting in condensation in the glass tube above.

A sequence of salt solutions was prepared containing a known mass of salt in a known mass of solution (salt + water). A volume of gas of known pressure and temperature measured by a gas meter was passed through the atomizer, removing a mass of solution determined by weighing the seeder before and after. Then the atomizer constant, the mass of solution removed per unit mass N_2 passed, is calculated. Knowing the mass of salt in a known mass of solution gives the information necessary to calculate the mole fraction of Na, K, or Cs in the gas stream, which is the seeding ratio N.

The salts used were Na NO_3, K NO_3 and Cs NO_3. These salts were dissolved in water.

V-C. Temperature Measurement

The standard technique of reversal of the Na D line[34] was used to measure temperature of the plasma seeded with sodium. The tungsten filament temperature is varied until the Na D lines have the same intensity as the nearby continuum of the tungsten. At filament temperatures lower than the plasma, the D lines appear bright compared to the background continuum, and at higher filament temperatures than the plasma, the D lines appear darker than the continuum. The tungsten filament temperature is measured with a Leeds and Northrup optical pyrometer.

The plasma must be in complete thermal equilibrium for this method to be valid. Hottel and Williams[34] indicate most of the excitation is due to collisions at atmospheric pressure. Even though radiation equilibrium does not exist in an optically thin plasma such as this one, the error due to radiation non-equilibrium is $< 3^{o}K$, but will increase, of course, at lower pressures, since a lesser proportion of the total excitation is due to collisions.

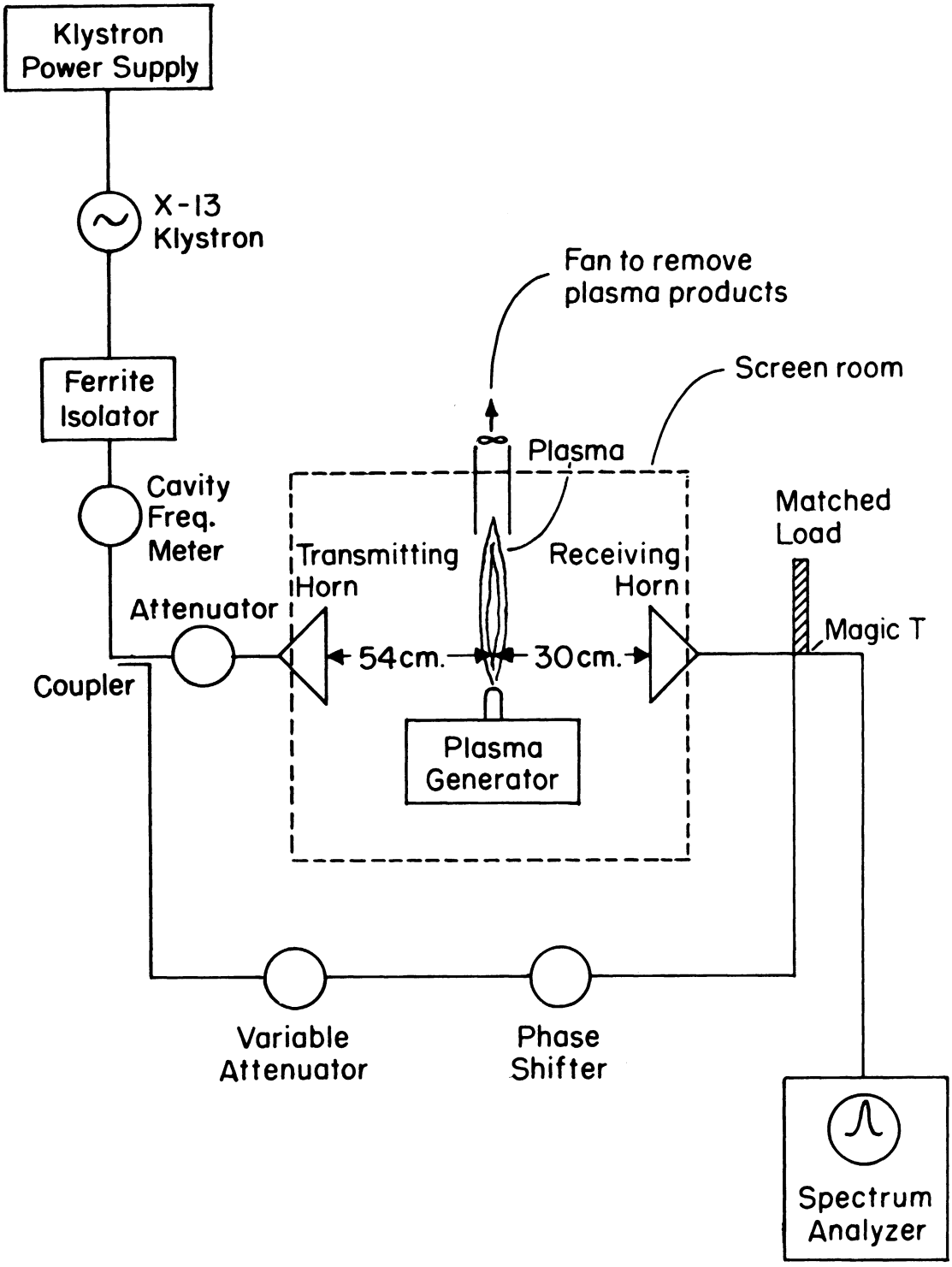

FIGURE 37. SCHEMATIC OF MICROWAVE INTERFEROMETER

The sodium D line temperature measures the Boltzmann energy distribution between two bound electron energy states of a neutral sodium atom, in terms of a temperature. This temperature is used for the free electron temperature and in the Saha equation equilibrium.

The measured Na D line temperature in the center of the plasma was $2754 \pm 37^{o}K$.

Figure 39 shows the experimental setup.

The question of electric fields giving nonequilibrium and its effects are discussed in the section on errors.

V-D. Schematic and Operation of Microwave Interferometer

The microwave interferometer shown schematically in Figure 37 and in Figure 38 is of standard design and operation.[6] The X-13 Klystron, operating continuous wave, generates 3 cm waves measured by the absorbtion in the cavity frequency meter. A coupler divides the signal into two parts. The signals are recombined in the Magic T and fed into a Polarad model STU-3A spectrum analyzer. The spectrum analyzer generates a local frequency modulated signal which is mixed with the incoming signal, whose spectrum is displayed on the oscilloscope.

When the phases of the recombined waves differ by 180^{o} and are of equal amplitude, a null is observed on the spectrum analyzer. This null is obtained by adjustment of the variable attenuator and phase shifter. The attenuator in the direct leg allows one to work in the most sensitive region of the variable attenuator in the parallel leg. In operation, the phase and db to produce a null without a plasma present are subtracted from the phase and db necessary with plasma present. Referring to the accompanying sketch, we write:

$$\beta = \beta_{\text{plasma}} - \beta_{\text{no plasma}} \tag{5-1}$$

$$db = db_{plasma} - db_{no\ plasma}$$

$$= 20 \log \frac{E_{tot}}{E_o} \tag{5-2}$$

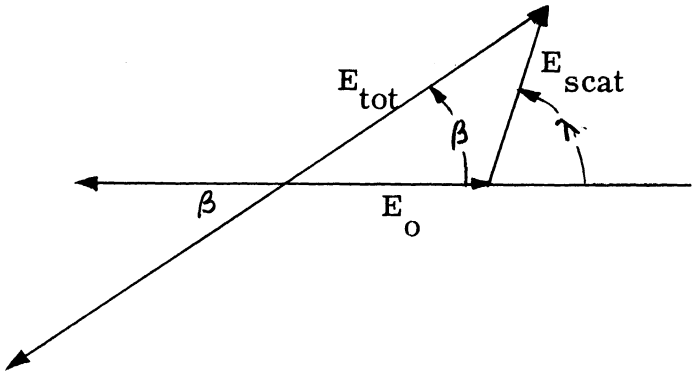

Knowing the ratio of two sides and the included angle of the triangle enables one to calculate $\frac{E_{scat}}{E_o}$ and λ, the phase of E_{scat} relative to E_o using

$$\frac{E_{tot}}{E_o} = \log^{-1} \left(\frac{db}{20}\right) \tag{5-3}$$

$$\frac{E_{scat}}{E_o} = \sqrt{1 + \left(\frac{E_{tot}}{E_o}\right)^2 - 2 \frac{E_{tot}}{E_o} \cos \beta} \tag{5-4}$$

$$\sin \lambda = \left(\frac{E_{tot}}{E_o}\right)\left(\frac{E_o}{E_{scat}}\right) \sin \beta \tag{5-5}$$

Considerable difficulty was experienced in zero shifts when power was applied to the plasma generator before the plasma was ignited. Considerable frequency shift (5 mc) of the X-13 Klystron and breakup of the CW "δ-function" spectrum into several peaks were eliminated by shielding all cables, particularly from the Klystron power supply to the Klystron, as well as by capacitor bypassing at both ends of this

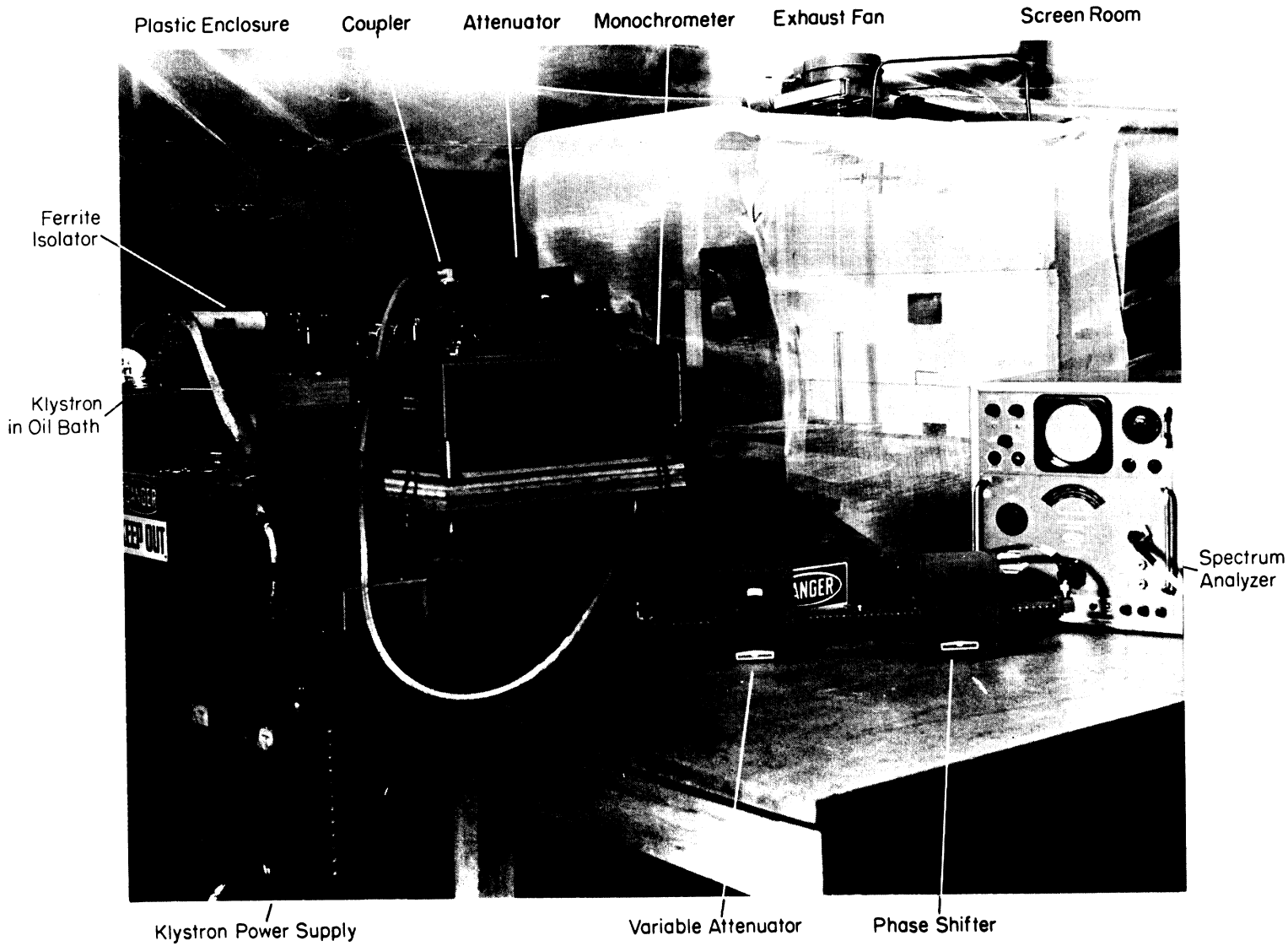

FIGURE 38. VIEW OF MICROWAVE INTERFEROMETER

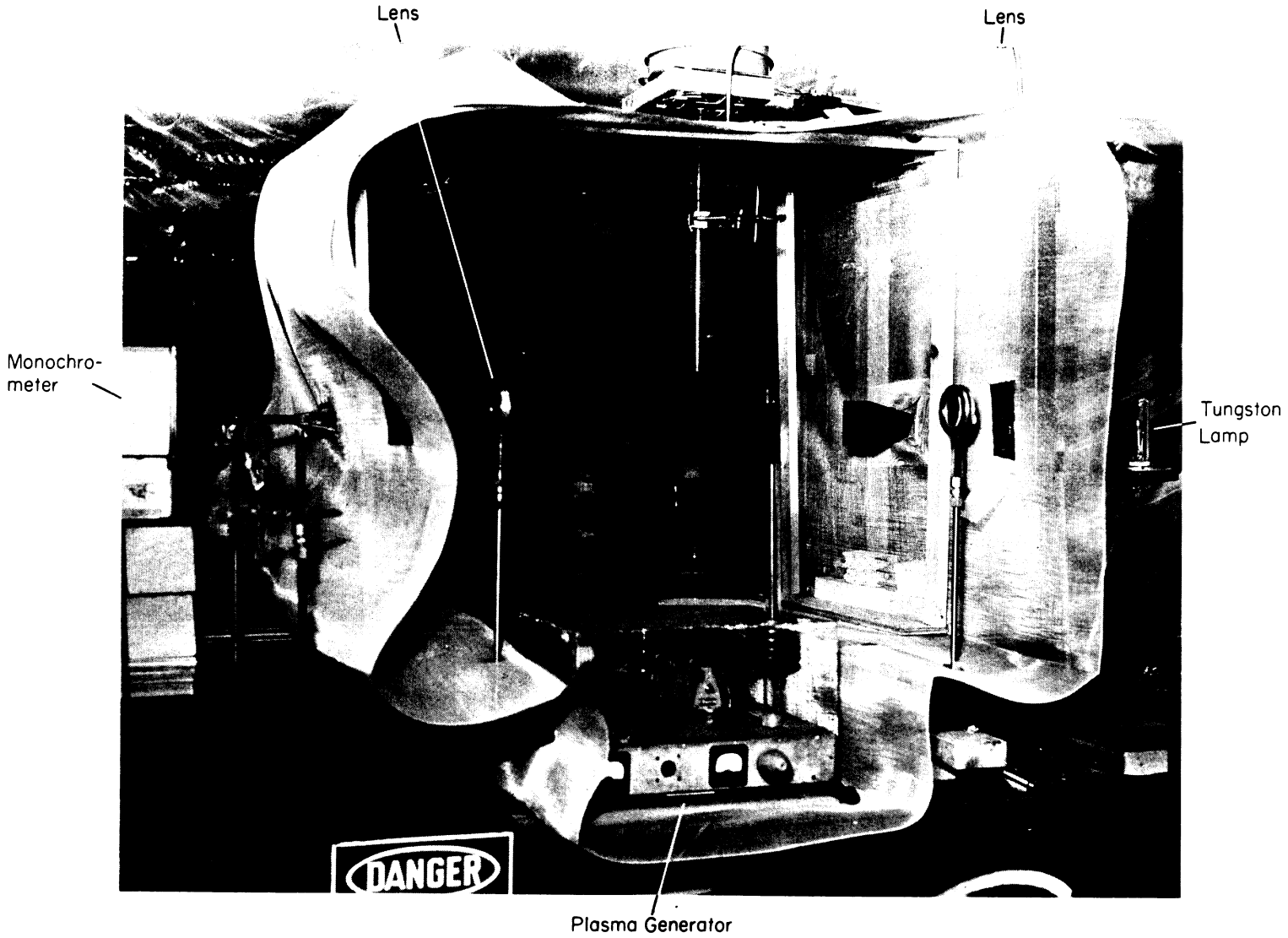

FIGURE 39. VIEW OF SODIUM D LINE MEASUREMENT SETUP

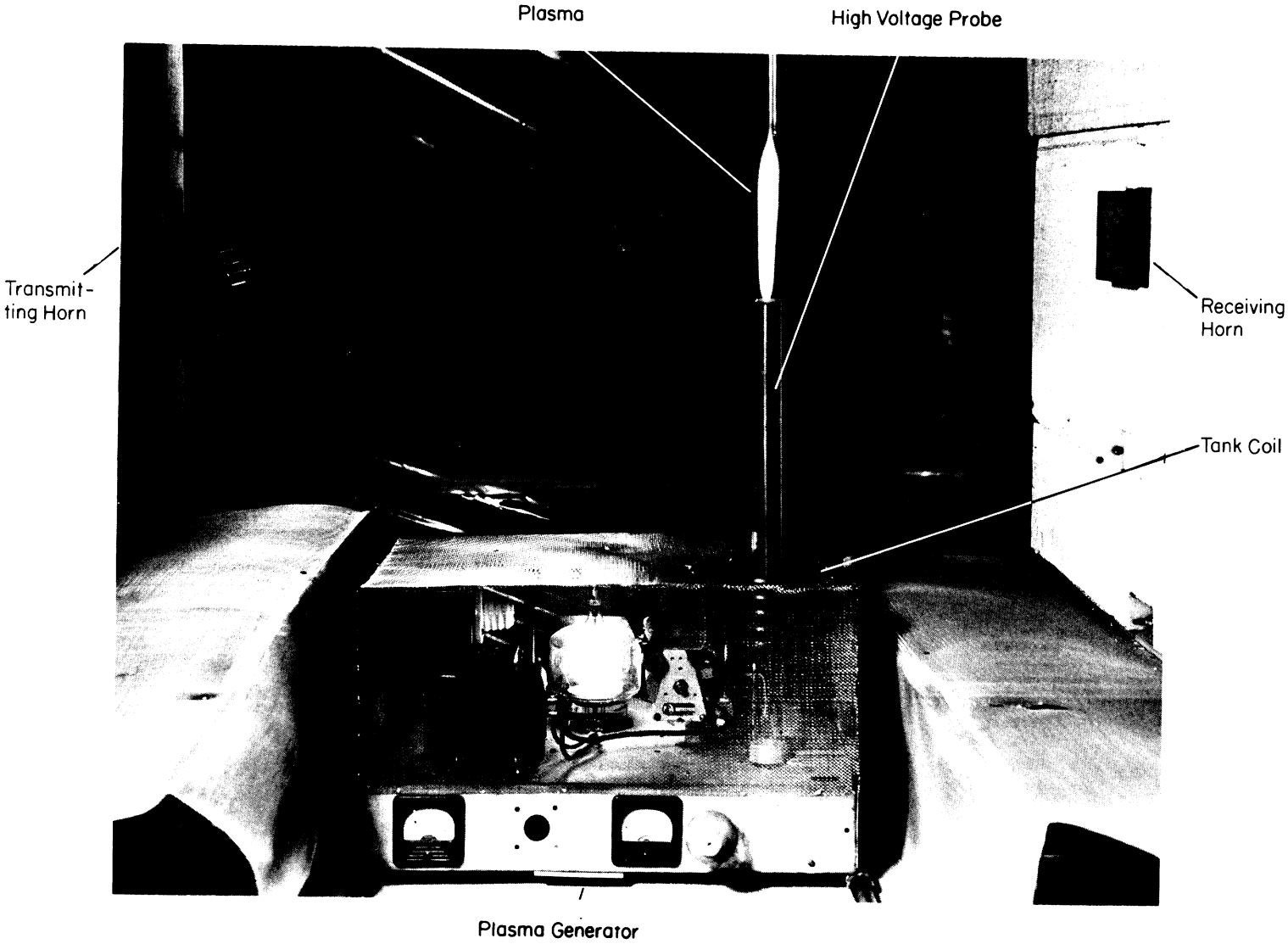

FIGURE 40. VIEW OF PLASMA GENERATOR

cable. It was also found necessary to enclose the plasma generator in a partial screen room.

The spectrum analyzer technique was used because of crystal detector noise problems and subsequent null sensitivity loss. This occurred when the combined output of the two legs with the X-13 square wave modulated at 1 KC/sec was fed directly to a crystal and the output measured using a standing wave meter. The IF strip of the spectrum analyzer operated at 150 mc, which gave a large improvement in crystal noise and hence null sensitivity. For example, using a IN23B crystal at 1 KC, phase shift variations of $\pm 10^{o}$ and db shifts of $\pm$. 5 db about a null produced no detectable unbalances in the null. Using the spectrum analyzer, shifts of $.2^{o}$ in phase and . 02 db were clearly evident as unbalancing the null.

The microwave horns were truncated pyramids, 15 cm long with faces 8. 9 by 7. 75 cm in the direction of $\overline{E}_p$, opening out from 2. 5 x 1. 25 cm waveguide.

The interferometer is shown in the accompanying photographs, Figures 38, 39, and 40.

VI. EXPERIMENTAL RESULTS

VI-A. Predicted Amplitude and Phase of the Scattered Wave

Using Figures 33 and 34, ω_p and ν were predicted for each seeding ratio. Together with the experimentally determined visible radius from Figure 41 these values of R, ω_p and ν were inserted into Equations (3-31), (3-28) and (3-29) to give E_{scat}/E_o and λ from Equation (3-31).

The notation used is given on the sketch in Section III-C.

For convenience, Table 4 lists the values of the seeding ratio vs. the measured radius, expected plasma frequency, collision frequency, and the computed E_{scat}/E_o and λ.

TABLE 4

PREDICTED VALUES OF PHASE AND AMPLITUDE vs. SEEDING RATIO

N	Measured R cm	Predicted ω_p rad/sec	Predicted ν $\frac{\text{coll}}{\text{sec}}$	Predicted E_{scat}/E_o	Predicted λ Radian
Sodium					
7.123×10^{-5}	.639	1.34×10^{11}	8.906×10^{10}	.1326	3.5112
1.201×10^{-4}	.593	1.53×10^{11}	8.906×10^{10}	.1317	3.4974
2.689×10^{-4}	.541	1.87×10^{11}	9.07×10^{10}	.1319	3.4780
6.212×10^{-4}	.565	2.30×10^{11}	9.20×10^{10}	.1498	3.4768
1.078×10^{-3}	.537	2.60×10^{11}	9.36×10^{10}	.1482	3.4626
Cesium					
1.356×10^{-4}	.510	5.70×10^{11}	9.56×10^{10}	.1637	3.4223
2.673×10^{-4}	.427	6.70×10^{11}	9.82×10^{10}	.1456	3.3831
5.194×10^{-4}	.359	7.85×10^{11}	1.02×10^{11}	.1306	3.3448
1.196×10^{-3}	.282(*)	9.70×10^{11}	1.094×10^{11}	.1129	3.2921
Potassium					
9.982×10^{-5}	.421	3.18×10^{11}	9.18×10^{10}	.1265	3.4059
1.974×10^{-4}	.387	3.96×10^{11}	9.30×10^{10}	.1246	3.3794
3.866×10^{-4}	.321	4.70×10^{11}	9.49×10^{10}	.1114	3.3369
9.088×10^{-4}	.235(*)	5.88×10^{11}	9.81×10^{10}	.0923	3.2688

$\omega = 2\pi \times 10^{10}$

$T = 2754^{O}K$

(*) = Extrapolated from Figure 41

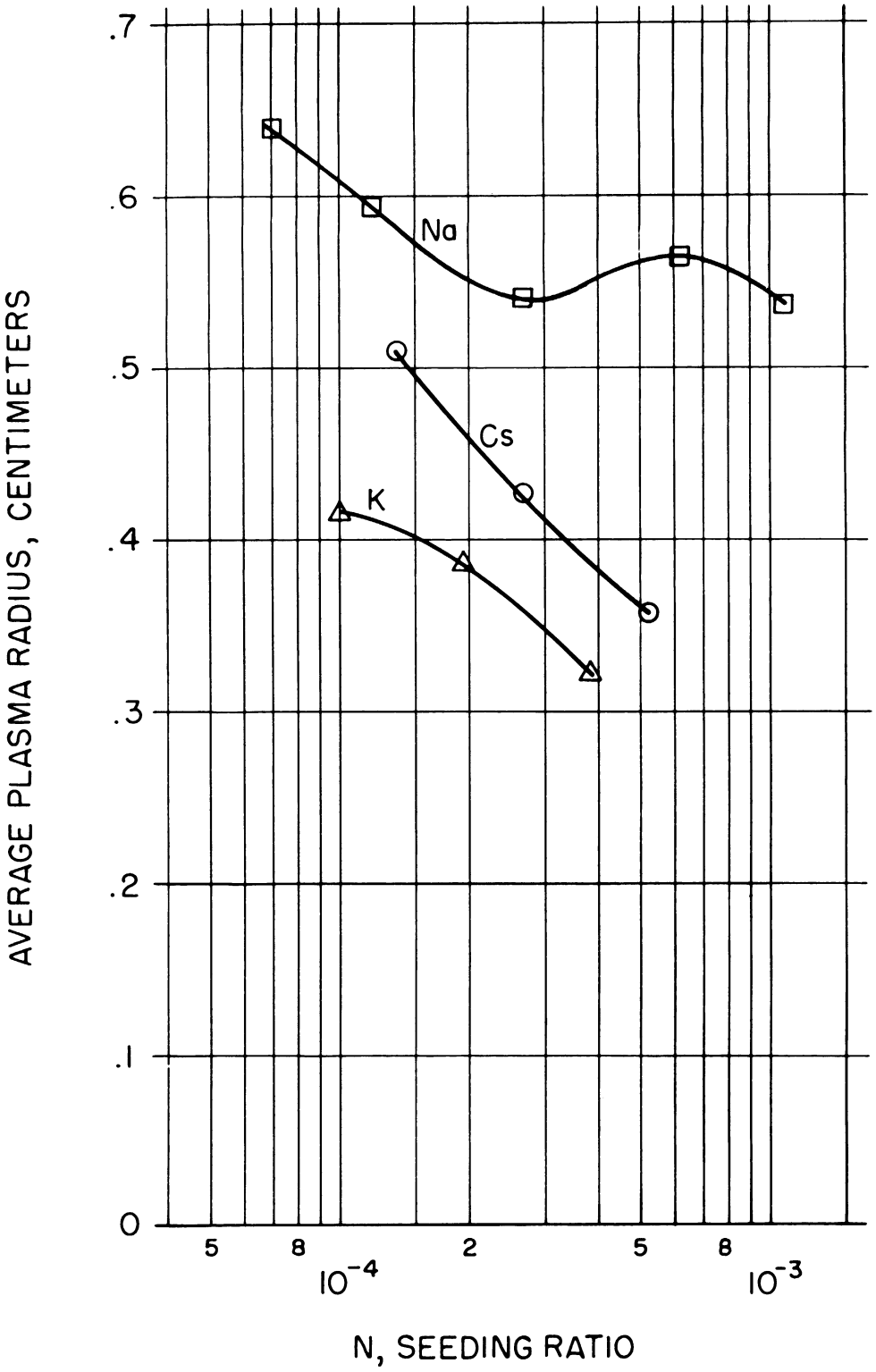

FIGURE 41. PLASMA RADIUS vs. SEEDING RATIO

VI-B. Measured Amplitude and Phase of the Scattered Wave

The experimentally determined values of db and β were reduced using Equations (5-3), (5-4) and (5-5) to give E_{scat}/E_o and λ as determined by the microwave measurements.

Table 5 lists the experimental microwave measurements of E_{scat}/E_o and λ.

TABLE 5

EXPERIMENTAL MICROWAVE VALUES OF PHASE AND AMPLITUDE vs. SEEDING RATIO

N	E_{scat}/E_o	λ Radians
Sodium		
7.123×10^{-5}	.03787	3.6250
1.201×10^{-4}	.04157	3.5563
2.689×10^{-4}	.05014	3.5699
6.212×10^{-4}	.06083	3.6250
1.078×10^{-3}	.06188	3.5375
Cesium		
1.356×10^{-4}	.09244	3.5015
2.673×10^{-4}	.1080	3.5059
5.194×10^{-4}	.1155	3.4897
1.196×10^{-3}	.1141	3.5581
Potassium		
9.982×10^{-5}	.07295	3.5479
1.974×10^{-4}	.08559	3.4163
3.866×10^{-4}	.1068	3.4883
9.088×10^{-4}	.1029	3.4203

At least three separate measurements were averaged to obtained these values.

These results are plotted vs. N in Figures 42-47. The curves pass through the values of E_{scat}/E_o and λ computed from the theoretically predicted values of ω_p and ν, using the measured visible radius. The experimental points are shown together with their probable errors calculated from Equations (7-6) and (7-7).

Table 6 lists the $\langle \delta\lambda \rangle$ and $\langle \delta E_{scat}/E_o \rangle$ computed from Equations (7-6) and (7-7).

TABLE 6

UNCERTAINTIES IN E_{scat}/E_o AND λ FOR EXPERIMENTAL MEASUREMENTS

N	$\langle \delta\lambda \rangle$ Radians	$\langle \delta E_{scat}/E_o \rangle$
Sodium		
$.7123 \times 10^{-4}$	.1768	2.540×10^{-3}
1.201×10^{-4}	.1883	2.454×10^{-3}
2.689×10^{-4}	.1523	2.448×10^{-3}
6.212×10^{-4}	.1072	2.498×10^{-3}
1.078×10^{-3}	.1330	2.399×10^{-3}
Cesium		
1.356×10^{-4}	9.823×10^{-2}	2.335×10^{-3}
2.673×10^{-4}	7.931×10^{-2}	2.269×10^{-3}
5.194×10^{-4}	7.720×10^{-2}	1.871×10^{-3}
1.196×10^{-3}	6.450×10^{-2}	2.321×10^{-3}
Potassium		
$.9982 \times 10^{-4}$	.1084	2.385×10^{-3}
1.975×10^{-4}	.1369	2.230×10^{-3}
3.866×10^{-4}	.08466	2.261×10^{-3}
9.088×10^{-4}	.1101	2.102×10^{-3}

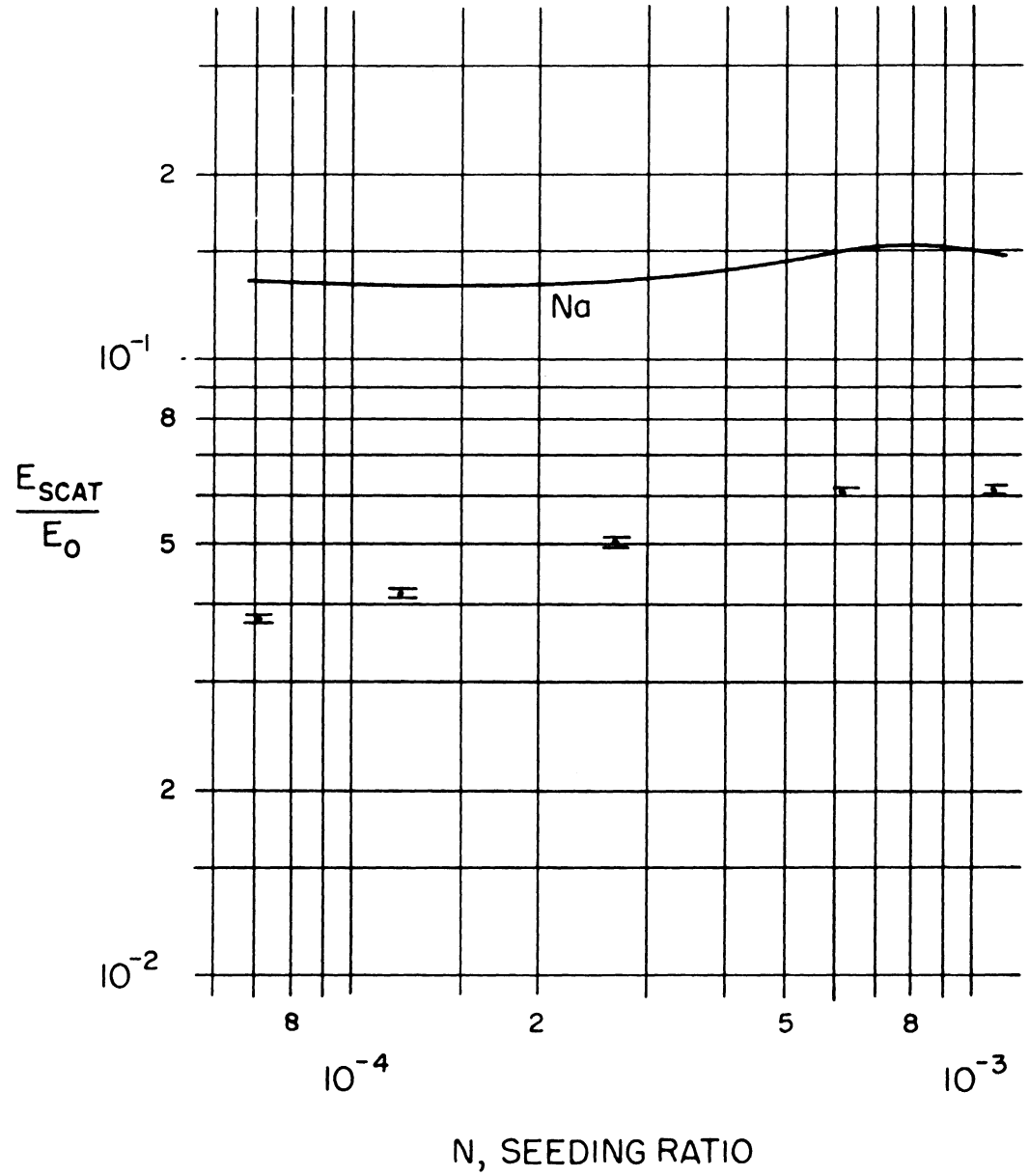

FIGURE 42. EXPERIMENTAL AND PREDICTED VALUES OF THE AMPLITUDE OF THE SCATTERED WAVE, Na, N_2

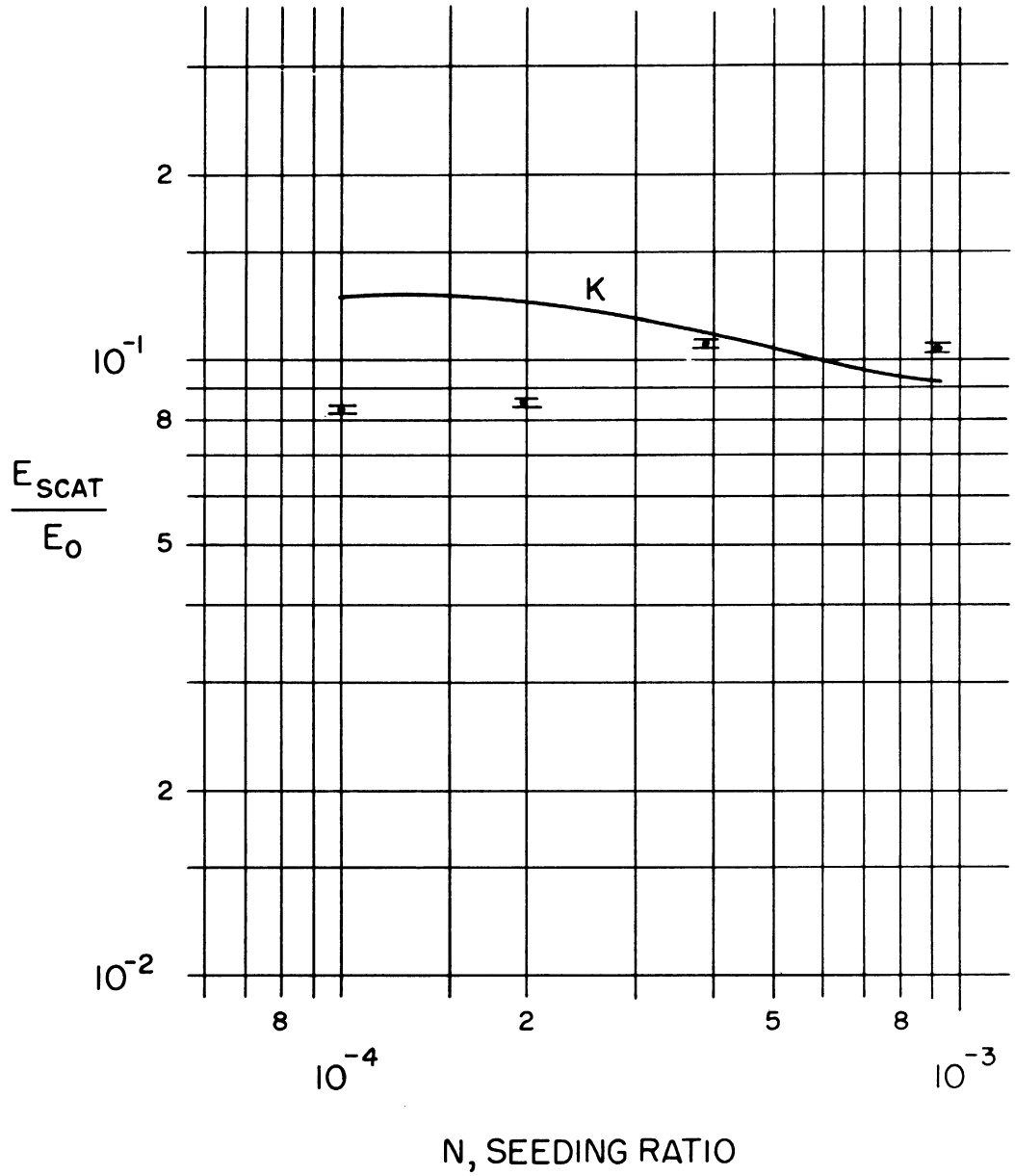

FIGURE 43. EXPERIMENTAL AND PREDICTED VALUES OF THE AMPLITUDE OF THE SCATTERED WAVE, K, N_2

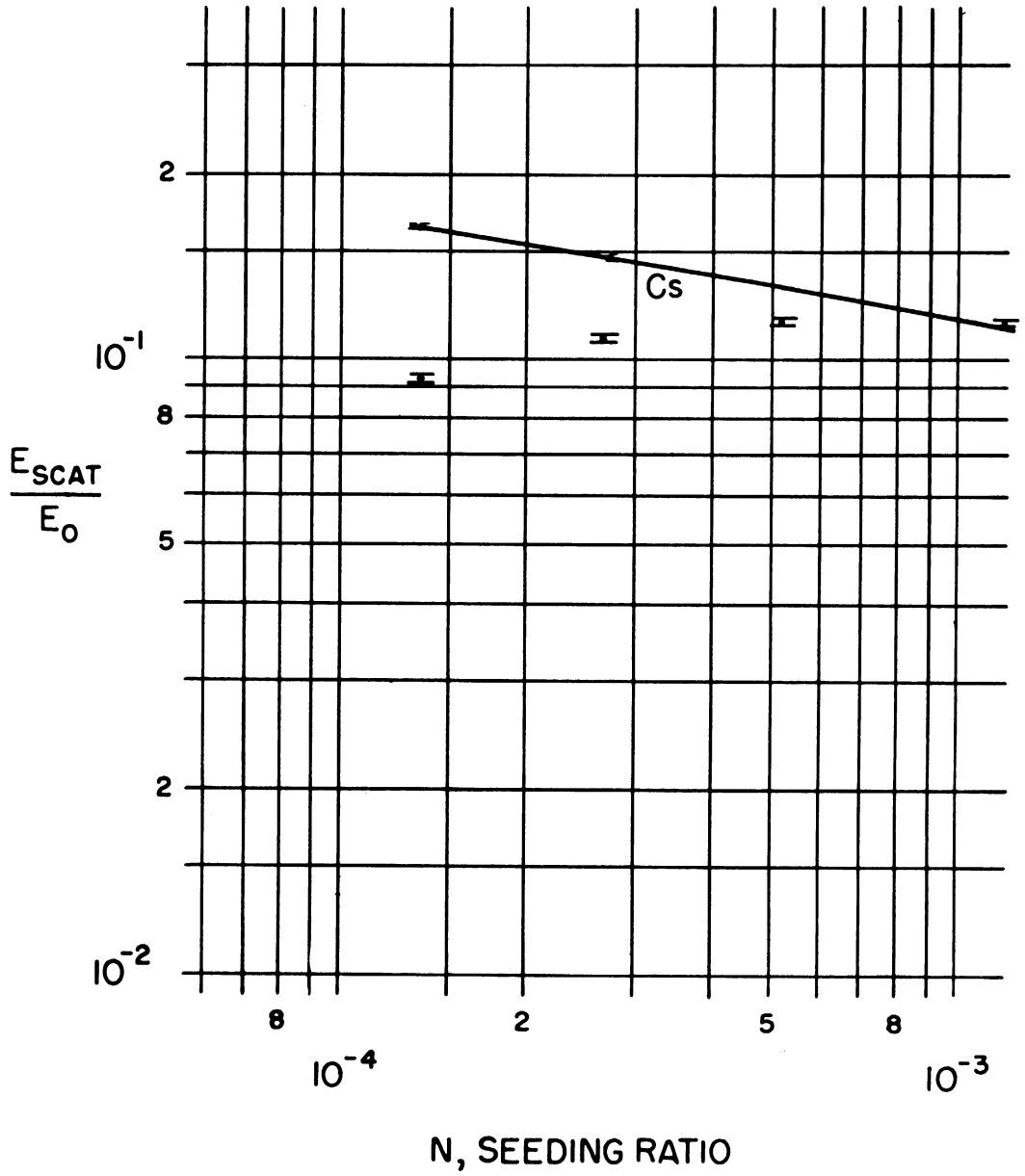

FIGURE 44. EXPERIMENTAL AND PREDICTED VALUES OF THE AMPLITUDE OF THE SCATTERED WAVE, Cs, N_2

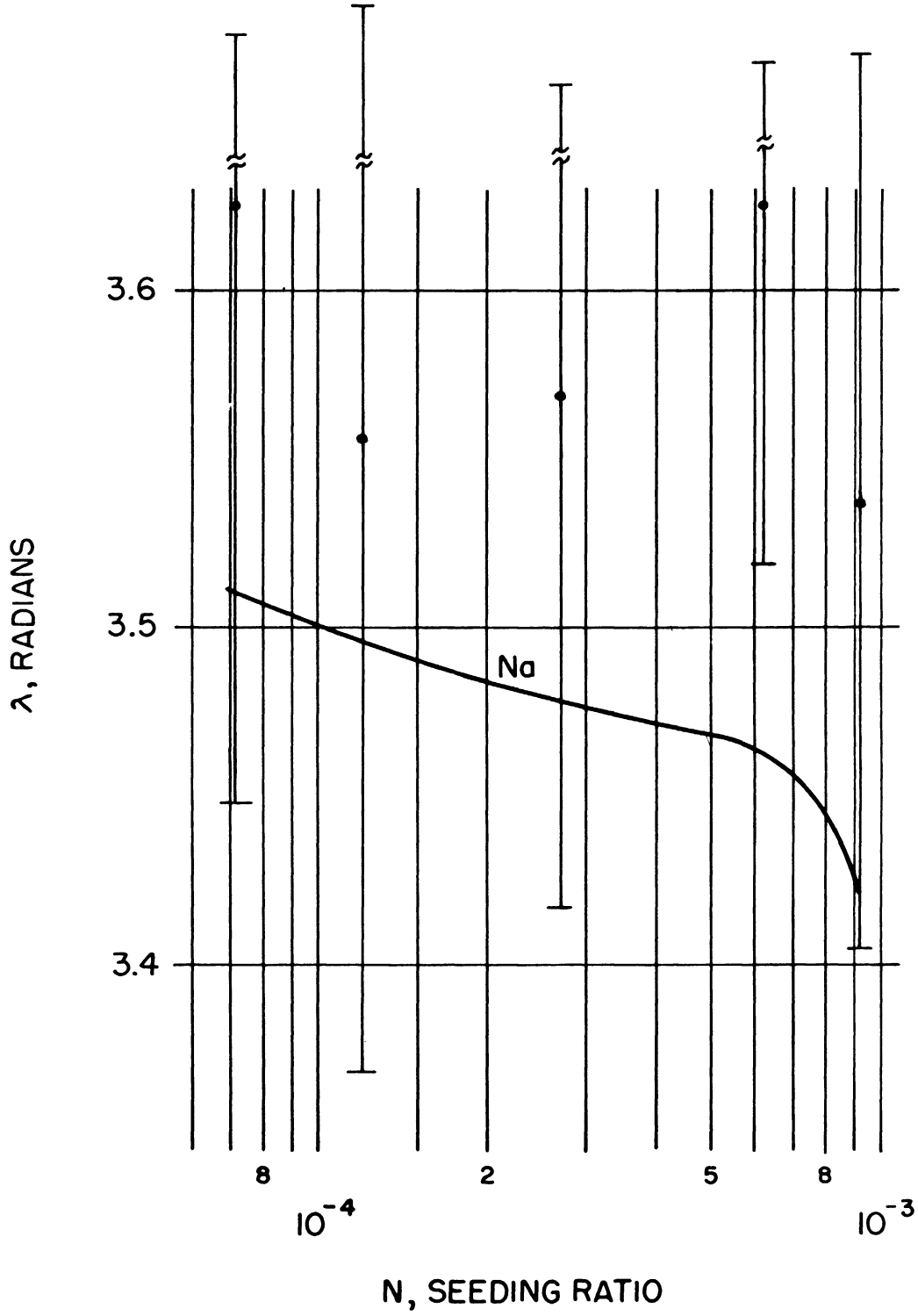

FIGURE 45. EXPERIMENTAL AND PREDICTED VALUES OF THE PHASE OF SCATTERED WAVE, Na, N_2

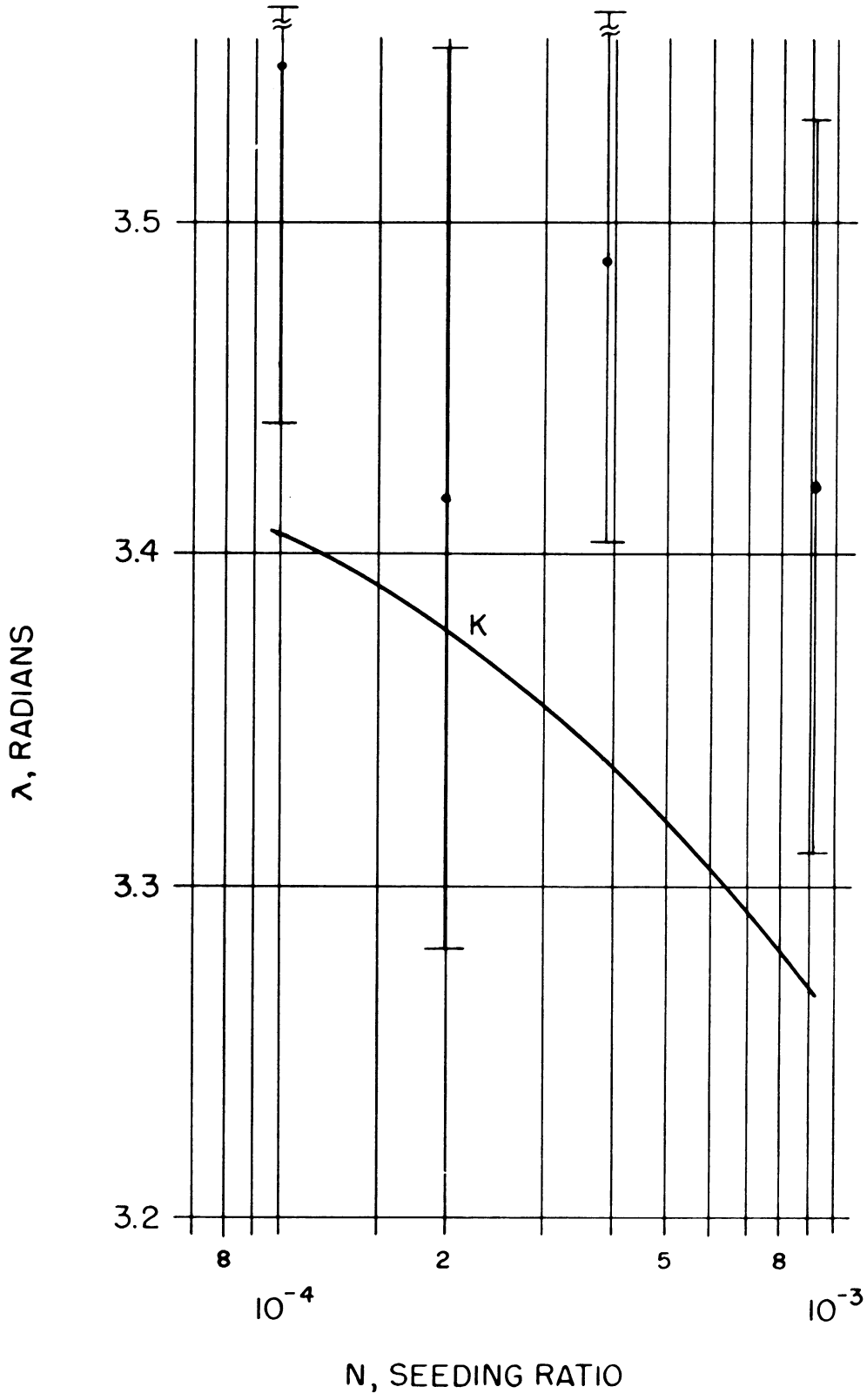

FIGURE 46. EXPERIMENTAL AND PREDICTED VALUES OF THE PHASE OF SCATTERED WAVE, K, N_2

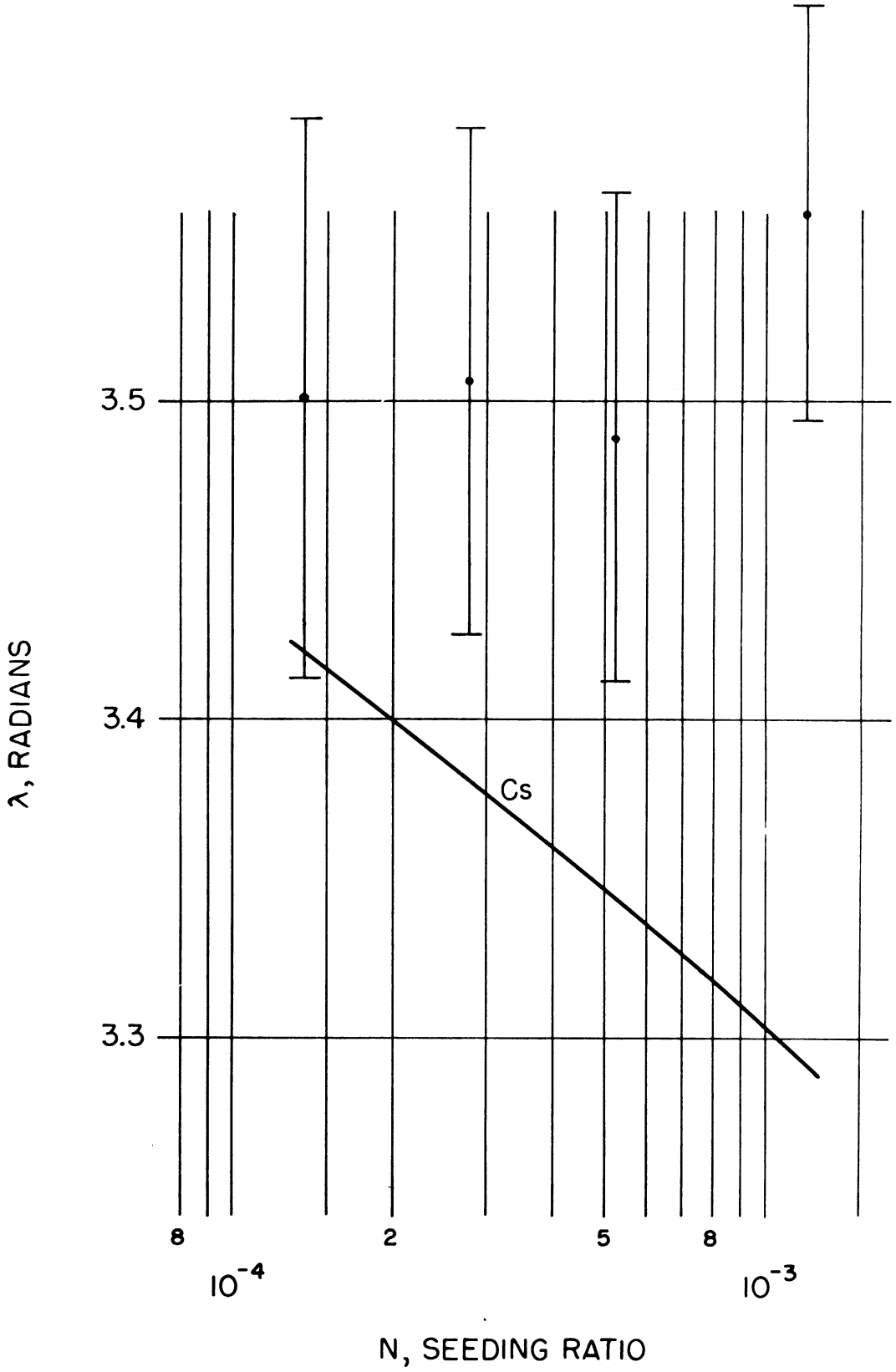

FIGURE 47. EXPERIMENTAL AND PREDICTED VALUES OF THE PHASE OF SCATTERED WAVE, Cs, N_2

VI-C. Discussion

There are two ways to compare theory and experiment. One is to insert the predicted plasma properties into the theoretical model and derive the predicted phase and amplitude of the scattered wave as done here. This predicted phase and amplitude is compared to the microwave measured phase and amplitude. Due to the complexity of the expressions, the origin of differences between theory and experiment is not clear.

One could alternatively use the observed phase and amplitude to work backward using the intersection of crossplots of ω_p vs. ν for both E_{scat}/E_o and λ to give the ω_p and ν necessary on the basis of the theoretical model. These plasma properties derived from the scattering data could be compared to the predicted properties. Of course the question of whether differences between the predicted and observed properties are real or due to inapplicability of the theoretical model to the actual situation still remains.

In view of the serious discrepancies between theory and experiment the first method was adopted. Some of the measurements were reduced using the second method but it was felt the difficulty was not justified commensurate with information obtained.

VII. ERRORS

VII-A. Introduction

Several sources of error are present, which can be grouped into three categories:

1. Errors affecting the predicted values of the plasma, i. e., errors in the quantities necessary to compute theoretical values of E_{scat}/E_o and λ. These are temperature error, plasma radius error, cross section data uncertainty, seeding ratio error, and deviations from the 760 mm atmospheric pressure assumed.
2. Errors in the experimental determination of E_{scat} and λ, which are due to db and phase measurement errors.

3. Errors due to neglected factors and simplifying assumptions. These include the effects of temperature gradients in the radial and axial directions, finite length, nonequilibrium due to high electric fields, use of an arbitrarily defined visible radius, attachment of electrons to O_2 and H_2O, the fact that the microwave plane wave is stronger at the plasma than at the receiving horn with no plasma and the finite size of the receiving horn introduces phase error in the measured signal.

Many of these possible sources of error are discussed in the following.

VII-B. DB and Phase Sensitivity

Errors in the db and phase measurements of E_{tot} relative to the plane wave will give errors in the values of E_{scat} and λ. Some idea of the magnitude of these errors can be obtained by calculating sensitivity coefficients in the triangle formed by E_{tot} and E_{scat}.

The relations between E_T, E_S, λ, ϕ, are shown on the diagram.

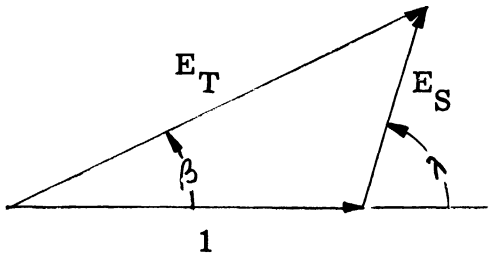

$$E_S^2 = 1 + E_T^2 - 2E_T \cos \beta \qquad (7\text{-}1)$$

$$E_T \sin \beta = E_S \sin \lambda \qquad (7\text{-}2)$$

Taking differentials

$$\left.\begin{aligned} 2E_S\,\delta E_S &= 2E_T\,\delta E_T - 2\cos\beta\,\delta E_T + 2E_T \sin\beta\delta\beta \\ \sin\beta\delta\,E_T + E_T\cos\beta\delta\beta &= \sin\lambda\,\delta E_S + E_S\cos\lambda\,\delta\lambda \end{aligned}\right\}$$

Considering δE_T, $\delta\beta$ as known

$$\left.\begin{aligned} E_S\,\delta E_S &= (E_T - \cos\beta)\,\delta E_T + E_T \sin\beta\delta\beta \\ \sin\lambda\,\delta E_S + E_S\cos\lambda\,\delta\lambda &= \sin\beta\,\delta E_T + E_T\cos\beta\delta\beta \end{aligned}\right\}$$

Solving for δE_S, $\delta\lambda$

$$\delta E_S = \left(\frac{E_T - \cos\beta}{E_S}\right)\delta E_T + \left(\frac{E_T}{E_S}\sin\beta\right)\delta\beta$$

$$\delta\lambda = \left[\frac{\sin\beta}{E_S\cos\lambda} - \left(\frac{E_T - \cos\beta}{E_S^{\,2}}\right)\tan\lambda\right]\delta E_T + \left[\frac{E_T}{E_S}\,\frac{\cos\beta}{\cos\lambda} - \frac{E_T\tan\lambda\sin\beta}{E_S^{\,2}}\right]\delta\beta$$

Simplifying using Equation (7-2)

$$\delta E_S = \left(\frac{E_T - \cos\beta}{E_S}\right)\delta E_T + (\sin\lambda)\,\delta\beta \qquad (7\text{-}3)$$

$$\delta\lambda = \left[\frac{\tan\lambda}{E_T} - \left(\frac{E_T - \cos\beta}{E_S^{\,2}}\right)\tan\lambda\right]\delta E_T + \left[\frac{E_T\cos\beta}{E_S\cos\lambda} - \frac{\tan\lambda\sin\lambda}{E_S}\right]\delta\beta \qquad (7\text{-}4)$$

Note $db = 20\log E_T$

$$= 8.686\ln E_T$$

so $$\delta E_T = \frac{E_T}{8.686}\,\delta\,db \qquad (7\text{-}5)$$

The root mean square errors are

$$\left\langle \delta E_{scat}/E_o \right\rangle = \sqrt{\left[\left(\frac{E_T - \cos\beta}{E_S}\right)\frac{E_T}{8.686}\,\delta\,db\right]^2 + (\sin\lambda\,\delta\beta)^2} \tag{7-6}$$

$$\left\langle \delta\lambda \right\rangle = \sqrt{\left[\left(\frac{\tan\lambda}{E_T} - \frac{E_T - \cos\beta}{E_S^2}\right)\frac{E_T}{8.686}\,\delta\,db\right]^2 + \left[\left(\frac{E_T\cos\beta}{E_S\sin\lambda} - \frac{\tan\lambda\sin\lambda}{E_S}\right)\delta\beta\right]^2} \tag{7-7}$$

It was found experimentally that phase shifts $\delta\beta = .2^o = 3.49 \times 10^{-3}$ radian and db changes $\delta\,db = .02$ caused detectable unbalance in the null measured on the spectrum analyzer throughout the measurements.

For example if $R = .5$ cm, $\nu = 10^{11}$, $\omega_p = 10^{11}$ then from Figures 27 and 28, $\lambda = 197.65$, $E_S = .07$, so $\beta = 358.7$, $E_T = .935$.

Therefore

$$\delta E_{scat}/E_o = -.925\,\delta E_T + .303\,\delta\beta \tag{7-8}$$

$$\delta\lambda = 4.55\,\delta E_T + 12.63\,\delta\beta \tag{7-9}$$

The necessity for accurate phase measurements is clearly evident in $\delta\lambda$.

Equations (7-6) and (7-7) were used to calculate $\delta E_{scat}/E_o$ and $\delta\lambda$ for the experimental determinations of E_{scat}/E_o and λ. Note that Equations (7-6) and (7-7) indicate only the precision of the measurement of E_{scat}/E_o and λ that can be expected. They do not indicate the error possible in E_{scat}/E_o and λ.

Since E_{scat}/E_o results essentially from the difference of two relatively large numbers and λ depends so critically upon both δ db and $\delta\beta$, the accuracy of measurement in the range of small E_{scat}/E_o is not large. Other methods of measuring the scattered field should be investigated.

VII-C. Plasma Radius Error

The plasma radius was evaluated by measuring three photographs of the plasma at a given seeding ratio. The three results were averaged. The visible radii are reproducible to ± .02 cm.

A serious question is whether the visible radius of the plasma, which is principly due to emission from neutral atoms gives an accurate picture of the free electron distribution. The values of E_{scat}/E_o and λ appear to depend fairly strongly on the value of R so the error due to this effect will be large. No measurements were undertaken to measure the free electron distribution so one can only speculate upon this question.

VII-D. Temperature Error

The sodium D line temperature measured in the center of the plasma directly between the horns was:

$$2754 \pm 37^{o}K$$

where $\pm 37^{o}K$ was the sample standard deviation of 13 temperature values. This temperature uncertainty is the principle factor in the electron density uncertainty.

For the sodium plasmas, Table 7 lists the relative errors in plasma frequency due to this temperature uncertainty.

TABLE 7

EFFECTS OF TEMPERATURE ERROR ON PLASMA FREQUENCY, Na

N	$\Delta\omega_p/\omega_p$
$.7123 \times 10^{-4}$	.208
1.20×10^{-4}	.200
2.689×10^{-4}	.169
6.21×10^{-4}	.164
1.078×10^{-3}	.161

TABLE 8

EFFECTS OF WEIGHT ERROR ON SEEDING RATIO AND PLASMA FREQUENCY Na

N	$\Delta N/N$	$\Delta\omega_p/\omega_p$
$.7123 \times 10^{-4}$	.0607	.030
1.201×10^{-4}		
2.689×10^{-4}	.0319	.013
6.212×10^{-4}	.0141	.009
1.078×10^{-3}	.0085	.005

A 5 mg error in the atomizer calibration gives errors substantially less than those above, and is therefore neglected.

It is concluded that seeding ratio errors are a fairly small source of error.

VII-G. Non-Standard Pressure

The calculations were made for 760 mm pressure but the actual pressure during the experiments was 740 mm. This introduces a particle density error $\Delta n/n = .026$, which is small in comparison to other effects.

VII-H. Strong Electric Fields

The presence of electric fields will accelerate the rather light electrons and raise their average energy compared to the heavy ions and neutral particles. On the other hand, collisions of the electrons with the other species will tend to equilibrate the electron energy with the energy of the other species. It is clear therefore that strong fields or low collision frequencies can give electron energies or temperatures much higher than plasma temperatures measured by sodium D line reversal techniques for instance. The sodium D line gives a temperature appropriate to a bound electron transition of a neutral sodium atom. As noted before the important quantity for microwave interaction is the free electron temperature. The Saha equation equilibrium will also be disturbed by an increased electron

temperature. High energy electrons may force a rise in the sodium D line temperature to some value between the ion or molecular translational temperature and the free electron temperature.

Let us calculate the error due to an electric field E exp (iωt). The equation of motion of an electron in this field is given by

$$m_e\ddot{x} = eE - m_e\dot{x}\nu \tag{7-10}$$

Assuming the time variation to be exp (iωt) then

$$\dot{x} = \frac{eE}{m_e(i\omega + \nu)}$$

and

$$|\dot{x}| = \frac{eE}{m\sqrt{\omega^2 + \nu^2}} \tag{7-11}$$

The average ordered oscillatory electron energy is

$$K = \frac{m_e|\dot{x}|^2}{2}$$

$$= \frac{e^2E^2}{2m_e(\omega^2 + \nu^2)} \tag{7-12}$$

Some of this ordered motion is converted into disordered heat at each collision.

Let ΔK = average electron energy loss at collision

$$= f(K_e - K_g) \tag{7-13}$$

where K_e = electron thermal energy

K_g = gas thermal energy

f = fraction of the excess energy $K_e - K_g$ of the electron lost at collision.

From elementary billiard ball mechanics one finds

$$f = \frac{2m_e}{M} \tag{7-14}$$

where M = mass of particle collided with

and m_e = electron mass.

Equilibrium occurs when the average ordered energy K gained during oscillation equals the average energy ΔK lost at each collision.

Therefore

$$K = \Delta K \tag{7-15}$$

or

$$f(K_e - K_g) = \frac{e^2E^2}{2m_e(\omega^2 + \nu^2)} \tag{7-16}$$

Since

$$K_e = \frac{3\ kT_e}{2} \tag{7-17}$$

$$K_g = \frac{3\ kT_g}{2} \tag{7-18}$$

Then

$$\frac{T_e - T_g}{T_g} = \frac{e^2E^2}{3fm_ekT_g(\omega^2 + \nu^2)} \tag{7-19}$$

For equilibrium $\frac{T_e - T_g}{T_g} << 1$

So

$$E << \frac{1}{e}\sqrt{3fm_ekT(\omega^2 + \nu^2)} \tag{7-20}$$

It is interesting to note that Margenau[28] obtains for the distribution function to be Maxwellian in the presence of electric fields

$$kT >> \frac{M\left(\frac{eE}{m_e}\right)^2}{6\frac{v^2}{\lambda^2} + \omega^2} \tag{7-21}$$

where λ = mean free path.

Using

$$\lambda^2 = \frac{v^2}{\nu^2} \approx \frac{3kT}{m_e \nu^2}$$

$$f = \frac{2m_e}{M}$$

then

$$E << \frac{1}{e}\sqrt{3 f m_e kT\,(\omega^2 + \nu^2)}$$

as obtained in Equation (7-20).

Considering N_2 as the massive particle, $f \sim 3.8 \times 10^{-5}$. Massey and Burhop[36] indicate experimental values for f on the order of 10^{-3} at electron energies of .5 ev, due to the presence of a few inelastic collisions for which $f \sim 1$.

Taking

$$f = 10^{-3}$$
$$\nu = 10^{11} \text{ as constant} >> \omega$$
$$T = 2750^{\circ}K$$

Equation (7-20) gives

$$E << 6.35 \times 10^3 \text{ volts/m}$$

An order of magnitude for the electric field off the tip of the probe is obtained by considering that just above the tip, the probe looks somewhat like a sphere of 3/8" diameter charged to about twice the plate potential (2000 v) of the plasma torch

The factor of two is due to the fact the tank coil is tapped like an auto transformer. Note that for 30 mc/sec, $\omega = 1.88 \times 10^8 << \nu = 10^{11}$ so the plasma generator field can be considered DC.

The capacitance of an isolated sphere of radius r_o is

$$C = 4\pi\epsilon_o r_o \tag{7-22}$$

If V_o = sphere voltage, Q = charge on sphere, then Gauss' law gives at some distance r

$$4\pi r^2 \epsilon_o E = Q = CV_o = 4\pi\epsilon_o V_o r_o$$

Therefore

$$E = \frac{V_o r_o}{r^2} \tag{7-23}$$

Now $r_o = .5$ cm $= 5 \times 10^{-3}$ m , $V_o = 4 \times 10^3$. At the tip $r = r_o$ so Equation (7-23) gives $E \sim 8 \times 10^5$ volts/m. This is considerably in excess of the allowable field strength, given by Equation (7-20).

For r = 7 cm, which is the plasma region directly between the microwave horns, Equation (7-23) becomes

$$E = 4.09 \times 10^3 \text{ V/m} \tag{7-24}$$

If

$$f = 10^{-3}$$
$$\nu = 10^{11} \text{ constant} >> \omega = 1.88 \times 10^8$$
$$T_g = 2750^{\circ}\text{K}$$

then Equation (7-19) gives

$$\frac{T_e - T_g}{T_g} = 2.48 \times 10^{-8} E^2 \tag{7-25}$$

Thus in the region between the horns

$$\frac{T_e - T_g}{T_g} \sim .413 \tag{7-26}$$

Therefore $T_e \sim 3890^{\circ}K$ which is considerably above the gas temperature $T_g = 2750^{\circ}K$.

In nonequilibrium cases, an adequate approximation[35,37] is to insert the electron temperature T_e into the Saha equation. For the sodium plasma, using $T_e = 3890^{\circ}K$, the electron density would be increased by a factor ranging from 27 at $N = 10^{-4}$ to 40 at $N = 5 \times 10^{-3}$ over the value using $2750^{\circ}K$, using Figure 5.

An estimate for the microwave electric field is found by noting that the time average flux density in a plane wave is

$$S = \frac{c\epsilon_o E_o^2}{2} \tag{7-27}$$

A maximum value of 100 milliwatts from the X-13 klystron is distributed by the horn over an area on the order of 20 cm x 20 cm or $.04\ m^2$ at the plasma position. Therefore $S = .1/.04 = 2.5\ watts/m^2$ giving

$$E_o = \sqrt{\frac{2S}{\epsilon_o c}} = \sqrt{\frac{5}{8.854 \times 10^{-12}\ 3 \times 10^8}} \tag{7-28}$$

$$= 43.6\ volts/m.$$

For the microwave electric field $\omega = 2\pi \times 10^{10}$, $\nu = 10^{11}$, $T_g = 2750^{\circ}K$, giving $\frac{T_e - T_g}{T_g} = 3.38 \times 10^{-5}$. Therefore $T_e - T_g = .093^{\circ}K$ at $T_g = 2750^{\circ}K$, which is negligible.

It is concluded that thermal equilibrium for the electrons probably does not exist, assuming Equation (7-23) represents the RF electric field at distances less than 15 cm in the region of the plasma. Of course the presence of the plasma may seriously affect the electric field strength as given by Equation (7-23).

VII-I. Temperature Gradients

There exist both axial and radial temperature gradients in the plasma. The radial variation is about $100^{o}K$ from center to visible radius of . 5 cm and about $60^{o}K$ per cm in the axial direction. These temperature differences will affect the plasma frequency and collision frequency in the plasma.

Some idea of the effect of axial variation may be obtained as follows. Consider the plasma divided into two halves by a plane normal to the plasma axis. In this plane the phase of the scattered wave from the upper half is the same as the phase of the scattered wave from the lower half. The upper and lower halves each contribute 1/2 of the magnitude of E_{scat}. Rather than taking the temperature throughout the entire plasma as that at the center where this plane passes through the plasma, for comparison we patch a two temperature plasma together at the mid plane. For the purposes of this calculation the temperatures used were those measured in the real plasma at the center of its upper half and the center of its lower half.

For each of these temperatures E_{scat} computed for the infinite length plasma is divided in half and added the other half, each with its own phase. The result is compared to that obtained for the full plasma taken at the average temperature of the two halves.

Assume upper half at $2520^{o}K$, lower half at $3000^{o}K$, with average $2760^{o}K$, $R = .5$, $\nu = 10^{11}$, $\phi = 0^{o}$, Na in N_2.

The ratio of E_{scat}/E_o, computed using the average plasma properties, to E_{scat}/E_o, computed using the composite plasma, is plotted vs. the plasma frequency of the average plasma in Figure 48. One could use this graph to get a correction factor to be applied to the observed E_{scat}/E_o.

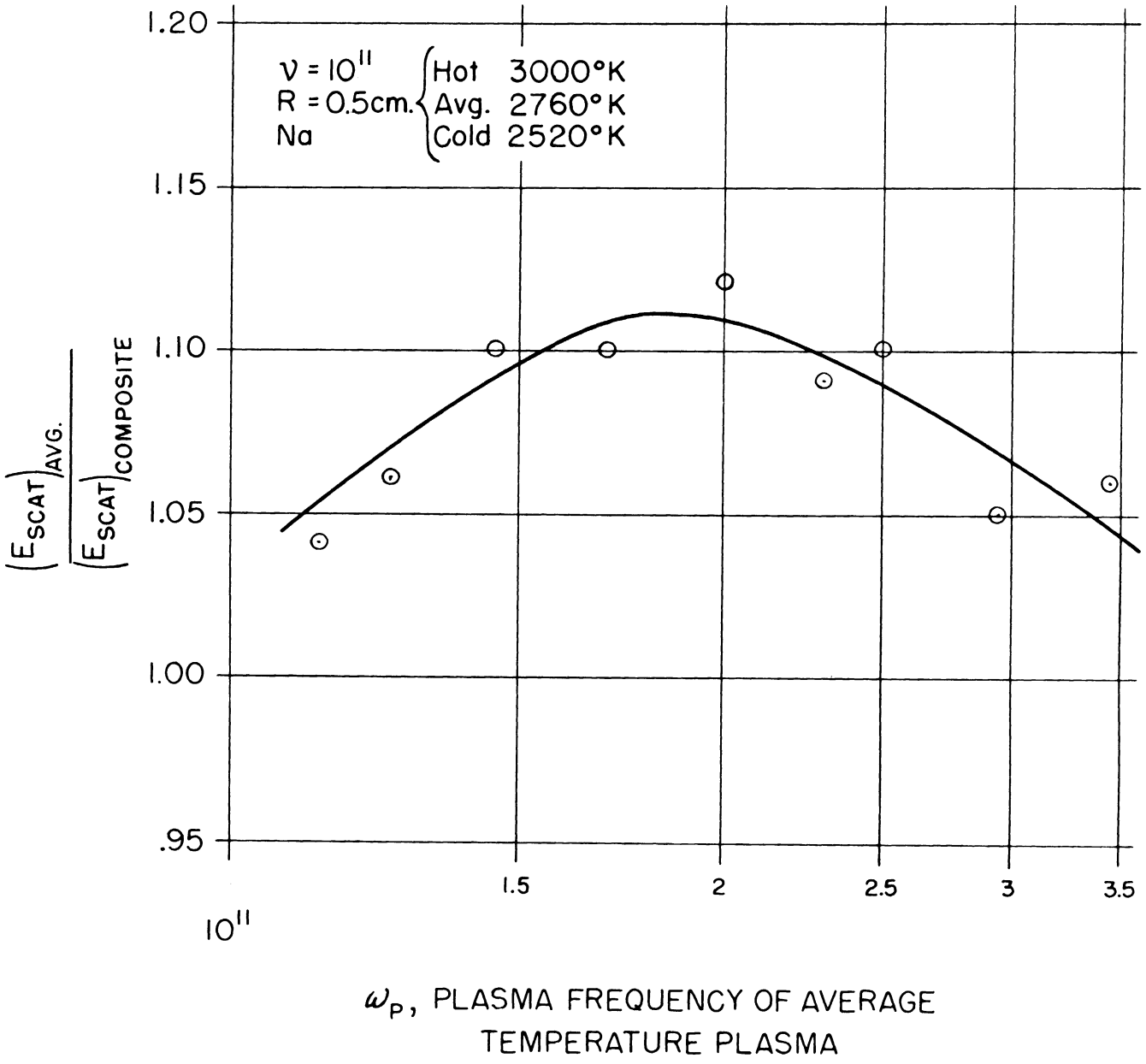

FIGURE 48. RATIO OF SCATTERED AMPLITUDES OF THE AVERAGE PLASMA TO THE COMPOSITE PLASMA

DeRidder and Edelberg[13] assumed arbitrary polynomial radial variation of ω_p, and found significant changes in the phase and amplitude of the scattered wave as compared to the homogeneous case. The scattered amplitude from the radially varying plasma generally decreases because of better matching of the plasma properties to the outside free space. For a sodium plasma of $N = 2 \times 10^{-4}$, the $100^{o}K$ decrease from $2754^{o}K$ decreases the electron concentration by a factor of 1.7. No attempt was made to determine the form of the radial variation.

VII-J. Finite Length

To evaluate the effects of finite plasma length on the phase and amplitude of the scattered wave, copper rods, and rods made of plaster of paris mixed with 2%, by volume wood charcoal (both of varying length, representing plasmas) were made and the phase and amplitude of the scattered wave plotted as a function of rod length.

The phase and amplitude data scatter was large but the conclusion was made that for lengths greater than 15 cm no large length effect was present. This is approximately the length of plasma illuminated by the microwaves.

VII-K. Electron Attachment and Ionization Rates

Due to the presence of O_2 and H_2O in the plasma, electron attachment is possible.[31]

$$e^- + H_2O \longrightarrow H_2O^-$$

$$e^- + O_2 \longrightarrow O_2^-$$

This attachment effectively immobilizes the electron for microwave purposes because of the heavy mass of these negative ions relative to the electrons. The microwave is sensitive only to the free electrons.

The rate of change of electron density due to attachments is[31]

$$\frac{dn_e}{dt} = - n_e (\nu_{H_2O} h_{H_2O} + \nu_{O_2} h_{O_2}) \frac{\text{electrons}}{\text{cc sec}}$$

where n_e = electron density

ν_{H_2O} = electron collision frequency with water molecules

h_{H_2O} = probability of electron attachment to water molecule, etc.

Balancing this removal of electrons is new ionization of seeding material, perhaps by the following process[35]

$$Na + e^- \xrightarrow{k_f} Na^+ + 2e^-$$

This ionization process produces electrons at the rate,

$$\frac{d[e^-]}{dt} = k_f [Na][e^-] \frac{\text{moles}}{\text{cc sec}}$$

or

$$\frac{dn_e}{dt} = k_f \frac{[Na][e^-]}{N_0} \frac{\text{electrons}}{\text{cc sec}}$$

N_0 = Avagadros' number, [ ] = concentration, $\frac{\text{moles}}{\text{cc}}$. The total rate of change of electron density is

$$\frac{dn_e}{dt} = - n_e (\nu_{H_2O} h_{H_2O} + \nu_{O_2} h_{H_2O} - k_f [Na])$$

Values of k_f could not be found so whether $\frac{dn_e}{dt}$ is positive or negative was not determined.

VII-L. Microwave Amplitude Error

The microwave is stronger at the plasma than at the receiving horn when the horn is put at x = 30 cm, $\phi = 0$, by 3. 65 db.

Therefore $E_{p\ plasma}/E_{p\ 30\ cm} = 1.525$. Since the amplitude of E_{scat} is directly proportional to the strength of the plane wave while the phase of E_{scat} is unchanged, the measured raw values of E_{scat} should be divided by 1. 525.

During these experiments the transmitting horn to plasma distance was 54 cm and the plasma to receiving horn distance was 30 cm.

VII-M. Errors Due to Altered Phase Relations of "Plane" and Scattered Waves Across Finite Horn

The receiving horn is not a point receiver but averages the signal which occupies roughly a spherical cap ℄ to E over the horn mouth with center of curvature at the horn apex.

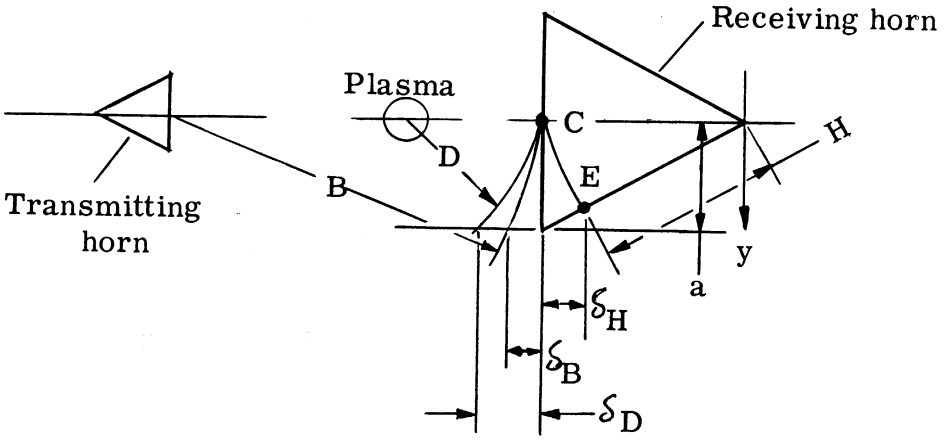

At the center C of the receiving horn the phase relations between E_p and E_{scat} are as shown:

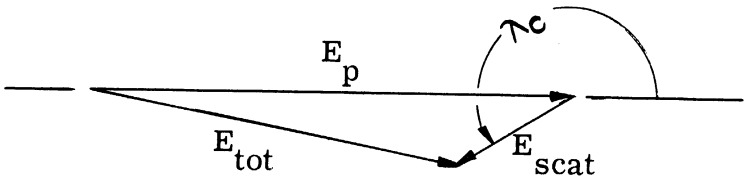

At the edge of the horn E these phase relations are as shown

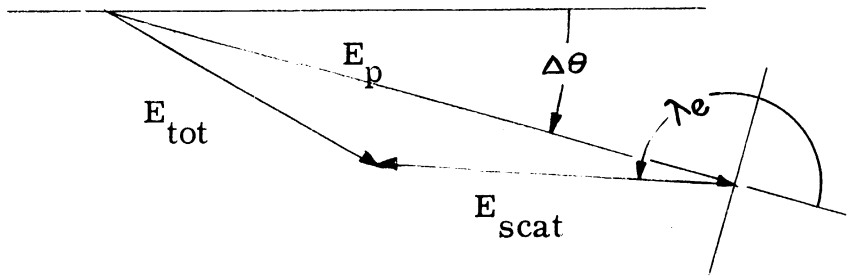

$\Delta\theta$ is the phase shift of the plane wave E_p due to the difference in distance of E and C from the receiving horn.

Let $\lambda_c - \lambda_y = \Delta\lambda$ be the phase shift due to the differences in the distance to the spherical cap of the "plane" wave and scattered wave.

If y = distance away from the center line

δ_H = distance spherical receiving cap departs from the planar horn face

δ_D = distance of the surface of constant phase of scattered wave from planar horn face

δ_B = distance of surface of constant phase of plane wave from planar horn face

δ_{scat} = distance scattered wave surface of constant phase is from the spherical cap

δ_p = distance "plane" wave surface of constant phase is from the spherical cap

then

$$\delta_{scat} = \delta_D + \delta_H$$

$$\delta_p = \delta_B + \delta_H$$

Since $\delta_D = \frac{y^2}{2D}$, etc., the change of phase between E_{scat} and E_p at y is

$$\lambda_c - \lambda_y = (\delta_{scat} - \delta_p) \frac{2\pi}{W}$$

$$\approx (\frac{1}{2D} - \frac{1}{2B}) \frac{2\pi y^2}{W}$$

where W = wave length of radiation.

Since all δ's are much less than B or D it has been assumed E_{scat}, E_p have nearly constant amplitude. E_{scat} and E_p fall off as $1/\sqrt{D}$ and $1/\sqrt{B}$ respectively.

If 2a = horn width, and each portion of the horn contributes equally to the total signal, an average $\Delta\lambda$ is

$$\langle \Delta\lambda \rangle \sim (\frac{1}{2D} - \frac{1}{2B}) \frac{2\pi}{W} \frac{1}{2a} \int_{-a}^{a} y^2 \, dy \sim (\frac{B - D}{BD}) \frac{\pi}{W} \frac{a^2}{6}$$

For the present case

W = 3 cm

B = 84 cm

D = 30 cm

a = 4.45

so $\langle \Delta\lambda \rangle$ = .074 radian. This should be algebraically added to the measured λ (which is an average) to give λ at the horn center.

VII-N. Error Summary

The principle errors are felt to be:

1. Possible nonequilibrium due to the high RF fields present.
2. Use of an arbitrary visible radius.
3. Nonuniform properties in the radial and axial directions.

Those corrections which can be made to E_{scat}/E_o and λ, i. e, the microwave amplitude error and altered phase relations due to the finite size horn, make the differences between theory and experiment larger.

It is apparent that the discrepancy between theory and experiment is too large to be satisfactorily accounted for. It should also be clear that serious doubts can be entertained as to whether the theoretical model in any but a qualitative manner describes the interaction of a plane wave and a finite nonuniform cylindrical plasma.

The errors affecting the predicted E_{scat}/E_o and λ were not used to obtain uncertainties for E_{scat}/E_o and λ.

VIII. CONCLUSIONS

Examining Figures 42 through 47, giving the comparison of theory and experiment, shows serious consistent differences between the predicted phase and amplitude using predicted values of ω_p and ν and the visually determined radius, compared to the microwave measurements of phase and amplitude.

The measured phase is seen to be larger than predicted even though the precision is of the same order as the differences. The corrections noted in Section VII-M however, increase the discrepancy between prediction and experiment.

The measured amplitudes are smaller than predicted. The precision of measurement is better but the corrections in Section VII-L indicate the experimental points should be divided by a factor which makes the disagreement between predicted and experimental amplitudes even larger.

The general uncertainty of the conditions in the experimental plasma indicate more work must be done to satisfactorily resolve these questions. It is anticipated that further studies of cylindrical plasmas with improved models will yield data which may explain some of the difficulties encountered here.

REFERENCES

1. Murphy, E. L., Edelberg, S., Pippert, G. F., Electro Magnetic Studies of Ionized Wakes, Massachusetts Institute of Technology, Lincoln Lab., Tech. Rept. No. 266, 20 Apr. 1962.

2. Ginzburg, V. L., Propagation of Electro Magnetic Waves in Plasma, Gordon and Breach Science Publishers, Inc., 1961.

3. Klein, M. M., Greyber, H. S., King, J. I. F., Breckner, K. A., Interaction of a Non-Uniform Plasma with Microwave Radiation, General Electric Company, Aero.Sci. Lab., Rept. R59SD467, Nov. 1959.

4. Albini, F. A., Jahn, R. G., "Reflection and Transmission of Electro Magnetic Waves at Electron Density Gradients," J. App. Phys., Vol. 22, No. 1, Jan. 1961 or California Institute of Technology, Guggenheim Jet Prop. Cntr., Tech. Note 3, Oct. 1960.

5. Mitra, S. K., The Upper Atmosphere, The Asiatic Soc., 2nd ed., 1952.

6. Golant, V. E., "Microwave Plasma Diagnostic Techniques," Soviet Phys. Tech. Phys., Vol. 5, No. 11, pp. 1197-1310, May 1961.

7. Daiber, J. W., Glick, H. S., "Plasma Studies in a Shock Tube," Midwest Research Institute Symp. Proc., Electromagnetics and Fluid Dynamics of Gaseous Plasma, Vol. XI, Apr. 1961.

8. Jahn, R. G., "Microwave Probing of Ionized Gas Flows," Phys. Fluids, Vol. 5, No. 6, pp. 678-686, June 1962.

9. Talbot, L., Katz, J. E., Brundin, C. L., Microwave Electron Density Measurements, University of California, Tech. Rept. No. HE-150-186, Jan. 1961.

10. Kuhns, P. W., Flame Temperature 2000 to 3000^{o}K Microwave Absorption, NASA Tech. Note 3254, 1954.

11. "Round Table Discussion," Microwave Research Institute, Proc. of Symp. on Electro Magnetic's and Fluid Dynamics of Gaseous Plasma, Vol. XI, Brooklyn Polytechnic Institute, New York, Apr. 1961.

12. DeRidder, C. M., Peterson, L. G., Scattering from a Homogeneous Plasma Cylinder of Infinite Length, Massachusetts Institute of Technology, Lincoln Lab., Rept. No. 312G-4, 15 Jan. 1962 (AD 274067).

13. DeRidder, C. M., Edelberg, S., "Electromagnetic Scattering from Plasma Cylinders with Varying Radial Electron Density and Collision Frequency Distributions, and the Effects of These Variations on the Plasma Diagnostic Problems in Hypervelocity Ballistic Range Experiments," presented at AFCRL Second Symp. on the Plasma Sheath, 10-12 Apr. 1962.

14. Hochstim, A. R., "Electron Concentration in Closed Form for High Temperature Air and Air with Additives," Proc. of the Symp. on the Plasma Sheath, Dec. 1959 or Electromagnetic Effects of Reentry, Pergamon Press, 1960.

15. Buchanan, R. S., Study of a Seeded Plasma, Doctoral Thesis, The University of Michigan, Sept. 1961, and ARL 62-310, Mar. 1962.

16. Chinitz, W., Ersen, L., Gross, R., "Aerothermodynamic and Electrical Properties of Some Gases to M = 20," paper presented at ARS Thirteenth Annual Meeting, Nov. 1958.

17. Shkarofsky, I. P., Bachynski, M. P., Johnston, T. W., Collision Frequencies Associated with High Temperature Air and Scattering Cross-Section of the Constituents, Radio Corporation of America Victor Company, Ltd., Montreal, Res. Rept. No. 7-801, Dec. 5, 1959.

18. Chapman, S., Cowling, T. G., The Mathematical Theory of Non-Uniform Gases, Cambridge, 1960.

19. Drummond, J. E., Plasma Physics, McGraw-Hill, 1961.

20. Logan, J. G., Treanor, C. E., Tables of Thermodynamic Properties of Air from 3000°K and 10,000°K at Intervals of 100°K, Cornell Aeronautical Lab., Inc., Rept. NOBE-1007-A-3, Jan. 1957.

21. Gilmore, F. R., Equilibrium Composition and Thermodynamic Properties of Air to 2400°K, The Ranel Corporation, Res. Mem. RM-1543, Aug. 24, 1955.

22. Stull, D. R., Sinke, G. C., Thermodynamic Properties of the Elements, American Chemical Society, Advances in Chemistry, Series 28, 1956.

23. Brewer, L., Chandrasekharaiah, M. S., Free Energy Functions of Gaseous Monoxides, University of California, Lawrence Rad. Lab., UCRL-8713 (Rev.), June 1960.

24. Penner, S. S., Chemistry Problems in Jet Propulsion, Pergamon Press, 1957.

25. Saha, M. N., Srivastava, B. N., A Treatise on Heat, The Indian Press, Ltd., 2nd ed., 1935.

26. Margenau, H., Stillinger, S., "Microwave Conductivity of Slightly Ionized Air," J. App. Phys., Vol. 30, No. 9, Sept. 1959.

27. Margenau, H., "Conductivity of Plasmas to Microwaves," Phys. Rev., Vol. 109, No. 1, Jan. 1958.

REFERENCES (continued)

28. Margenau, H., Phys. Rev., Vol. 69, p. 508, 1946.

29. Hilsenrath, J., et al., "Tables of Thermal Properties of Gases," NBS Circular 564, Nov. 1955.

30. Molmud, "The Electrical Conductivity of Weakly Ionized Gases," ARS Preprint 2586-62, Part I.

31. Brown, Basic Data of Plasma Physics, Wiley and Massachusetts Institute of Technology, 1959.

32. Spitzer, Physics of Fully Ionized Gases, Interscience, 2nd ed., 1962.

33. Roddy, Green, Electronics World, p. 29, Feb. 1961.

34. Hottel, Williams, Jensen, Optical Methods of Measuring Plasma Jet Temperatures, WADD Tech. Rept. 60-676, June 1961 (AD 266723).

35. Robben, Experimental Studies of Non-Equilibrium Ionization in an Magneto-hydrodynamic Generator, General Electric Company, Space Sci. Lab., Rept. No. R62 SD13, Feb. 1962 (AD 275444).

36. Massey, Burhop, Electronic and Ionic Impact Phenomena, Oxford, 1952.

37. Shair, Theoretical Performance of Magnetohydrodynamic Generators Utilizing Magnetically Induced Nonequilibrium Ionization in Pure Alkali Metal Vapors and in Seeded Gas Systems, Proc. of Fourth Symp. on the Engineering Aspects of MHD, Apr. 10, 1963.

38. Ratcliff, The Magneto Ionic Theory and Its Applications to the Atmosphere, Cambridge, 1959.